Preparation and Characterization of Proton Exchange Membranes for Direct Methanol Fuel Cells

by

Xiao Zhang

Department of Chemical Engineering
Universitat Rovira i Virgili (URV)
Spain

October 2005

Thesis Supervisor: Dr. Ricard Garcia Valls

Preparation and Characterization of Proton Exchange Membranes for Direct Methanol Fuel Cells

Xiao Zhang
Department of Chemical Engineering
Universitat Rovira i Virgili
URV
Tarragona, Spain

Ph.D. Thesis
October, 2005
ISBN-10: 84-689-3990-0

Aquest treball ha estat desenvolupat en major terme als laboratoris del Grup de Recerca de Biopolímers Vegetals, del Departament d'Enginyeria Química de la Universitat Rovira i Virgili (Av. Països Catalans, 26, 43007 – Tarragona, Catalunya, Espanya) sota finançament de la Universitat Rovira i Virgili i del projecte: "*Evaluación de cultivos energéticos para la obtención de derivados celulósicos*", referència PPQ2001-1215-C03-01, concedit pel "*Ministerio de Ciencia y Tecnología*" i 2001SGR-00323 de la Direcció General de Recerca de la Generalitat de Catalunya. El treball presentat en aquest document no ha estat usat també per l'obtenció de qualsevol altre títol o qualificació, i ha estat fruït íntegrament del treball realitzat pel sotasignant, excepte els casos que específicament s'indiqui el contrari.

Xiao Zhang

Septiembre de 2005

Tribunal de la Tesis

Dra. Juana Benavente
Universidad de Málaga, España

Dr. José Luís Toca
Universitat Rovira i Virgili, España

Dr. Oscar Miguel
Centro de Tecnología Electroquímica, España

Dr. Andreas Glüsen
IWV-3, Forschungszentrum Jülich, Germany

Dr. Philippe Sistat
Institut Européen des Membranes, UMI
Université Montpellier II, France

Suplentes

Dra. Laura Palacio Martínez
Universidad de Valladolid, España

Dr. Francisco Medina
Universitat Rovira i Virgili, España

Evaluadores externos

Dra. Signe Kjelstrup
Norwegian University of Science and Technology, Norway

Dr. João Paulo Serejo Goulão Crespo
Universidade Nova de Lisboa, Portugal

"All men have been created to carry forward an ever-advancing civilization."

---------- Bahá'u'lláh

Preface

This thesis presents researches of two stages. The first stage which consisted of the membrane preparation and characterization was mainly performed in the Universitat Rovira i Virgili (URV - Spain), some parts of the membrane characterization were in collaboration with Universidad de Málaga (Spain) and Universidad de Valladolid (Spain). The second stage consisted of the fuel cell test, which was performed in IWV-3, Forschungszentrum Jülich, Germany.

I would like to begin by acknowledging those professors who were instrumental in the development of my PhD research. First I would like to acknowledge Prof. Ricard Garcia Valls of URV because through him my research in fuel cell membrane began three years ago and to Universitat Rovira i Virgili (URV) for providing the doctoral scholarship. As we started we only had a manual casting knife in our lab to prepare membrane. After one year's struggle with material, equipment and testing conditions, we finally found an exciting direction ----- Lignosulfonate Membranes (LS membranes). The optimization and characterization of the membrane were difficult since we were the first to use porous membrane in fuel cells and it was the first time that LS was used in polymeric membranes. Second, I would like to acknowledge Dr. Laura Palacio Martínez and Dr. Javier Carmona del Rio of Universidad de Valladolid for their help with contact angle measurement and some of the atomic force microscopic (AFM) characterization. The rest of the members in their groups also deserve recognition for their help. Third, I would like to acknowledge Dr. Juana Benavente of Universidad de Málaga who helped with the measurement of the membrane ion conductivity.

Finally, I would like to acknowledge Dr. Andreas Glüsen of IWV-3 (Forschungszentrum Jülich, Germany) for his support and guidance and to Deutscher Akademischer Austauschdienst (DAAD) for providing the grant for my research there.

Under Dr. Glüsen's supervision the electrochemical and electrical characterizations (or fuel cell test) of the LS membranes were performed. He showed extreme patience with the membrane test, encouraged and instructed me when I was disappointed after many failures to fabricate Membrane Electrode Assembly (MEA). His support made me understand much better about fuel cell membranes and made my research stay fruitful ---- one chapter of the thesis and one paper were based on these efforts. I would also like to take this chance to thank Mr. Jürgen Mergel

and his group members for their kind help; Furthermore, I would like to thank the Bahá'í community in Jülich for the hospitality and spiritual support.

Looking back into the past, Prof. Shenyi Tong led me into polymer science during my Master study. His devotion into the polymer science contributed to my interests in polymer synthesis and application field. Through him, I learned how to start a research project which made my PhD research easier.

My stay in Spain has been pleasant because of the support and friendship of many. I would have never imagined that upon my arrival at the airport at midnight, I would have my professor Dr. Ioanis Katakis picking me up with my heavy luggage and helping me settle down at the beginning. He also helped me get started in the university. Of course, I would like to thank all the professors and my colleagues in the group for their support, especially to Claudia Barba for her warmest welcome and friendship. Also I would like to thank those professors and colleagues of the department, the scientific service center and the language service center who gave me kindly support. During these four years, my friends Paulo, Luciana, Baltazar, Chimentão, Oscar, Costanza, Xavier, Justyna and Haydée made great efforts helping my Spanish, embracing me into their social activities and giving me valuable suggestions. Their friendship will always last in my heart. I am also grateful for the support of the Bahá'í community in Tarragona. They provided a peaceful environment around me and made me feel at home. Especially to Mr. & Mrs. Mohabbat, who took care of me as their own child. May God bless them.

I would like to thank those who gave me support at any moment; their actions filled my heart with gratitude and to those who gave me challenges, which taught me to be strong.

I dedicate this thesis to my loving family. Without their help, understanding, support and love, I would never achieve my goals. Mainly to my mother who has been by my side in all situations; she has been so patient, open-minded, and instructive all these years, she believes in me more than I believe in myself.

In memory of my dear grandmother who passed away three months after I came to Spain, and my grandfather, who loved me always.

To God, the All-Glorious, the Supreme Helper.

Summary

This thesis presents the preparation and characterization of three novel proton exchange membranes: **poly(ethylene glycol) (PEG) composite membranes**, **polyamide (PA) composite membranes** and **Lignosulfonate (LS) membranes**. Among them, LS membranes were tested in a direct methanol fuel cell. LS membranes were the innovation of this thesis, through which we pointed out that porous membrane can also be considered in the fuel cell application.

- **Two kinds of composite membranes were prepared by separately coating poly(ethylene glycol) (PEG) and polyamide (PA) skin layers onto polysulfone (PSU) porous supports.** Lignosulfonate (LS) and the derivative of phosphoric acid were incorporated into the PA network to perform as "proton carriers". Skin layer and support were optimized separately for the two types of membranes. PEG composite membranes showed water-dependent proton conductivity, while PA composite membranes showed proton hopping mechanism through acid groups and base groups. Comparing to Nafion 117, these two kinds of membranes had lower proton transport ability and need to be further improved if they are to be considered for applications in fuel cells.

- **Hybrid LS membranes were also prepared by blending LS with PSU and then by immersion precipitation method.** Influential factors were investigated such as PSU/LS proportion, the temperature of the casting solution, the precipitation temperature and the composition of the precipitation bath. The best results were obtained for membranes prepared from the casting solution at 35 ^{o}C, precipitated at 15 ^{o}C in a water bath. High LS content in the membrane gave better mass transport ability.

  Membrane morphology changes detected by scanning electron microscopy (SEM) and atomic force microscopy (AFM) led us to

analyze the transport ability from the microscopic point of view. Proper nodule size or aggregation and orientated distribution on the membrane surface favored for the proton transport.

The electrochemical properties of LS membranes were also characterized. LS membranes achieved acceptable proton conductivities with very low ion exchange capacity (IEC).

- **Membrane electrode assemblies (MEAs) were fabricated and their cell performances were measured in a single direct methanol fuel cell (DMFC).** The MEA fabrication conditions were not optimized, the contact between electrodes and membranes was the difficult part of the fabrication. It proved the possibility for LS membranes to be used in DMFC.

Resumen

En esa tesis se presentan tres nuevas membranas de intercambio de protón; los tres siguientes temas fueron llevados a cabo:

- Dos clases de membranas compuestas fueron preparadas utilizando polisulfona (PSU) como soporte poroso sobre las cuales se depositó una capa activa. En un caso se utilizó polietilenglicol (PEG) y en el otro poliamida (PA). Derivados del ácido fosfórico y lignosulfonados (LS) fueron incluidos en la estructura de la PA para actuar como agentes transportadores de protones. Las capas y el soporte fueron optimizados por separado para los dos tipos de membranas. Las membranas compuestas preparadas utilizando PEG mostraron una conductividad de protón que dependía de la presencia del agua, mientras que las membranas compuestas preparadas utilizando PA siguieron el mecanismo de "hopping", a través de grupos de ácidos y grupos de base. Comparadas a Nafion 117, estas dos clases de membranas presentaron capacidad para el transporte de protones más baja y deberían ser mejoradas para su aplicación en celdas de combustible.
- Se obtuvieron también membranas híbridas de LS, preparadas mediante la mezcla de los dos polímeros, LS y PSU, siguiendo el método de precipitación en inmersión. Los parámetros influyentes investigados fueron la proporción de PSU / LS, la temperatura de la solución polimérica de "casting", la temperatura de precipitación y la composición del baño de precipitación. Los mejores resultados fueron obtenidos para membranas preparadas con la solución polimérica "casting" a 35 ºC, baño de precipitación a 15 ºC con una composición al 100% de agua. Las membranas con altos contenidos en LS presentaron mejor transporte de materia.

Los cambios detectados en la morfología de las membranas utilizando Microscopía de Barrido Electrónico (SEM) y de Fuerza Atómica (AFM) nos permitieron a analizar la habilidad de transporte del punto de vista microscópico. Un tamaño de nódulo correcto y el de sus agregados, y una distribución orientada sobre la superficie de la membrana favorecen el transporte de protones.

- Las propiedades electroquímicas de las membranas de LS fueron caracterizadas. Las membranas de LS alcanzaron conductividades de protón aceptables con capacidad de intercambio iónico muy baja (IEC).

  "Membrane electrode assemblies" (MEAs) fueron preparadas y sus rendimientos de celda fueron medidos en una celda individual directa de metanol (DMFC). Las condiciones de preparación de las MEA no fueron optimizadas debido a que éste no era un objetivo inicial de la tesis y a que el contacto entre electrodos y membranas era la parte difícil de la fabricación. Este objetivo queda para trabajos posteriores.

Abbreviations

AFC	Alkaline fuel cell
DMFC	Direct methanol fuel cell
DMF	N,N-Dimethylformamide
DEHPA	Di-(2-ethyl-hexyl) phosphoric acid
GDE	Gas diffusion electrode
IEC	Ion exchange capacity
IPA	Iso-propanol
LS	Lignosulfonate
MEA	Membrane electrode assembly
MCFC	Molten carbonate fuel cell
OCV	Open cell voltage
PSU	Polysulfone
PEG	Poly(ethylene glycol)
PA	Polyamide
PAD	Polyamide membrane containing DEHPA
PALS	Polyamide membrane containing LS
PEM	Proton exchange membrane
PEMFC	Proton exchange membrane fuel cell
PAFC	Phosphoric acid fuel cell
PFSA	Perfluorosulfonic acid membrane
PEEK	Poly(ether ether ketone)

PS	Polystyrene
PBI	Poly(benzimidazole)
PEO	Poly(ethylene oxide)
PVP	Polyvinyl pyrrolidone
PTFE	Polytetrafluoroethylene
SD	Swelling degree
SOFC	Solid oxide fuel cell
SPSU	Sulfonated polysulfone
SPEEK	Sulfonated poly(ether ether ketone)
TFC	Thin film composite membrane

Contents

Chapter 1

Introduction

1 Background

1.1 Main categories of fuel cells

Fuel cells were invented in 1839 by William Grove. They are a kind of electrochemical device that converts chemical energy directly into electrical energy. After the petrol crisis and the emission problems resulting from it, fuel cells gained an important place in the application of alternative energy. They do not need a particular environment to work well in and are highly efficient both electrically and physically. Other advantages include the fact that they are silent and non-polluting and their emissions are ultra low.

After over 150 years of research, fuel cells can be divided into five major categories [1]: alkaline, phosphoric acid, solid oxide, molten carbonate and proton exchange membrane.

Alkaline fuel cells (AFC) were developed by F.T. Bacon in 1930. They use alkaline potassium hydroxide as the electrolyte and generate power efficiencies of up to 70 percent. AFC were long used by NASA on space missions—on the Apollo spacecraft to provide electricity and drinking water, for example. Their operating temperature is 150 ^{o}C to 200 ^{o}C. However, they were too costly for commercial applications and several companies are now examining ways to reduce costs and improve operating flexibility.

Phosphoric acid fuel cells (PAFC) were manufactured in the 1970s in the background of the energy crises. This type of fuel cell is the one that has been commercially developed the most and is used in a wider range of applications in hospitals, nursing homes, hotels, office buildings, schools, utility power plants and airport terminals. These cells generate electricity with an efficiency of over 40% and their operating temperatures are around 150 ^{o}C.

Another highly promising fuel cell, the solid oxide fuel cell (SOFC), is used for stationary power plants. A solid oxide system usually uses a hard ceramic material instead of a liquid electrolyte. This allows operating temperatures to reach 1,100 ^{o}C. Power generating efficiencies can reach 60% and 85% with cogeneration and with a cell output of up to 100 kW.

Molten carbonate fuel cells (MCFC) use a liquid solution of lithium, sodium and/or potassium carbonates soaked in a matrix for an electrolyte. They promise high fuel-to-electricity efficiencies normally of about 60%, or 85% with cogeneration, and operate at about 650 ^{o}C.

Proton exchange membrane fuel cells (PEMFC) operate at relatively low temperatures (about 80 ^{o}C), have high power density, can vary their output quickly to meet shifts in power demand, and are suitable for automobile applications. In the 1960s, driven by the need for very compact units for producing electricity and water, NASA developed PEMFC in their Gemini space program. They were chosen for the Apollo program and launched in the space shuttles, but were found to be inferior to the AFC in terms of performance and durability. In the 1980s PEMFCs achieved significant progress when membranes with greater stability and performance were discovered. PEMFCs use polymer membranes, which are able to conduct hydrogen protons, as the electrolyte. . The electrolyte is sandwiched between two electrodes, which contain Pt-based catalysts that help the oxidation and reduction reactions to take place. According to the U.S. Department of Energy, they are "the primary candidates for light-duty vehicles, for buildings, and potentially for much smaller applications such as replacements for rechargeable batteries in video cameras." PEMFCs mainly include hydrogen fuel cells and direct methanol fuel cells (DMFC).

1.2 Introduction of direct methanol fuel cell (DMFC)

1.2.1 Methanol as the fuel

In DMFCs, methanol is fed directly as the fuel. Methanol systems have several advantages over fuel cell systems based on hydrogen and compressed natural gas [2]. The liquid nature of methanol under room

temperature and atmospheric pressure simplify the methanol transport and application since it can be pumped from existing gasoline infrastructures without an external compressor or refrigeration equipment. This makes the volume of DMFCs is as small as possible.

Methanol has the highest hydrogen-to-carbon ratio among alcohols, which means that the highest energy could be generated and the least carbon dioxide emitted. The miscibility of methanol with water means that DMFCs can be fueled with different concentrations of a methanol aqueous solution. Other advantages of methanol are that it can be obtained through biomass and is more environmentally friendly than gasoline since it breaks down quickly in the environment.

1.2.2 Working principle of DMFCs

Figure 1 illustrates the working principles of DMFCs.

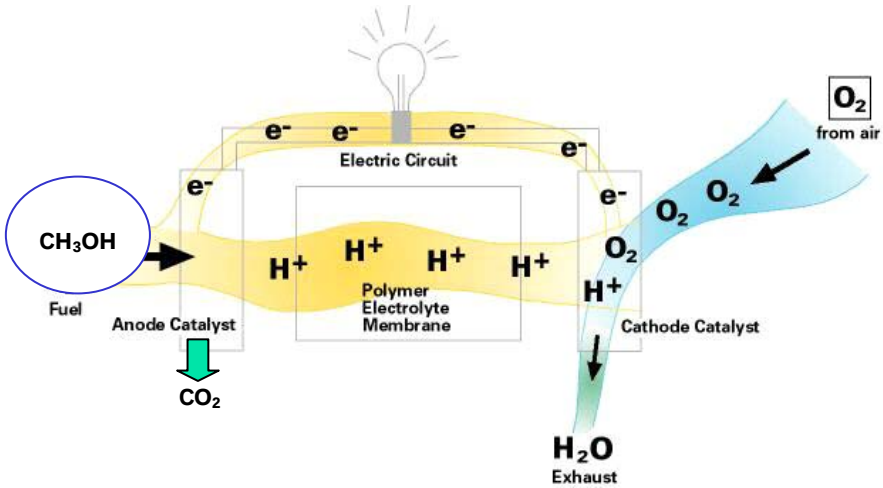

Figure 1. Working principles of DMFCs [3].

Methanol is introduced to the anode, where it is split into protons and free electrons and gives out carbon dioxide. The hydrogen ions flow through the polymer electrolyte membrane to the cathode, where the air or oxygen is introduced. At the cathode, the hydrogen ions are bonded with oxygen to form water and the movement of free electrons from anode to cathode creates a current that can be used to power an electrical device.

CH_3OH (l) + H_2O (l) -------> $6H^+ + 6e^- + CO_2$ (g) (anodic half reaction)

$6H^+ + 6e^- + \frac{3}{2} O_2$ (g) -------> $3H_2O$ (l) (cathodic half reaction)

CH_3OH (l) + $\frac{3}{2} O_2$ (l) -------> CO_2 (g) + $2H_2O$ (l) (overall reaction)

Pt-Ru (Platinum - Ruthenium) catalysts are currently considered to be the best anode catalysts and Pt (platinum) catalysts are considered to be the best cathode catalysts [4, 5]. These catalysts are often mixed with carbon black to increase reaction area and may be sprayed, pressed or "glued" onto the membrane. The function of a polymer membrane in a DMFC is to separate the anode and cathode feed and create a chemical potential when the electrochemical reaction occurs. The ideal membrane should tolerate high temperatures, present free resistance of proton transport, be an insulator to electrons, totally separate chemical species from the anode and cathode, possess good mechanical strength and be inexpensive.

2 Problem statement and development of DMFCs

Although DMFC technology is considered to be the most suitable alternative power source for certain applications, it still faces several challenges.

2.1 Proton exchange membranes

Perfluorosulfonic acid membranes (PFSAs) (e.g. Nafion, by Dupont) are widely considered as standard because of their high proton conductivity. However, PFSA membranes are good proton conductors only when they are saturated with water. For example, as we can see in Figure 2, the proton is transported through the micropores or ion channels of the Nafion together with its solvating water [6-9].

This water-dependence of proton conductivity creates a severe problem in the DMFC—the so-called "methanol crossover"—because methanol is transported through PFSA membranes by means of diffusion and active transport with proton and water (electroosmotic drag) [9]. This high methanol crossover has reduced cell efficiency in various aspects [10, 11].

Firstly, the methanol that crosses over is oxidized in the cathode, thus consuming extra energy.

Secondly, overall fuel efficiency is reduced because fuel that could have been separated into protons and carbon dioxide is wasted.

Finally, the catalyst on the cathode side is easily poisoned by carbon atoms that stick to the catalyst and inactivate it.

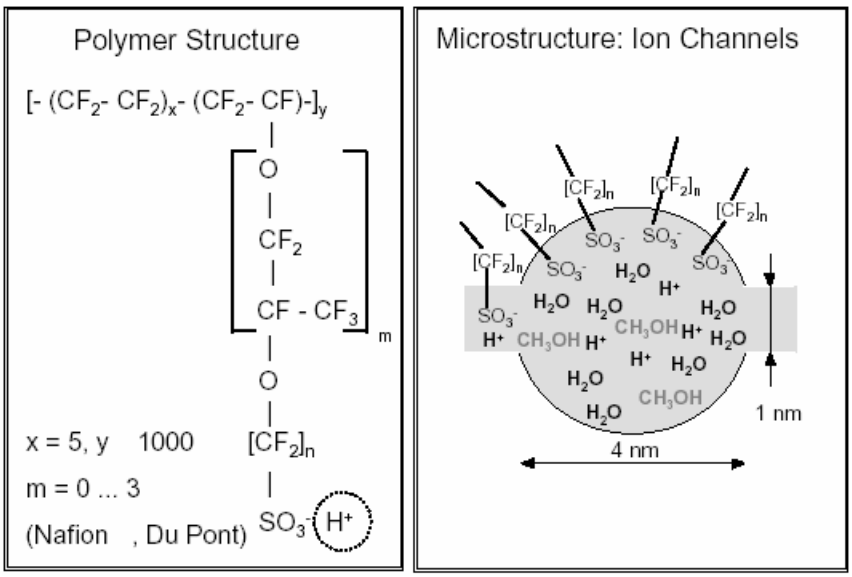

Figure 2. Structure of Nafion and water-filled micropores [9].

Another disadvantage of PFSA membranes is the high level of swelling. Nafion, for example, swells in water by about 10%. This limits how membrane electrode assembly (MEA) is produced. New attempts to directly coat the catalyst on the membrane to provide better contact are not producing good results with PFSA membranes because of this swelling.

The high cost of PFSA membranes also help significantly to make the fuel cell system as a whole expensive.

For these reasons, new types of membranes based on different concepts are being developed.

One type of membrane developed with the same proton transport concept as PFSA membranes are sulfonated hydrocarbon membranes and blends such as sulfonated poly(ether ether ketone) (PEEK), polysulfone (PSU) and polystyrene (PS), etc. [12-14]. The aromatic polymer-based

membranes are cheaper than PFSAs and their low degree of swelling enables them to form thinner films with relatively lower methanol crossover. Suitable polymers and a carefully controlled sulfonation degree should be thoroughly investigated in order to obtain membranes with good proton conductivity and low methanol crossover. At a low sulfonation degree, the conductivities of this kind of membrane are lower because the acid sites on sulfonated aromatics are less acidic than those of PFSAs. At a high sulfonation degree, the membranes present high water swelling, which leads to high methanol crossover and poor chemical and mechanical stabilities. Some inorganic materials such as SiO_2, TiO_2 and ZrO_2 have been blended with sulfonated hydrocarbon. In this case, the generated membranes can be applied to DMFCs operating at over 100 ^oC and the methanol crossover is lower [15-20].

Another type of membrane was generated by filling the phosphate and other acids into a polymeric matrix, which improved proton conductivity [21-24]. The main problem with this type of composite membrane could be the limited long-term stability since the acids that are introduced may be washed out in the fuel cell operation.

Polymers with proton donors and acceptors are another concept in the preparation of proton exchange membranes [25-28]. The membranes are usually synthesized by combining a basic polymer with N as a proton acceptor and an acidic polymer with sulfonic acids groups as a proton donor. The sulfonic acid groups interact with the N-base by forming hydrogen bridges and by protonation of the basic N. For example, poly(benzimidazole) (PBI) blend membranes use this mechanism to transport protons (Figure 3).

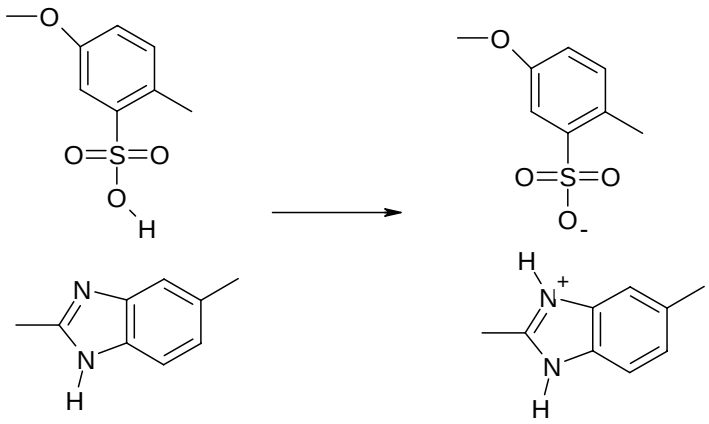

Figure 3. Proton transport in sPEEK-PBI acid-base blends by imidazole group protonation [28].

As we can see, here proton is mobile in the matrix without the solvating water, so the methanol cannot be transported accompanying the proton, and methanol crossover is significantly lower. Improvements in proton conductivity and long-term stability are being further investigated.

2.2 Catalysts and cell performances

Another reason for the high cost of DMFCs is that large amounts of expensive platinum and platinum-ruthenium catalysts are used. The reaction kinetics (rate) in the oxidation of methanol limits the practicality of the fuel cell.

The mechanism behind methanol oxidation is not yet fully understood. General agreement supports the theory that surface-bound CO is the long-living intermediate responsible for the slow overall reaction kinetics [29, 30]. Since the anodic reaction rate is far slower than the cathodic one, it is assumed to be the rate-determining step under most operating conditions.

A catalyst must be resistant to the poison from the CO and crossed methanol. Raising the operating temperature is one way to increase the tolerance of the catalyst to CO. Low catalyst loading is another way to reduce fuel cell costs.

The theoretical open cell voltage (OCV) E^0 of a DMFC at STP condition is calculated as [31]:

$$E^0 = \frac{-\Delta\bar{g}_f}{zF} = \frac{702.5}{6F} = 1.214\ \text{V}$$

where $\Delta\bar{g}_f$ is the change in Gibbs free energy of formation per mole (kJ),

z is the number of electrons transferred in the reaction, and

F is the Faraday constant, the charge on one mole of electrons (96,485 Coulombs).

Because of the oxidation of crossed methanol, the values of the experimental data of OCV are significantly lower than the theoretical values. This undesired oxidation of methanol leads to a mixed potential formation at the cathode, which leads to a reduced electrode potential and causes the overall reduction in cell voltage.

The characteristic shape of the voltage-current density graph (U-I) for an irreversible DMFC is shown in Figure 4. Three major irreversibilities are presented in the U-I curve [2].

1. Activation losses. At the start of the U-I curve (region 1), there is a rapid voltage drop. This is caused by the slowness of the reactions taking place on the surface of the electrodes.

2. Ohmic losses. Region 2 represents the drop in ohmic voltage due to the resistance of MEA and various interconnections.

3. Mass transport losses. In region 3, the voltage begins to drop faster at higher currents because the reactant concentration is lower and is not enough for the reactant to be transported to the electrode surface.

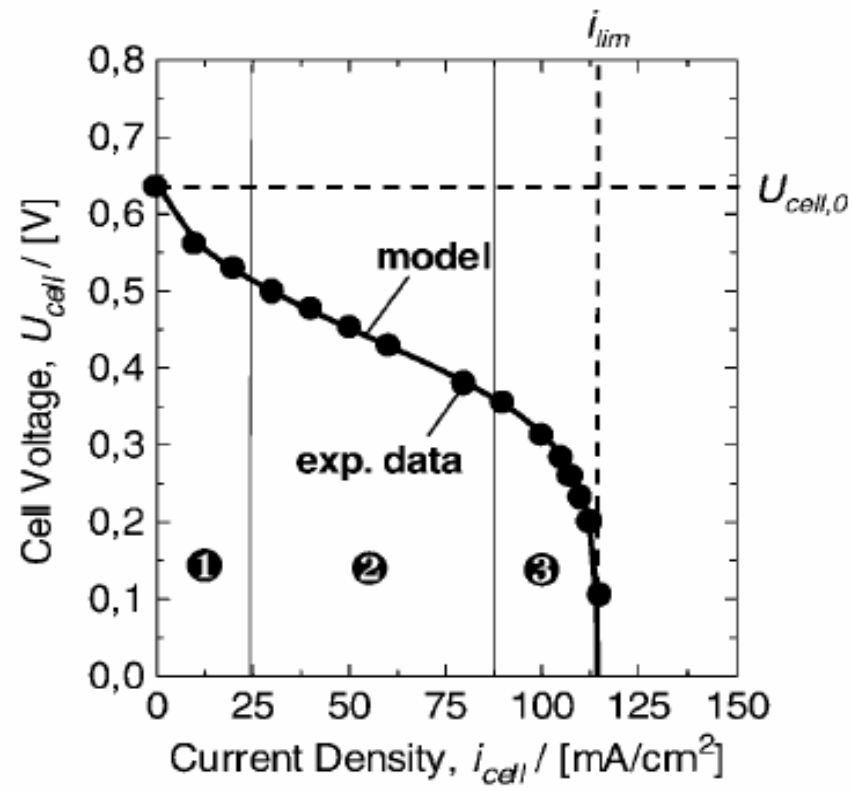

Figure 4. U-I characteristics of a DMFC at three operating regions [2].

Presently, the performance levels of DMFCs have achieved in the range of 180 mA/cm^2 to 250 mA/cm^2 when cell voltage is at 0.30 V. Further effort is needed in order to further improve the power density.

3 The aims of the thesis

The main aim of this thesis is to prepare novel proton exchange membranes to apply in the DMFC. Specific objectives related to this aim are:

1. To prepare hybrid and composite membranes with acceptable or good proton conductivity (10 – 100 mS/cm) and less methanol crossover than Nafion 117.
2. To characterize membranes in order to explain the proton and methanol transport abilities and mechanisms from membrane morphologies and to define the optimal conditions for preparing membranes.
3. To fabricate membrane electrode assemblies based on novel membranes and obtain the preliminary results of cell performance.

4 The outline of the thesis

Chapter 2 describes the two kinds of membrane preparation methods—phase inversion by immersion and coating. The characterization methods are also documented in detail.

Chapter 3 presents two kinds of composite membranes—the poly(ethylene glycol) (PEG) composite membranes and the polyamide (PA) composite membranes. Membrane preparation and characterization are discussed.

Chapter 4 presents the lignosulfonate (LS) hybrid membranes. The novel porous proton exchange membranes are developed with potential application in DMFCs. Some of these results are published in the Journal of Power Sources (see Appendix C) and a new publication is in preparation.

Chapter 5 describes work on the electrochemical and electrical characterization of LS membranes. It is a continuation of chapter 4 for a further LS membrane test in a real fuel cell.

Appendix A is an article published in the Journal of Power Sources in collaboration with Luizildo Pitol Filho of the URV. It presents the experimental results on PEG composite membranes from chapter 3 and makes a computational study of mass transport.

Appendix B is an article published in the Journal of Colloid and Interface Science in collaboration with Dr. Juana Benavente of Malaga University. It presents the preparation and ion conductivity of PEG and PA composite membranes based on the results from chapter 3.

Appendix C is an article published in the Journal of Power Sources. It presents some of the results from chapter 4.

Appendix D is a paper accepted by the Journal of Membrane Science. It presents some of the results from chapter 5 and was written in collaboration with Dr. Andreas Glüsen of Forschungszentrum Jülich, Germany.

References

[1] Karl Kordesch, Günter Simader, Fuel cells and their applications, Weinheim, Germany, ISBN: 3-527-28579-2, 1996, p. 2-8

[2] James Larminie, Andrew Dicks, Fuel cell systems explained, second edition, Wiley, England, ISBN: 0-470-84857-X, 2003, p. 142-156

[3] http://www.fuelcells.org/basics/how.html

[4] J.B. Goodenough, A. Hamnett, B.J. Kennedy, R. Manoharahn, S.A. Weeks, J. Electroanal. Chem. 240 (1988) 133

[5] A. Aramata, M. Masuda, J. Electrochem. Soc. 138 (7) (1991) 1949

[6] Anne-Laure Rollet, Gérard Gebel, Jean-Pierre Simonin, Pierre Turq, A SANS Determination of the Influence of External Conditions on the Nanostructure of Nafion Membrane, Journal of Polymer Science: Part B: Polymer Physics 39 (2001) 548-558

[7] M. Eikerling, A. A. Kornyshev, A. M. Kuznetsov, J. Ulstrup, S. Walbran Mechanisms of Proton Conductance in Polymer Electrolyte Membranes, J. Phys. Chem. B 105 (2001) 3646-3662

[8] M. Eikerling, Y. I. Kharkats, A. A. Kornyshev, Y. M. Volfkovich Phenomenological Theory of Electro-osmotic Effect and Water Management in Polymer Electrolyte Proton-Conducting Membranes J. electrochem. Soc. 145 (1998) 2684-2699

[9] Thorsten Schultz, Su Zhou & KaiSundmacher, Current Status of and Recent Developments in the Direct Methanol Fuel Cell, Chem. Eng.Technol. 24 (2001) 12, 1223

[10] A. Heinzel, V.M. Barragan, J. Power Sources 84 (1999) 70-74

[11] J. Cruickshank, K. Scott, J. Power Sources 70 (1998) 40-47

[12] Jinhwan Kim, Bokyung Kim, Bumsuk Jung, Proton conductivities and methanol permeabilities of membranes made from partially sulfonated polystyrene-block-poly(ethylene-ran-butylene)-block-polystyrene copolymers, Journal of Membrane Science 207 (2002) 129–137

[13] F.G. Wilhelm, I.G.M. Pünt, N.F.A. van der Vegt, H. Strathmann, M. Wessling Cation permeable membranes from blends of sulfonated poly(ether ether ketone) and poly(ether sulfone), Journal of Membrane Science 199 (2002) 167–176

[14] Carmen Manea, Marcel Mulder, Characterization of polymer blends of polyethersulfone/sulfonated polysulfone and polyethersulfone/sulfonated polyetheretherketone for direct methanol fuel cell applications, Journal of membrane Science 206 (2002) 443–453

[15] V. Baglio, A.S. Arico, A. Di Blasi, V. Antonucci, P.L. Antonucci, S. Licoccia, E. Traversa, F. Serraino Fiory, Nafion–TiO2 composite DMFC membranes: physico-chemical properties of the filler versus electrochemical performance, Electrochimica Acta 50 (2005) 1241–1246

[16] S.P. Nunes, B. Ruffmann, E. Rikowski, S. Vetter, K. Richau, Inorganic modification of proton conductive polymer membranes for direct methanol fuel cells, Journal of Membrane Science 203 (2002) 215–225

[17] Dae Sik Kim, Ho Bum Park, Ji Won Rhim, Young Moo Lee, Preparation and characterization of crosslinked PVA/SiO2 hybrid membranes containing sulfonic acid groups for direct

methanol fuel cell applications, Journal of Membrane Science 240 (2004) 37–48

[18] P. Dimitrova, K. A. Friedrich, U. Stimming, B. Vogt Modified Nafion-based membranes for use in direct methanol fuel cells, Solid State Ionics 150 (2002) 115-122

[19] N. Miyake, J. S. Wainright, R. F. Savinell Evaluation of a Sol-Gel Derived Nafion/Silica Hybrid Membrane for Proton Electrolyte Membrane Fuel Cell Applications, J. Electrochem. Soc. 148 (2001) A898-A909

[20] A. Glüsen, D. Stolten Membranen für Polymerelektrolyt Brennstoffzellen, Chemie Ingenieur Technik 75 (2003) 1591-1597

[21] Young-Sun ParkT, Yohtaro Yamazaki, Low methanol permeable and high proton-conducting Nafion/calcium phosphate composite membrane for DMFC, Solid State Ionics 2005 in press

[22] F. Bauer, M. Willert-Porada, Microstructural characterization of Zr-phosphate–Nafion® membranes for direct methanol fuel cell (DMFC) applications, Journal of Membrane Science 233 (2004) 141–149

[23] L. Tchicaya-Bouckary, D. J. Jones, J. Rozière Hybrid Polyaryletherketone Membranes for Fuel Cell Applications, Fuel Cells 2 (2002) 40-45

[24] G. Alberti, U. Costantino, M. Casciola, S. Ferroni, L. Massinelli, P. Staiti Preparation, characterization and proton conductivity of titanium phosphate sulfophenylphosphonate, Solid State Ionics 145 (2001)249-255

[25] M.K. Daletou, N. Gourdoupi, J.K. Kallitsis, Proton conducting membranes based on blends of PBI with aromatic polyethers containing pyridine units, Journal of Membrane Science 252 (2005) 115–122

[26] S.M. Javaid Zaidi, Preparation and characterization of composite membranes using blends of SPEEK/PBI with boron phosphate, Electrochimica Acta xxx (2005) xxx–xxx

[27] Qingfeng Li, Ronghuan He, Rolf W. Berg, Hans A. Hjuler, Niels J. Bjerrum, Water uptake and acid doping of polybenzimidazoles as electrolyte membranes for fuel cells, Solid State Ionics 168 (2004) 177–185

[28] Jochen Kerres , Andreas Ullrich, Frank Meier, Thomas Haring, Synthesis and characterization of novel acid–base polymer blends for application in membrane fuel cells, Solid State Ionics 125 (1999) 243–249

[29] M. Götz, H. Wendt, Electrochimica Acta 43 (24) (1998) 3637-3644

[30] H. Bönnemann, P. Britz, W. Vogel, Langmuir, 14 (1998), 6654-6657

[31] Fuel Cell Handbook, National Energy Technology Laboratory, fifth edition, October 2000, 1-8

Chapter 2

Methodology of membrane preparation and characterization

1 Introduction

There are many techniques for preparing polymeric membranes, including stretching, track-etching, phase inversion and coating [1]. In this thesis, we have prepared several types of composite membranes and hybrid membranes using coating and phase inversion.

Coating is used to prepare composite membranes. The thin dense layer is coated or deposited onto a porous support [2-4]. This layer is usually called the selective layer or skin layer.

Phase inversion starts from a homogeneous polymer solution or a mixture, then phase separation or liquid-liquid demixing takes place according to the thermodynamic principle. Finally, the polymer-rich phase solidifies and forms the membrane. Hybrid membranes are membranes prepared by mixing different polymers. This method combines the hydrophobic polymer and the hydrophilic polymer and, by changing the proportion of polymer, membranes with desired properties are finally formed [5-12].

The main techniques of membrane preparation used in the thesis are the solvent-nonsolvent phase inversion method and the coating method. In this chapter we only discuss solvent-nonsolvent phase inversion. The coating method is discussed in Chapter 3.

Characterization, to evaluate and improve the membranes obtained, is an important part of this thesis. We have used several methods to characterize the membrane surface and cross-section morphologies and evaluate the physical and chemical properties of the membranes.

2 Membrane preparation via solvent-nonsolvent phase inversion

A casting solution is prepared by dissolving the polymer in a solvent, then using a coating machine (Figure 1) to spread the casting solution onto a glass surface with a controlled thickness. The glass with a wet film on top is then immersed in a nonsolvent bath. The solvent diffuses into the precipitation bath, where the nonsolvent diffuses into the cast film. After a time in which the solvent and the nonsolvent are exchanged, the polymer solution (wet film) becomes thermodynamically unstable and demixing takes place. Finally, a solid polymer membrane forms with an asymmetric structure and peels off from the glass. This membrane has two surfaces, termed the film/glass surface and the film/bath surface. In general, pores close to the film/bath surface are larger than those close to the film/glass surface for an asymmetric membrane.

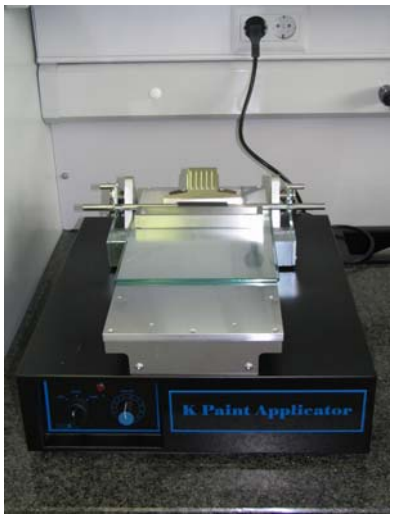

Figure 1. The coating machine.

Several factors can affect the membrane structure, including the concentration of the polymer solution, the compositions of the solvent and the nonsolvent, and the temperatures of the casting solution and precipitation bath. Under different conditions, the structures of the membranes can change from a very open porous structure to a closed porous structure with a dense nonporous top layer. This is mainly because of the demixing process, which includes instantaneous demixing and delayed demixing. When the solvent and nonsolvent have a high affinity, the demixing process is instantaneous. When they have a low affinity, the demixing process is delayed. Instantaneous demixing generates membranes with more pores, while delayed demixing generates denser membranes [1, 13]. For example, a solution of polysulfone (PSU) in dimethylformamide (DMF) when cast and immersed in a water bath shows instantaneous

demixing and produces a porous layer close to the film/bath surface. When it is cast and immersed in an iso-propanol solution, the membrane shows delayed demixing and a dense nonporous layer close to the film/bath surface is produced.

In an asymmetric membrane, macrovoids are often observed. Macrovoids are very large elongated pores that can extend over the entire thickness of the membrane. Macrovoids are usually associated with instantaneous precipitation. Most techniques that can be used to delay demixing usually lead to the suppression of macrovoids. Increasing the viscosity of the polymer solution decreases the tendency for macrovoid formation [1, 13].

3 Membrane characterization

3.1 Attenuated Total Reflectance Infrared (ATR-IR) Spectrometry

ATR-IR spectrometry can provide valuable information about the chemical structure of membranes. Infrared spectra are obtained by pressing small pieces of membrane against an internal reflection element (IRE). ATR-IR is illustrated in Figure 2. IR radiation is focused on the end of the IRE. Light enters the IRE and reflects down the length of the crystal. At each internal reflection, the IR radiation actually penetrates a short distance (about 1 μm) from the surface of the IRE into the polymer membrane.

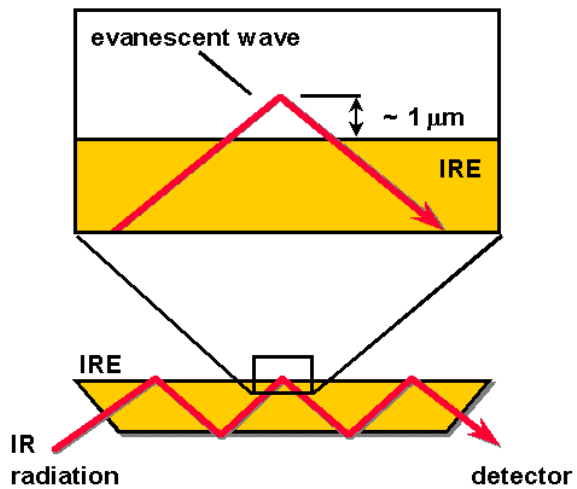

Figure 2. The working principle of ATR-IR [14].

This technique is useful for characterizing the composite membranes because it is impossible to make a homogeneous tablet with membranes and the composite membranes are not transparent enough to allow the light to pass through using the normal IR technique. Using the ATR-IR technique (Bruker-Tensor 27), we placed the different faces of a membrane in contact with IRE and then obtained information about its compositions.

3.2 UV-visible Spectrometry

A UV-visible spectrometer (HP8542A) was used to determine the stability of composite and hybrid membranes. After the membranes are soaked in water for a certain time, the water is detected by a UV-visible spectrometer to examine whether LS (Figure 3) has been washed out from the membranes.

At the same time, LS powder was dissolved in deionized water at a concentration of 0.005 M and the solution determined by UV-visible spectrometer, the spectra showed that the band at 280 nm corresponded to the aromatic ring absorption of LS [15].

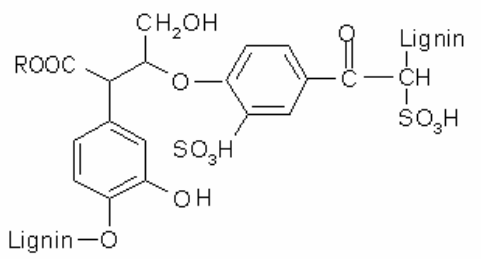

Figure 3. LS molecular structure.

For all membranes tested, no LS was leached from the membrane. This proved that LS was bonded chemically with the host polymers—PSU.

3.3 Scanning Electron Microscopy (SEM) and Energy Dispersive Spectrometry (EDS)

SEM (JEOL JSM-6400) uses an electromagnetic lens that focuses the beam of electrons onto the test sample (Figure 4). A probe of electrons is finely focused over the imaged area and an induced signal is simultaneously monitored. Turning the magnification knob located on the keyboard varies the current through the objective lens, which then changes the magnification of the sample. Our test conditions were: an acceleration voltage of 15-20KV and distance from lens to sample of 8–15 cm.

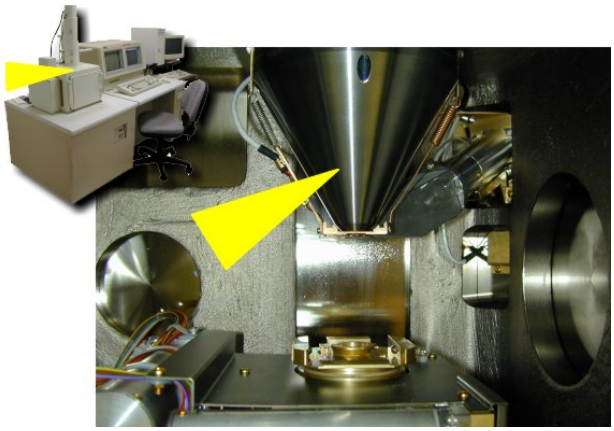

Figure 4. SEM [16].

SEM requires special sample preparation. To scan the membrane surfaces, the carbon tab was first stuck on top of the steel stub and the membrane was then cut into a small piece (about 1cm×1cm) and stuck on top of the carbon tab. To scan the membrane cross section, the membrane was first dipped into a pure ethanol solution and then rapidly broken in liquid nitrogen. This allowed the frozen membrane to break without changing its structure. The cut membrane was then fixed straight up on top of the steel stub by an adhesive.

Gold or carbon was then spurted on top of the membrane's scanning area. A sputter machine was used to spurt gold or carbon under vacuum. The gold or carbon atoms were deposited onto the sample to form an ultra-thin conductive layer that would not change the morphology of the membrane.

The microscope was equipped with an energy dispersive X-ray detector i.e. EDS, which was used to obtain information about the elemental compositions of the membrane surface.

Figure 5 shows a cross-section SEM image of an asymmetric membrane. The membrane presents a gradually enlarged porous structure. The membrane has two regions, called the top layer and the sublayer. The top layer is located near the film/bath surface and the sublayer is located near the film/glass surface. The top layer is also called the skin layer or the selective layer. There are two types of top layer: an integrated top layer and a composite top layer.

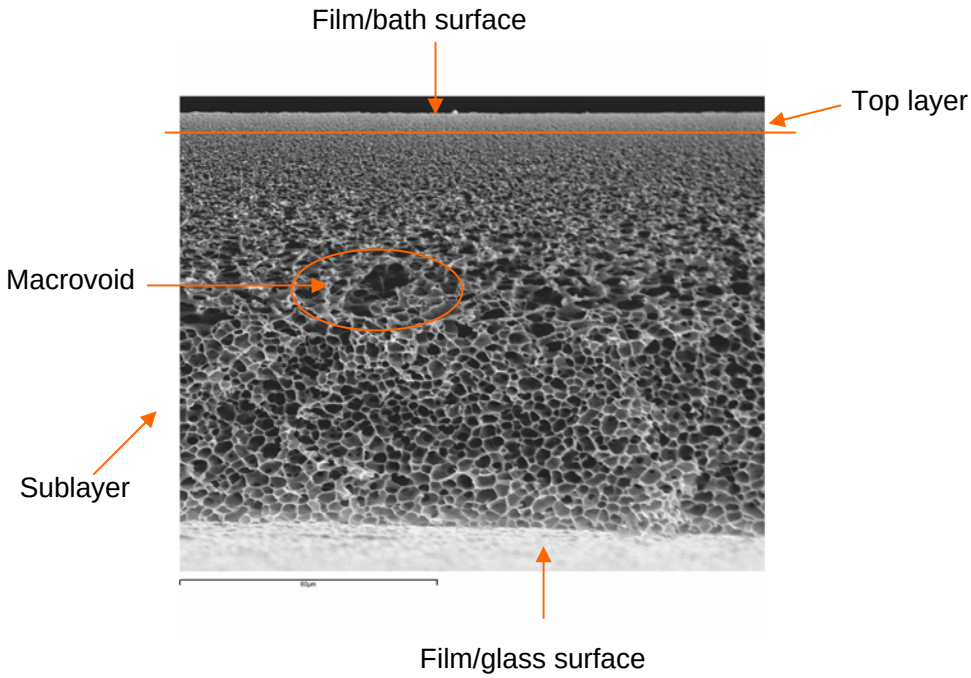

Figure 5. Membrane cross-section structure by SEM.

3.4 Atomic Force Microscopy (AFM)

AFM is a new characterization technique applied in the microscopic characterization of non-conducting material surfaces [17-19]. The aim of AFM is to detect interactions between the tip and the substrate. With this

technique, the tip is placed on a cantilever whose deflection can be detected by the reflection of a suitably focused laser beam (see figure 6). In the tapping mode AFM, the cantilever is oscillated at a certain resonant frequency with a high amplitude to allow the tip to touch the sample during the oscillation. This method maintains high resolutions and eliminates lateral friction forces.

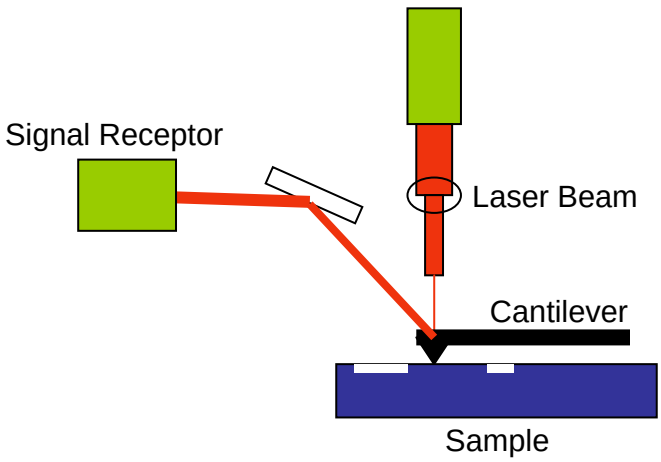

Figure 6. The working principle of AFM [20].

In our case, we used tapping mode (TM AFM) (Pico Scan, Molecular Imaging) to characterize membrane surfaces. The membrane sample was attached to a stainless steel stub. The n-type silicon TM AFM tip was mounted on a cantilever with a constant force of 42 N/m. The resonance frequency was adjusted to between 270 and 290 kHz.

The topology and phase images were obtained using SPIP software in the flattening treatment. Depending on the topology, the software synthesized the three-dimensional image as shown in Figure 7.

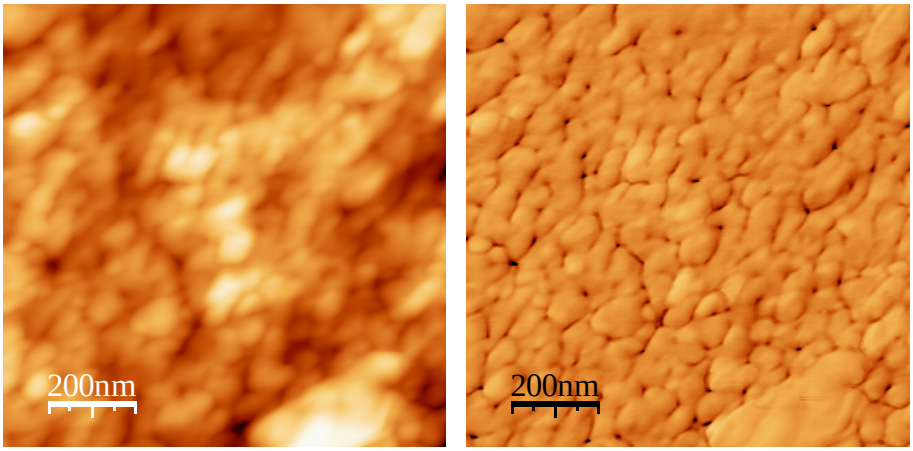

a b

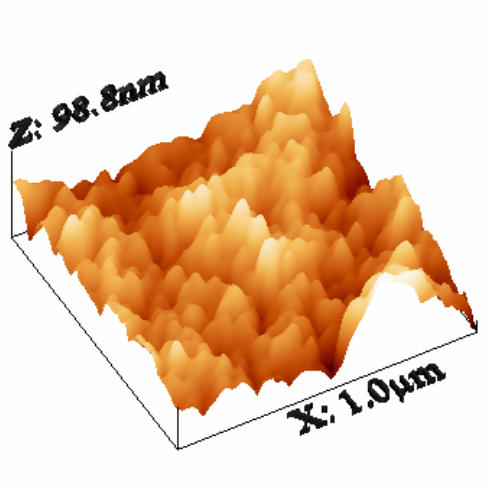

c

Figure 7. Membrane surface morphology through AFM (a: topology; b: phase image; c: 3-D image).

The membrane surfaces were compared using roughness R_q (nm) -- mean square (rms) of the surface height (Z, nm) [17-19]. R_q is the standard deviation of the Z values within the given area, and is calculated as

$$R_q = \left(\sum_i \left(Z_i - Z_{avg} \right)^2 / N \right)^{1/2} \quad (1)$$

where, Z_{avg} is the average of the Z values, Z_i, is the current Z value, and N is the number of events or the number of examined points.

Using the above equation, SPIP analyzed the Z data of image 7.a at each surface point and the Z distribution was plotted as Figure 8. The R_q was then calculated to be 26.08 nm.

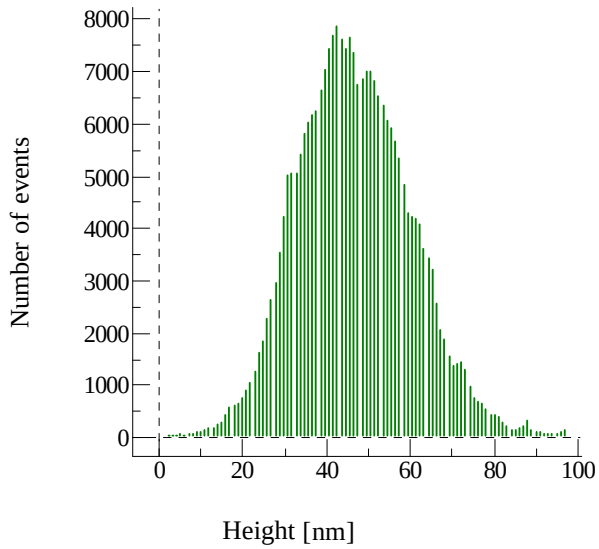

Figure 8. Normal distribution of Z data of a given membrane area by SPIP software.

However, if the topology has several defects (Figure 9), the Z data analysis does not show a normal distribution (Figure 10). In this case, we did not take into count the roughness calculated from it. For each membrane, we analyzed 3 or 4 surface areas and the roughness was shown as an average value. The error was within 28%. We should point out that roughness depends on the curvature and size of the TM AFM tip and on the treatment of the captured surface data (raw, flattening,

filtering), and should not be considered as absolute roughness values [17, 18].

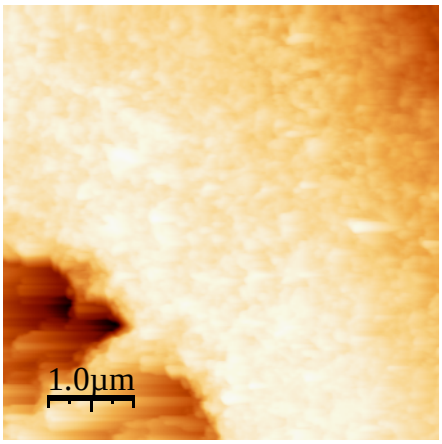

Figure 9. Membrane topology with defects.

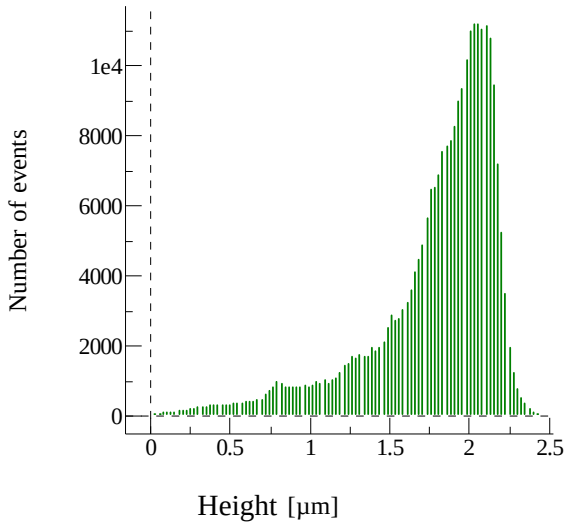

Figure 10. Z data analysis for a defective membrane surface.

3.5 Contact angle measurement (CA)

The sessile drop [21] was used to measure the contact angle of membrane. It describes the shape of a liquid droplet resting on a solid surface. When drawing a tangent from the droplet to the solid surface, the contact angle is the angle formed between the tangent and the solid surface (Figure 11). The larger the angle, the more hydrophobic the membrane surface.

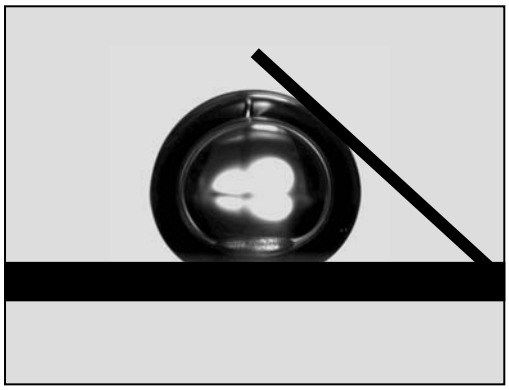

Figure 11. Contact angle measurement.

Membrane samples were cut to 5cm×5cm, then washed with deionized water and dried at 30°C in a vacuum oven. The sample was attached to a smooth glass surface and placed on a black support. After a droplet of liquid (10 μL) was placed automatically onto the sample surface, a video camera revealed the profile of the droplet on the computer screen. Reported values were the average contact angle (right and left) of a series of images of the droplet. Contact angles do not provide absolute values but allow a comparison of each material. For each membrane, we measured up to five regions to obtain the average contact angle and the error was within 12%.

3.6 Proton and methanol transport experiments

Transport experiments were carried out using a test cell (Figure 12), which included two compartments separated by the tested membrane. The solutions in the two compartments were called feed and stripping. The volumes of the feed and stripping were 200 ml and the effective membrane area was 8.51 cm^2.

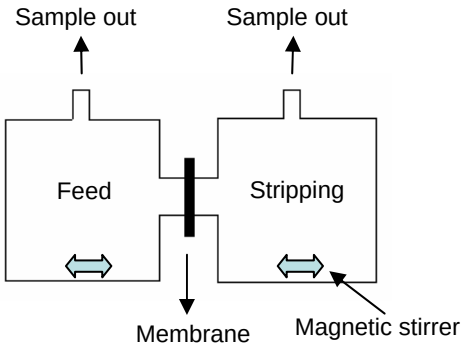

Figure 12. Transport cell.

For methanol crossover experiments, the feed was the aqueous methanol solution (1.0 M) and the stripping was deionized water. Both compartments were continuously stirred by magnetic stir bars during permeability measurements. The methanol concentration in the stripping (C_s, mol l^{-1}) was determined over time by HPLC (Agilent 1100) using a XDB-C8 column.

In the case of the proton transport, the initial feed was 1.0 M HCl aqueous solution and the stripping was 1.0 M NaCl aqueous solution. The pH of the stripping was measured every 1-2 seconds by the Crison Compact Titrator.

Eq. (1) describes the permeability coefficient of proton or methanol (p, $cm^3\,cm^{-2}s^{-1}$) [1]:

$$-\ln\frac{C_f}{C_0} = \frac{Ap}{V_f}t \qquad (2)$$

where C_0 (mol l^{-1}) is the initial concentration of the feed solution, C_f (mol l^{-1}) is the feed concentration calculated from the concentration of the stripping solution at time t (s):

$$C_f = C_0 - C_s \qquad (3)$$

V_f is the feed volume (ml) and A is the actual membrane area (cm^2). From Eq. (2) we observed the linear relationship between $-\ln(C_f/C_0)$ and time. The slope of the corresponding plot determines the value of p.

Under steady state condition, proton and methanol fluxes (mol $cm^{-2}s^{-1}$) were calculated by Fick's First Law:

$$J = \frac{P\Delta C}{l} \qquad (4)$$

Where, l (cm) is the membrane thickness, ΔC is the difference in concentration between the initial feed and the final stripping. In our experimental conditions, C_0 was much greater than the final stripping concentration, so we considered $\Delta C \approx C_0$.

P is the permeability ($cm^2\ s^{-1}$), which is defined as:

$$P = pl \qquad (5)$$

The flux is then related to the permeability coefficient as:

$$J = pC_0 \qquad (6)$$

Selectivity α of proton over methanol is a comprehensive evaluation of a membrane and is calculated by Eq. (7):

$$\alpha = \frac{J_{H^+}}{J_{Methanol}} \qquad (7)$$

Here we calculate the proton and methanol permeabilities of Nafion 117 in accordance with the above equations. In the following chapters, we used the proton and methanol permeabilities of Nafion 117 as the comparing standard.

To calculate the proton permeability of Nafion 117, we first drew the plot of $-\ln(C_f/C_0)$ versus time (Figure 13). From the slope we observed two different regions. The first region probably corresponded to the proton absorption and diffusion. Once the membrane was saturated by H^+, the

mechanism became hopping dominated, which corresponded to the second region of Figure 13. We used this second region to calculate the proton permeability of Nafion 117.

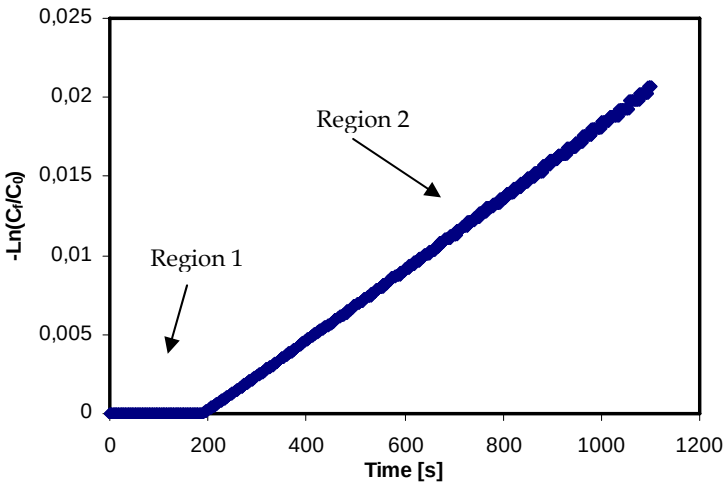

Figure 13. The plot of $-\ln\left(C_f / C_0\right)$ versus time for calculating the proton permeability coefficient of Nafion 117.

$$p = \frac{Slope \times V_f}{A} = 5.17 \times 10^{-4} \text{ cm}^3\,\text{cm}^{-2}\text{s}^{-1}$$

$$J = pC_0 = 5.17 \times 10^{-7} \text{ mol cm}^{-2}\text{s}^{-1}$$

$$P = pl = 9.56 \times 10^{-6} \text{ cm}^2\,\text{s}^{-1}$$

To calculate the methanol permeability through Nafion 117, we used HPLC to determine the methanol concentration in the stripping, which initially was zero. First we plotted the calibration curve of methanol concentration determined by HPLC (see Figure 14).

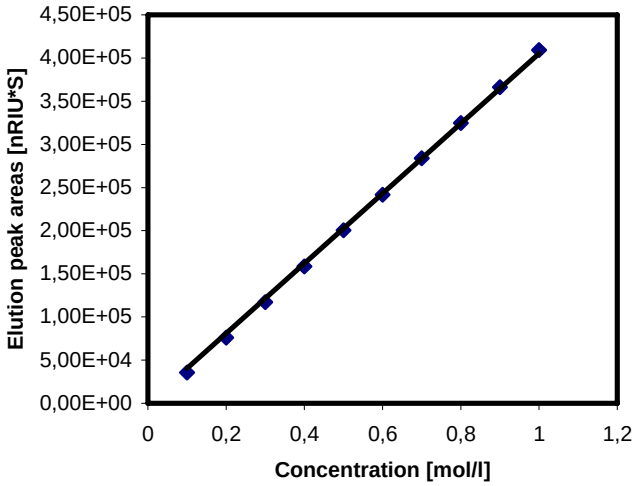

Figure 14. Calibration curve of methanol concentration.

We then drew the plot (Figure 15) according to equation (2) to calculate permeability.

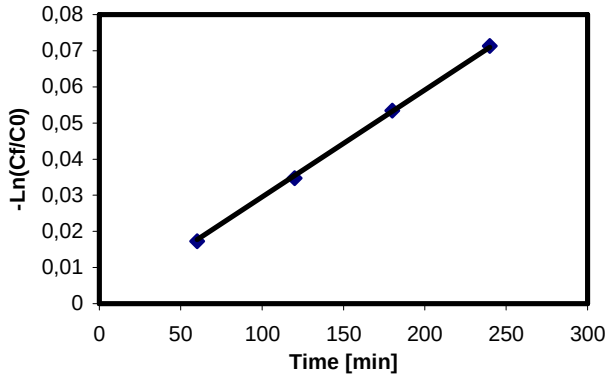

Figure 15. The plot of $-\ln\left(C_f / C_0\right)$ versus time for calculating the methanol permeability coefficient of Nafion 117.

$$p = \frac{Slope \times V_f}{A} = 1.18 \times 10^{-4} \text{ cm}^3\,\text{cm}^{-2}\text{s}^{-1}$$

$$J = pC_0 = 1.18 \times 10^{-7} \text{ mol cm}^{-2}\text{s}^{-1}$$

$$P = pl = 2.54 \times 10^{-6} \text{ cm}^2\,\text{s}^{-1}$$

The value was in perfect agreement with the result available (2.6×10^{-6} cm^2 s^{-1}) in the literature [22].

Therefore, the selectivity of proton to methanol for Nafion 117 was calculated by equation (6) to be: $\alpha = 4.55$

3.7 Impedance Spectrometry (IS)

Using IS, we tested the ion conductivity and proton conductivity of membranes. Here we discuss only the measurement of ion conductivity. Proton conductivity measurements are discussed in Chapter 5.

We measured the ion conductivities of hydrated membranes using impedance spectrometry (Solartron 1260) [23]. The cell has two compartments, each with a volume of 10 cm^3. The electrode used was Ag/AgCl. The membrane was tightly clamped between two half cells by silicone rubber rings. To minimize concentration-polarization at the membrane surfaces, a magnetic stirrer was placed at the bottom of each half cell. This enabled its speed rate to be controlled externally. IS data, as well as the influence of connecting cables and other parasitic capacitances, were corrected by software. We used several frequencies in the 10–10^6 Hz range and a maximum voltage of 0.01 V. Measurements were carried out at a stirring rate of 525 rpm at six different NaCl solutions (10^{-3} M to 5 × 10^{-2} M), at room temperature T = (25.0 ± 0.3) ^{o}C and standard pH (5.8 ± 0.3). The solutions on both sides of the membrane had the same concentration. Before the measurement, the membranes were soaked for at least 10 h in the NaCl solution at the test concentration.

Reference

[1] Marcel Mulder, Basic principles of membrane technology, 2nd ed. Kluwer Academic Publishers, The Netherlands, 2003

[2] R.J. Petersen, Composite reverse osmosis and nanofiltration membranes, J. membr. Sci. 83 (1993) 81-150

[3] J.E. Cadotte, R.J. Petersen, R.E. Larson, E.E. Erickson, A new thin film composite sea water reverse osmosis membrane, Desalination 32 (1980) 25-31

[4] R.L. Riley, R.L. Fox, C.R. Lyons, C.E. Milstead, M.W. Seroy, M. Tagami, Spiral-wound poly(ether/amide) thin film composite membrane systems, Desalination 19 (1976) 113-126

[5] A. Glüsen, D. Stolten Membranen für Polymerelektrolyt Brennstoffzellen, Chemie Ingenieur Technik 75 (2003) 1591-1597

[6] C.W. Lin, R. Thangamuthu, C.J. Yang, Proton-conducting membranes with high selectivity from phosphotungstic acid-doped poly(vinyl alcohol) for DMFC applications, Journal of Membrane Science 2005 in press

[7] Jinhwan Kim, Bokyung Kim, Bumsuk Jung, Proton conductivities and methanol permeabilities of membranes made from partially sulfonated polystyrene-block-poly(ethylene-ran-butylene)-block-polystyrene copolymers, Journal of Membrane Science 207 (2002) 129–137

[8] F.G. Wilhelm, I.G.M. Pünt, N.F.A. van der Vegt, H. Strathmann, M. Wessling Cation permeable membranes from blends of sulfonated poly(ether ether ketone) and poly(ether sulfone), Journal of Membrane Science 199 (2002) 167–176

[9] Carmen Manea, Marcel Mulder, Characterization of polymer blends of polyethersulfone/sulfonated polysulfone and polyethersulfone/sulfonated polyetheretherketone for direct methanol fuel cell applications, Journal of membrane Science 206 (2002) 443–453

[10] J. Kerres, A. Ullrich, F. Meier, T. Häring, Synthesis and characterization of novel acid-base polymer blends for application in membrane fuel cells, Solid State Ionics 125 (1999) 243-249

[11] J.M. Bae, I. Honma, M. Murata, T. Yamamoto, M. Rikukawa, N. Ogata, Properties of selected sulfonated polymers as proton-conducting electrolytes for polymer electrolyte fuel cells, Solid State Ionics 147 (2002) 189-194

[12] D. J. Jones, J. Rozière, Recent advances in the functionalisation of polybenzimidazole and polyetherketone for fuel cell applications, Journal of Membrane Science 185 (2001) 41-58

[13] P. van de Witte, P.J. Dijkstra, J.W.A. van den Berg, J. Feijen, Phase separation processes in polymer solutions in relation to membrane formation, Journal of Membrane Science 117 (1996) 1-31

[14] http://www.micromemanalytical.com/ATR_Ken/ATR.htm

[15] Kjell Magne Askvik, Svein Hetlesæther, Johan Sjöblom, Per Stenius, Properties of the lignosulfonate–surfactant complex phase, Colloids and Surfaces A: Physicochemical and Engineering Aspects 182 (2001) 175–189

[16] http://mse.state.edu/microscopy.html

[17] K.C. Khulbe, B. Kruczek, G. Chowdhury, S. Gagne, and T. Matsuura, Surface morphology of homogeneous and asymmetric membranes made from Poly(phenylene oxide) by tapping mode atomic force microscope, Journal of Applied Polymer Science 59 (1996) 1151-1158

[18] A. Lehmani, S. Durand-Vidal, P. Turq, Surface morphology of Nafion 117 membrane by tapping mode atomic force microscope, Journal of Applied Polymer Science 68 (1998) 503-508

[19] A. Hernández, J.I. Calvo, P. Prádanos and L. Palacio, A Multidisciplinary Approach Towards Pore Size Distributions of Microporous and Mesoporous Membranes, Surface Chemistry and Electrochemistry of Membranes, Surfactant Science serie 79: 39-90, 1999, Marcel Dekker Inc. Nueva York, EE.UU.

[20] http://www.aquila.infn.it/infm/labinfm/infm_oth/attr/afm/introeng.html

[21] T. Gumí, M. Valiente, K.C. Khulbe, C. Palet, T. Matsuura, Characterization of activated composite membranes by solute transport, contact angle measurement, AFM and ESR, Journal of Membrane Science 212 (2003) 123-134

[22] B.S. Pivovar, Y. Wang, E.L. Cussler, J. Mem. Sci. 154 (1999) 155–162.

[23] J. Benavente, X. Zhang, R. Garcia Valls, Modification of polysulfone membranes with poly(ethylene glycol) and lignosulfate: electrical characterization by impedance spectroscopy measurements, Journal of Colloid and Interface Science 285 (2005) 273–280

Chapter 3

Composite Proton Exchange Membranes

1 Introduction

Thin film composite (TFC) membrane is characterized by an ultra-thin separating "barrier" layer, also called the skin layer, supported on a chemically different asymmetric porous substrate. The advantage of composite membranes over single-material asymmetric membranes is that, as the film is formed in situ, the chemistry and performance of the top barrier layer and the bottom porous substrate can be independently studied and modified to optimize the overall membrane performance. Many TFC membranes have been successfully developed from several polymers [1-3] and have been successfully applied in the chemical separation fields [4, 5].

In this chapter, we discuss two kinds of TFC membranes as options for direct methanol fuel cells (DMFCs). These were achieved by coating a thin polymer film, also called the "skin layer", onto an asymmetric polymeric membrane surface to produce a barrier for methanol and assist proton transport.

Porous polysulfone (PSU) membrane was chosen as the support layer because PSU is a chemically stable polymer and PSU membrane has been very well characterized. By adjusting the morphology of the PSU membrane, e.g. porosity, pore size and hydrophilicity, we can optimize the support layer. In this work, we examined the thermal sulfonation treatment of the PSU layer to improve its hydrophilicity.

For the skin layer, we chose poly(ethylene glycol) (PEG) because of its cross-linking property due to the hydroxyl groups at the end of the chain (Figure 1). This kind of polymer is widely used in many fields [6-10]. Because of its flexible and hydrophilic chain, it may swell and form a "hydrogel" [11, 12] with -O- segments with an affinity for proton. At the same time, after the cross-linking, PEG is expected to form a dense skin layer, which will help to reduce the methanol crossover. Moreover, PEG is reasonably inexpensive and is compatible with many organic materials.

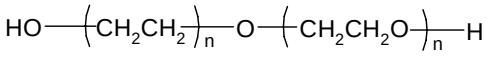

Figure 1. PEG molecular structure.

Polyamide (PA) is also widely used as a skin layer in the separation field. The PA skin layer can be formed by interfacial polymerization with monomers containing amino groups and acid chloride groups [13, 14]. In the chemical separation field, to select ions to transport through the polyamide layer, some organic compounds—the so called "carriers"—are trapped inside the skin layer [15, 16]. In our case, the proton is the ion that needs to be transported. Therefore, compounds with functional groups that have a strong affiliation with protons can be used as carriers. Di-(2-ethyl-hexyl) phosphoric acid (DEHPA) and lignosulfonate (LS) (Figure 2 and Figure 3) are incorporated into the polyamide network to serve as "proton carriers".

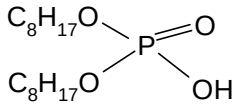

Figure 2. DEHPA molecular structure.

The molecular structure of DEHPA illustrates its proton transport potential. The fact that DEHPA is relative small may facilitate its mobility within the polyamide network and enable it to carry and release the proton.

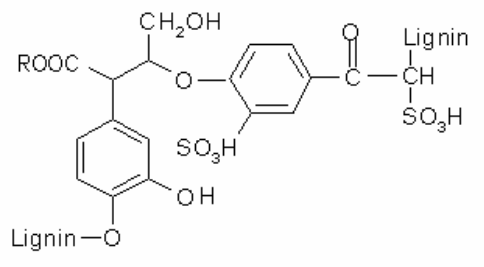

Figure 3. LS molecular structure.

Lignosulfonate, a highly anionic polymer and a byproduct of the sulfite method for manufacturing paper from wood pulp, is sometimes called sulfonated lignin. It is a complex mixture of small-to-moderate polymeric compounds made of the repetition of phenyl-propane units with $-SO_3H$, -COOH and -OH groups attached to the molecule [17]. Like other acidic compounds, LS could behave as good proton exchangers.

Currently, a huge amount of LS is produced all over the world. This polymer has applications as an additive [18] and as a surfactant [19, 20]. It has also been reported as a component in polymer blends, where it has proved to be bioactive and biocompatible [21]. It has also been applied in blends with thermoplastics [22]. Although LS research is receiving greater attention, most LS is incinerated as waste and is still a significant environmental burden. New research into LS applications could therefore be very significant from both the economical and the environmental points of view.

2 Experimental

2.1 Preparation of asymmetric PSU support layers

PSU casting solutions were prepared by dissolving different quantities of PSU (Mw. 35,000) purchased from Aldrich in N,N-dimethylformamide (DMF) with vigorous agitation for 12 h at room temperature. The solutions were cast onto a glass plate using a 200 μm-thick casting knife and then precipitated in different nonsolvent baths. PSU membranes were then taken from the bath and rinsed with distilled water. Several PSU membranes were formed. These are listed in Table 1.

Table 1. PSU porous membranes

Membranes	PSU concentration in the casting solution [wt.%]	Precipitation solution bath
PSU10	10	Water
PSU11	11	Water
PSU12	12	Water
PSU13	13	Water
PSU14	14	Water
PSU15	15	Water
PSU20	20	Water
PSU15D	15	15%DMF/85%H_2O

2.2 Thermal sulfonation process

The PSU membranes obtained were kept in 0.25 M H_2SO_4 aqueous solution at 80 °C for 3, 24 and 72 h, respectively. Excess acid on the surface was removed by a short water rinse. The membranes were then put into an oven at 80 °C for 1 h, soaked in distilled water and rinsed daily until the rinsed water reached neutral pH.

2.3 Synthesis of PEG skin layers

Wax-like PEG (M_W. 1000, from Aldrich) was dissolved in methanol in several concentrations. The solution (100 µl) was deposited consistently onto the top surface of a wet PSU15 membrane (8.51 cm^2). The PEG-covered PSU15 membranes were put into an oven to crosslink at 80 °C for 1 h, and then stored in water before use. Theoretical PEG loadings were calculated. The composite PEG membranes obtained are listed in Table 2.

Table 2. PEG composite membranes with different PEG loadings

PEG composite membranes	PEG 5	PEG 10	PEG 20	PEG 30	PEG 40	PEG 50	PEG 60	PEG 70
PEG loading [mg/cm^2]	0.46	0.93	1.86	2.79	3.72	4.65	5.58	6.51

2.4 Synthesis of Polyamide skin layers containing DEHPA and LS as proton carriers

The support PSU15D membranes were soaked into aqueous solutions of 3.00 wt.% 1,3-phenylenediamine for 10 min. Different amounts of DEHPA were added into hexane solutions containing 0.15 wt.% 1,3,5-triclorotricarbonyl benzene (acid chloride). DEHPA-acid chloride solution was then dropped onto the membrane surface, where interfacial polymerization took place. Finally, the excess solution was washed off by water rinse and put into an oven at 60 °C for 30 min to cure. The composite membrane obtained was soaked in water for use. The composite polyamide-DEHPA membranes (PAD) are listed in Table 3.

Table 3. PAD composite membranes obtained

PAD composite membranes	PAD1	PAD2	PAD3	PAD4	PAD5	PAD6
DEHPA concentration in hexane solution [mM]	250	400	550	700	850	1000

Skin layers of polyamide containing LS at different concentrations were obtained by interfacial polymerization. PSU15D membrane was immersed in 3.00 wt.% 1,3-phenylenediamine solution, which contained water-soluble LS (Mw. 7000, acid groups 8.4 wt%). The solution of 0.15 wt% acid chloride in hexane was then continuously dropped onto the membrane surface, where the interfacial polymerization took place immediately. The formed polyamide composite membrane was cured at 60 °C for 30 min

and then rinsed with water. All polyamide-LS membranes (PALS) were stored in distilled water before use.

The composite PALS membranes are listed in Table 4.

Table 4. PALS composite membranes obtained

PALS composite membranes	PALS 5	PALS 10	PALS 20	PALS 30	PALS 40	PALS 50
LS content in 1,3-phenylenediamine solution [wt.%]	5	10	20	30	40	50

2.5 Characterization of composite membranes

Attenuated Total Reflectance Infrared Spectrometry (ATR-IR) was used to detect the formation of the skin layer on top of the PSU support with the proton carrier. The morphology of the PSU support membrane and the skin layer was obtained by Scanning Electron Microscopy (SEM). Transport experiments determined proton and methanol permeability. Impedance Spectrometry (IS) determined the ion conductivity of composite membranes. All the characterization methods have been described in detail in Chapter 2.

3 Results and Discussion

3.1 Optimization of PSU support membranes

3.1.1 PSU support membrane morphologies

All the PSU support membranes we obtained were examined by SEM. From Figure 4 to Figure 11 we can see that casting solutions with high PSU concentrations generated thicker membranes and their membrane morphologies changed from open channels (Figure 4 to Figure 8) to nano or micro closed pores with some macrovoids (Figure 9 and Figure 10). The cross section images showed that the top layer became denser as the PSU concentration increased. All these changes in morphology were associated with solvent-nonsolvent demixing process [23].

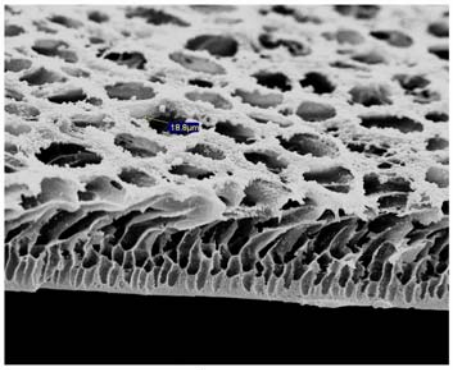

Figure 4. PSU10 cross-section.

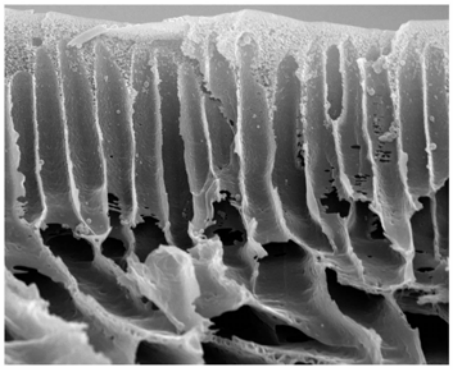

Figure 5. PSU11 cross-section.

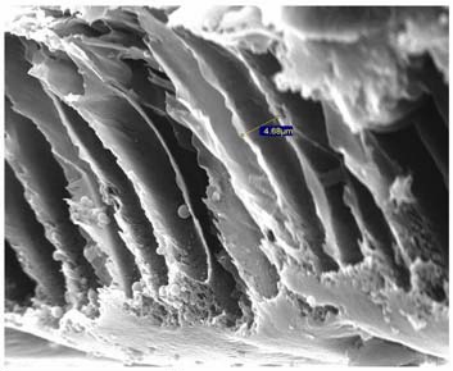

Figure 6. PSU12 cross-section.

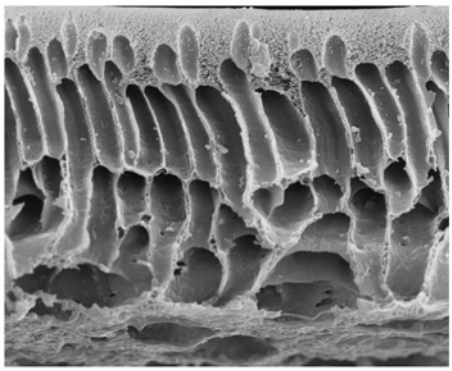

Figure 7. PSU13 cross-section.

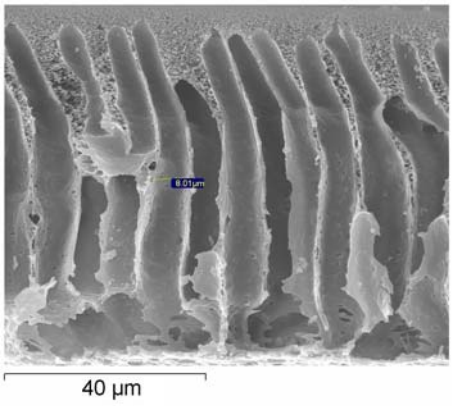

Figure 8. PSU14 cross-section.

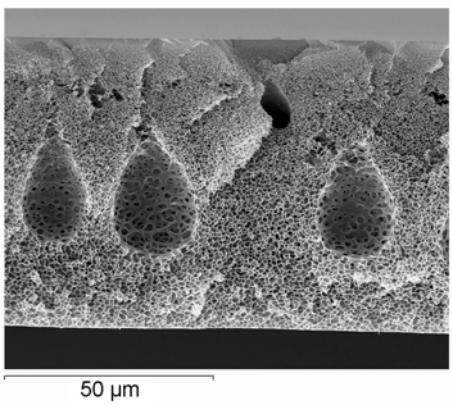

Figure 9. PSU20 cross-section.

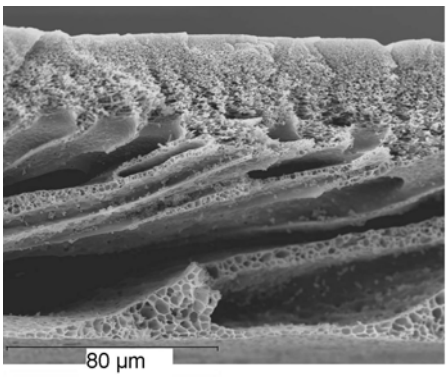

Figure 10. PSU15 cross-section.

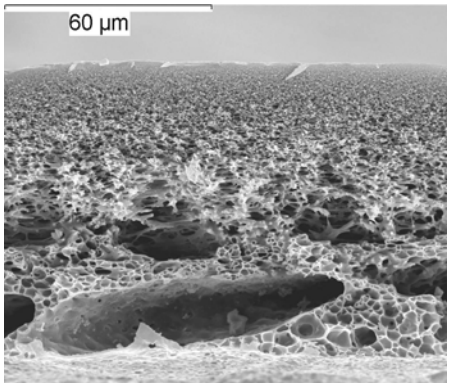

Figure 11. PSU15D cross-section.

The two surfaces of the membranes were different. The film/glass surface was more porous (several micrometer in diameter) than the film/bath surface. Here we present the surface images of PSU10 and PSU15 as examples (Figure 12 and Figure 13). At a low PSU concentration, the integrated skin layer formed with defects. At a high PSU concentration, the integrated skin layer was much denser and had fewer defects.

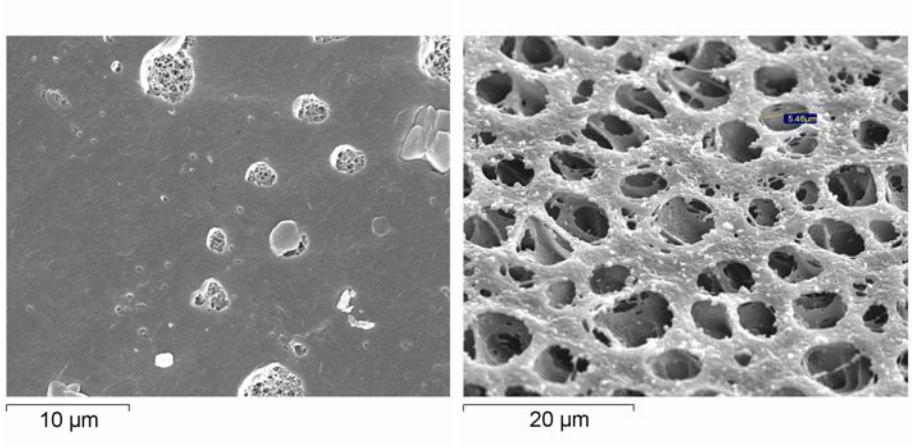

a b

Figure 12. Surface images of PSU10 (a) film/bath surface (b) film/glass surface.

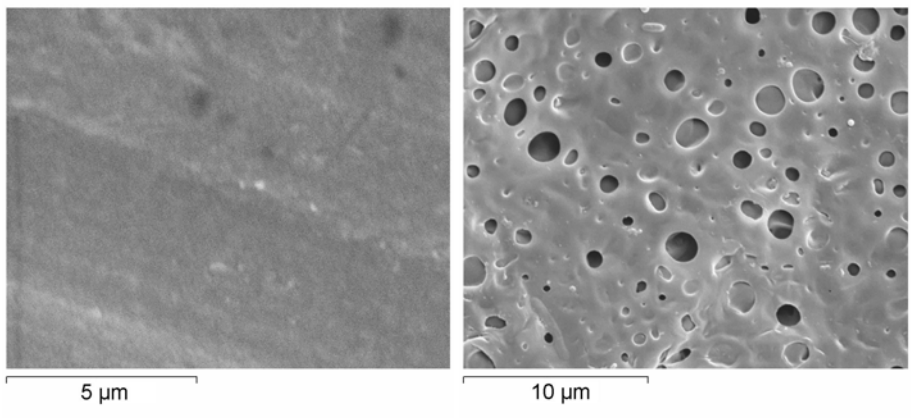

a b

Figure 13. Surface images of PSU15 (a) film/bath surface (b) film/glass surface.

To be a good support, a membrane should exhibit good mechanical properties and low mass transport resistance but should suppress methanol transport. An asymmetric structure with closed pores will have a lower mass transport resistance than the dense structure and will be a better methanol barrier than the channel structure. Based on this concept, we chose membranes PSU15, PSU15D and PSU20 and evaluated their mass transport ability.

3.1.2 Proton and methanol transport abilities of the chosen membranes

Through transport experiments, proton and methanol permeabilities were determined. The results are plotted in Figure 14.

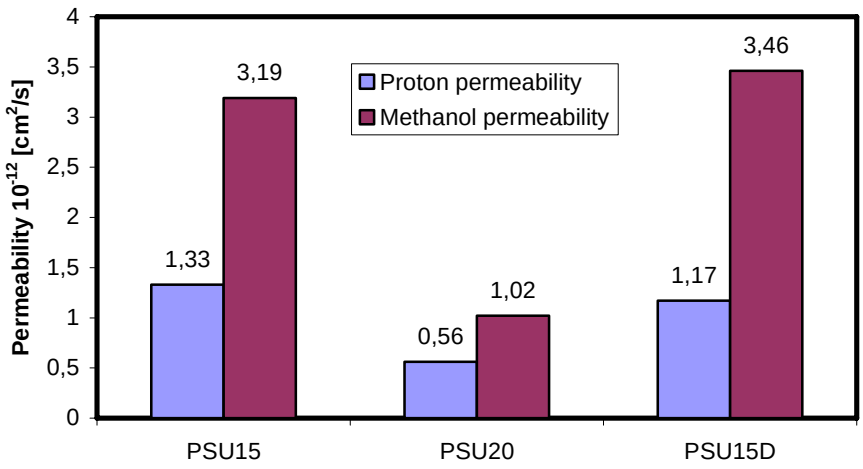

Figure 14. Mass transport ability of membranes PSU15, PSU20 and PSU15D.

We observed that the mass transport abilities of PSU15 and PSU15D were very close, while PSU20 showed much lower proton and methanol permeabilities than the other membranes. This was due to the membrane structures—a higher PSU concentration resulted in a denser membrane, so mass resistance was higher. We therefore concluded that PSU15 and PSU15D were suitable for the support layer.

3.1.3 Thermal sulfonation treatment of PSU support membrane

PSU15 was treated with thermal sulfonation. Proton permeability measurements were carried out for PSU15 and for the treated PSU15. After 3 h of treatment, proton permeability improved significantly from 1.33×10^{-12} cm²/s to 6.66×10^{-11} cm²/s. A longer sulfonation time did not improve proton permeability. We then assumed that some sulfonic acid

groups may have been introduced to the PSU chain (Figure 15) and this could be close to the optimum in our testing conditions. The final sulfonation degree was not determined.

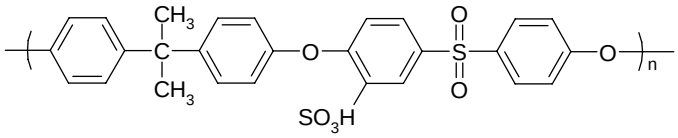

Figure 15. Molecular structure of sulfonated PSU.

3.2 ATR-IR characterization of PEG and PA composite membranes

Several PA structures may form during interfacial polymerization. Their molecular structures are illustrated in Figure 16 [24].

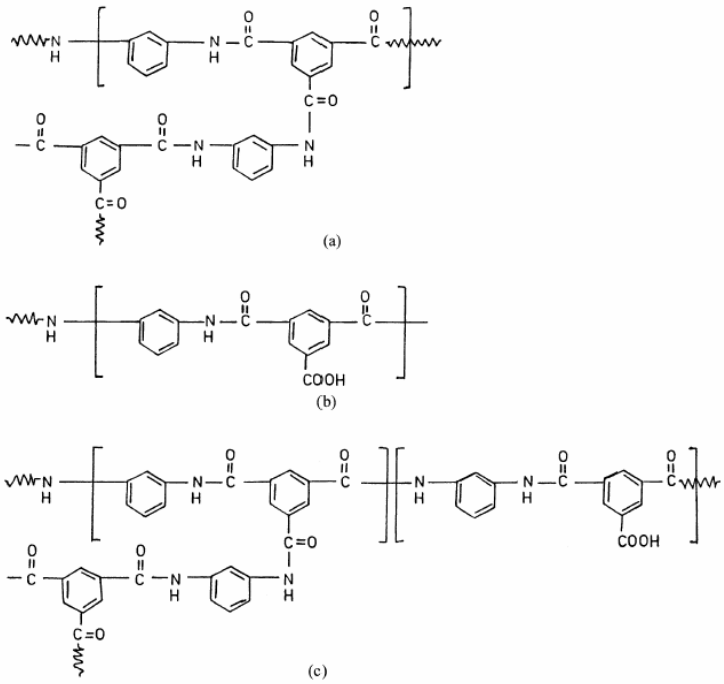

Figure 16. Several PA structures due to interfacial polymerization [24].

The IR spectra of PSU and PA are shown in Figure 17. If we compare the absorbance of PA with that of PSU, we find that both spectra show absorbance bands at 1583 cm^{-1} and 1477 cm^{-1}. These are characteristic of PSU, since the wavelengths penetrated the PSU support layer as well as the PA skin layer. The IR spectrum of PALS presents new absorbance bands at 1645 cm^{-1}, which is characteristic of the C=O band that may belong to the amide groups or to the carbonyl groups of LS. Other characteristic bands of polyamide are also observed at 1537 cm^{-1} (C–N stretch of the amide group) and 1602 cm^{-1} (polyamide aromatic ring breathing) [24]. There is no absorbance of the carboxylic acid groups in the spectrum, so we believe the PA formed was of structure (a).

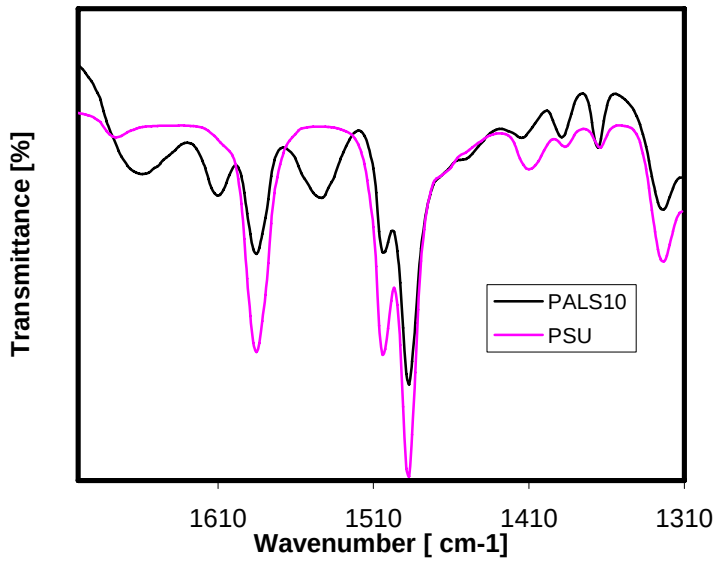

Figure 17. IR spectrum I of PALS10 and PSU membranes.

Figure 18 clearly demonstrates that new absorbance appeared with the PALS membrane at 3405 cm^{-1}, which corresponds to the –OH groups of LS.

We therefore conclude that the PA skin layer was formed on top of the PSU support and that LS, as a proton carrier, was incorporated into the PA network.

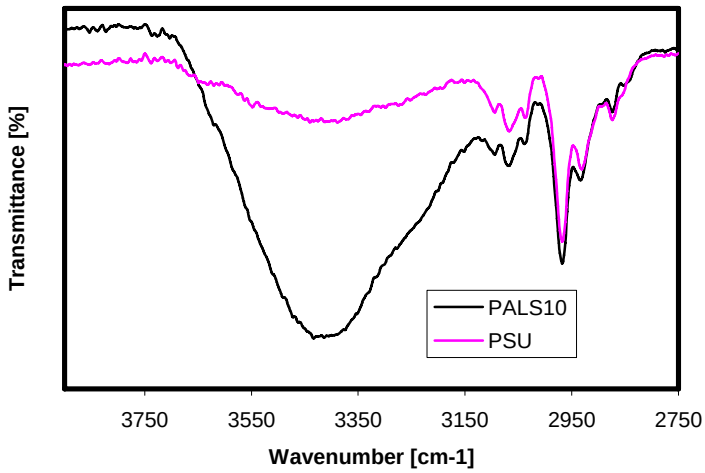

Figure 18. IR spectrum II of PALS10 and PSU membranes.

ATR-IR has also been used to determine PEG composite membranes (Figure 19). However, PSU absorbance was so strong that it covered the PEG absorbance at 1109 cm^{-1}, which is characteristic of C-O-C absorbance. At 3405 cm^{-1}, no significant absorbance of –OH groups was observed, which implies that PEG chains crosslinked through their end groups (-OH).

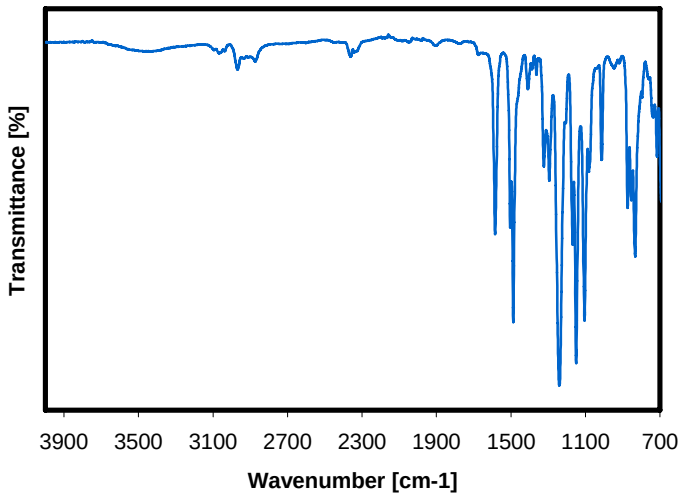

Figure 19. IR spectrum of PEG20 composite membrane.

3.3 SEM characterization of PEG and PA composite membranes

Using SEM, we obtained the cross-section images of PEG composite membranes (Figure 20). The image has two parts. The asymmetric porous structure shows the morphology of PSU15, and the dense continuous phase on top of the PSU corresponds to the PEG skin layer. The PEG skin layer did not change the underlying PSU15 morphology.

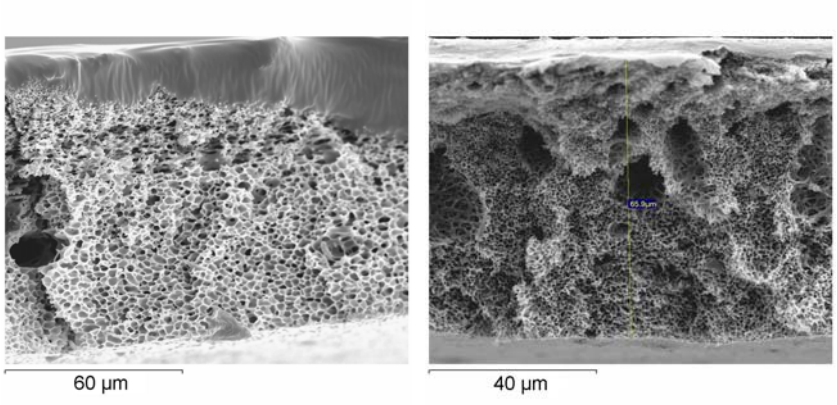

Figure 20. Cross section SEM image of PEG20 and PEG30.

The surface morphology of PSU15D and PALS membranes were also examined by SEM. Figure 21 shows the smooth morphology of the PSUD15 membrane surface. Figure 22 shows the denser and rough morphology of the PALS membrane surface. The rough PA surface may help to incorporate more active functional groups [25].

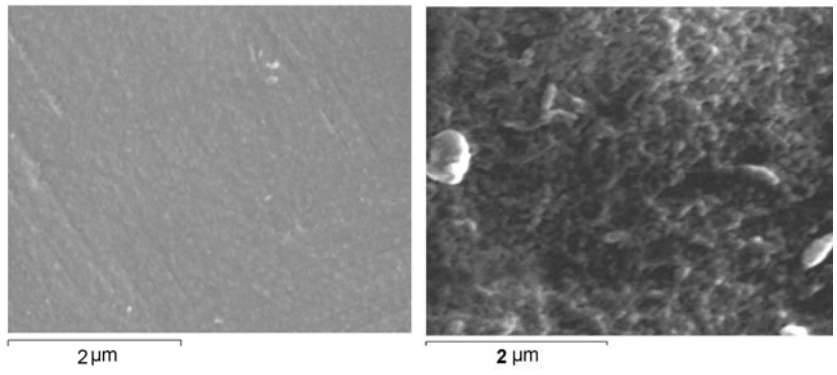

Figure 21. PSU15D surface.

Figure 22. PALS30 surface.

3. 4 Membrane swelling characteristics

Membranes should have suitable swelling characteristics in order to reduce diffusive resistance through the dense layer [26]. They should also have a low degree of swelling in order to avoid unwanted methanol permeation, since methanol migrates through the membrane by combining with its solvating water [27]. Swelling is therefore an important parameter for evaluating membrane transport ability.

The degrees of swelling (SD) of the PEG skin layer and the PSU15 support layer were calculated separately because these layers had totally different swelling characteristics. At 20 ^{o}C, the SD of PSU15 was 1.03 wt.% and was obtained from

$$SD_{PSU15} = \frac{W_{wetPSU15} - W_{dryPSU15}}{W_{dryPSU15}} \times 100\% \qquad (1)$$

Since some PEG composite membranes became brittle after they were put into an oven at over 80 ^{o}C, we immersed the PEG membrane immediately after taking them out of the oven and then weighed the wet PEG composite membrane. The theoretical SD for the PEG layer was calculated as:

$$SD_{PEG} = \frac{W_{PEGcomposite} - W_{wetPSU15}}{W_{PEG}} \times 100\% \qquad (2)$$

where, $W_{PEGcomposite}$ (g) is the weight of the wet PEG composite membrane, $W_{wetPSU15}$ (g) is the weight of the wet PSU15 membrane and W_{PEG} (g) is the theoretical weight of the PEG layer.

Figure 23 shows the degree of swelling of the PEG layer at different PEG loadings. This increased as the PEG loading increased until the maximum SD obtained for PEG50 membrane. The PSU15 support layer hardly swelled, so the SD changes of the PEG composite membranes mainly depended on the PEG loading. Since the thicker PEG layer took more water into its network, the SD of PEG composite membrane increased. When the PEG loading was even higher, the SD decreased slightly. The best explanation for this is that, during soaking, some slices of the PEG

layer peeled off from the PSU support. This resulted from the different swelling characteristics of PSU and PEG. The PSU porous membrane took little water into its pores without changing its dimensions, while PEG took water into its network and changed dimensions, so part of the PEG layer detached from the PSU surface when the PEG loading was over the 4.65 mg/cm^2 limit.

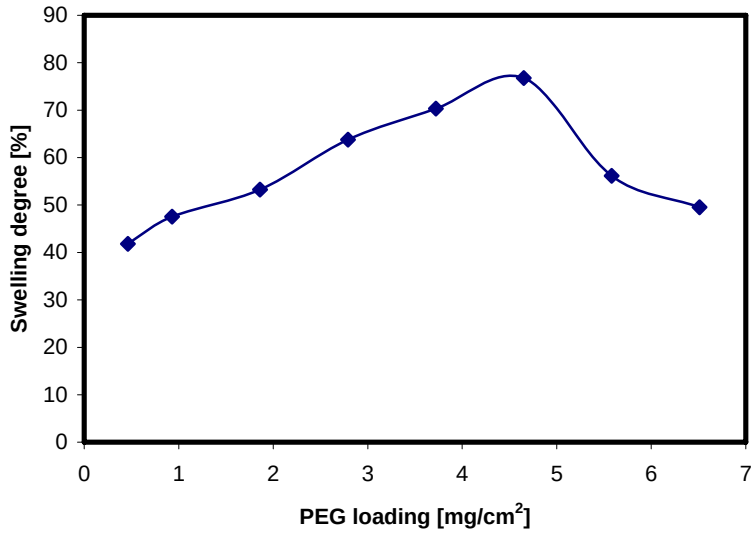

Figure 23. Degree of swelling of the PEG layer.

We also calculated the degree of swelling of the PALS membranes. These are shown in Table 5.

Table 5. The influence of LS content on the degree of swelling (SD) of PALS membranes

PALS membranes	PALS10	PALS25	PALS30	PALS50
SD (%)	4.43	4.76	4.84	6.08

It seems that as the LS content in the polyamide skin layer increased, the SD of the PALS membranes increased only slightly because of the relatively dense and rigid polyamide main chain.

3.5 Transport abilities through PEG and PA composite membranes

3.5.1 Proton and methanol permeabilities through PEG membranes

Figure 24 shows the proton and methanol permeabilities for PEG membranes. The PEG loading had the same influence on permeability of proton and methanol. High PEG loadings resulted in high permeabilities, which is consistent with the measurements of the degree of swelling. PEG swelled in water and produced a loose structure [28] that helped proton and methanol to permeate together with solvating water [29]. A study of the similar poly(ethylene oxide) (PEO) system [30] indicated that when the PEO system contained more water, the proton conducting was more likely to be dominated by the hopping mechanism. In the system that contained 35% water, both the hopping and the diffusion mechanisms were important. When the water content was less than 20%, the system was non-conducting. If we take into account the PEG composite membranes in our study, the results of the swelling and mass transport experiments suggest that the PEG composite membranes were water-dependent conductive. Also, high PEG loading membranes demonstrated that transport was dominated by the hopping mechanism.

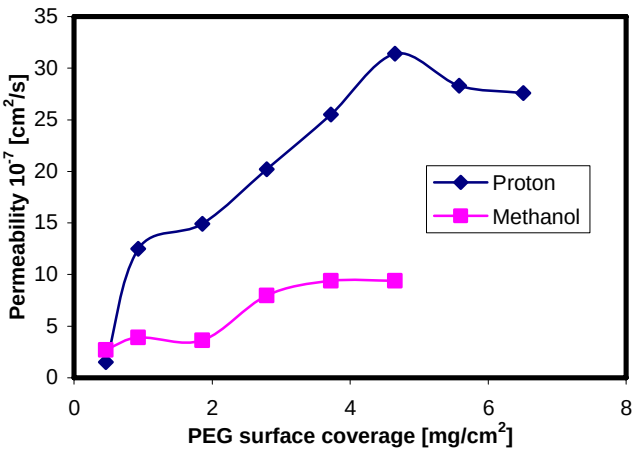

Figure 24. The effect of PEG loading on proton and methanol permeabilities.

A parallel computational study showed how the PSU porous membrane, the PEG skin layer and their interface contribute to mass transport resistance for proton and methanol [31]. Results suggested that the PEG loading at 4.65 mg/cm² provided the lowest resistance for proton transport through the skin layer. Choosing a suitable porous support could reduce mass transfer resistance and increase the selectivity of proton to methanol.

3.5.2 Proton and methanol permeabilities through PA membranes

Transport experiments determined the proton and methanol permeabilities through PA composite membranes with and without proton carriers. Without a proton carrier, the PA membrane showed very low proton permeability (3.72×10^{-12} cm²/s). However, when the carriers were incorporated into the PA network, the proton permeability increased dramatically. Figure 25 shows the influence of LS on proton and methanol transport. PALS membranes exhibited increasing proton permeability until the LS content was around 30 wt.%.

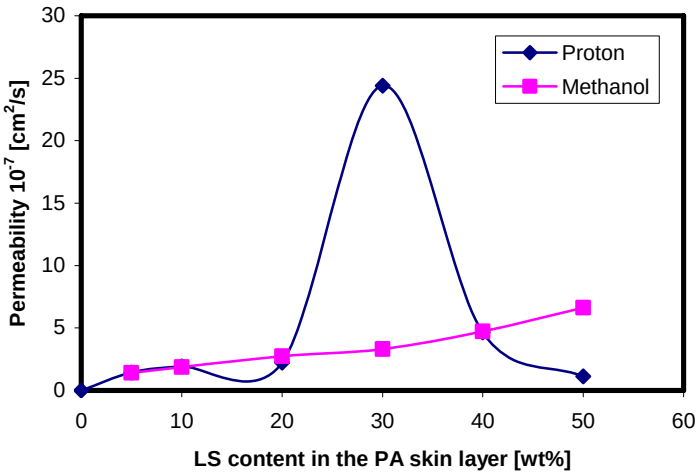

Figure 25. Effect of LS content on proton and methanol permeabilities.

Unlike proton permeability, methanol permeability increased slightly as the LS content increased. This was due to the low degree of swelling of

the PA dense layer and was in agreement with the results for degree of swelling. This indicates that methanol permeability was closely related to water content in the membrane and that methanol could only be transferred between sulfonic acid groups together with its solvating water. Proton permeability behaved quite differently, which implies a different transport mechanism. We suggest, as was found in similar studies [32], that the PALS membranes were one type of acid-base membranes through which the proton transferred from a sulfonic acid group to an amino group of polyamides by hydrogen bonds and polysalt. The lower proton permeability when the LS content was above 30 wt% may be explained as the partial blocking of the SO_3^- groups for proton transport by the polysalt formation (Figure 26). Also, the formed NH^+ group may have repulsed the proton diffusion and led to the lower proton permeability [33].

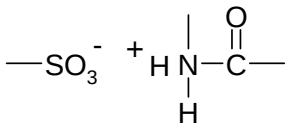

Figure 26. Structure of polysalt [33].

Proton permeabilities through PAD membranes were also determined by the proton transport experiment (Figure 27).

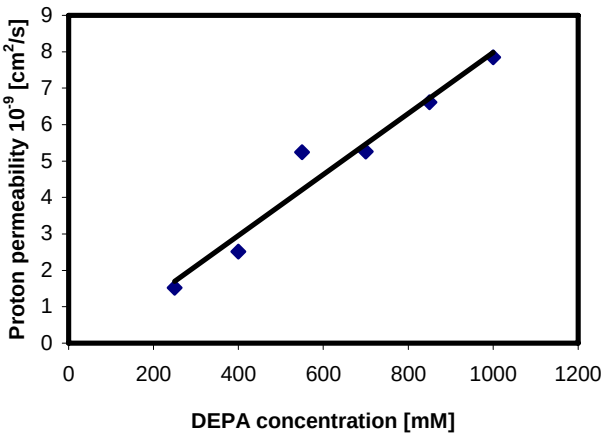

Figure 27. Effect of DEHPA concentration on proton permeability.

We found that DEHPA constantly improved proton permeability. However, proton permeability was too low even with a high DEHPA concentration. Although the permeation curve implied that proton permeability increased continuously as the DEHPA concentration increased, it was impossible to increase DEHPA concentration over 1000 mM because the membrane became very brittle with high DEHPA concentrations.

3.6 Electrochemical characterization of PEG and PA composite membranes

Ion conductivity was carried out by impedance spectrometry (IS) to confirm the transport results.

First, the electrical resistance of the PSU membrane treated with thermal sulfonation was about 15 times lower than that of the untreated PSU membrane [34]. This confirmed that sulfonic acid groups were introduced into the PSU chain.

Figure 28 shows the electrical resistance of PEG membranes in 0.5 M NaCl solution. A high PEG loading reduced membrane resistance and this then remained constant. The results of the transport experiment therefore showed a good correlation with those from IS analysis.

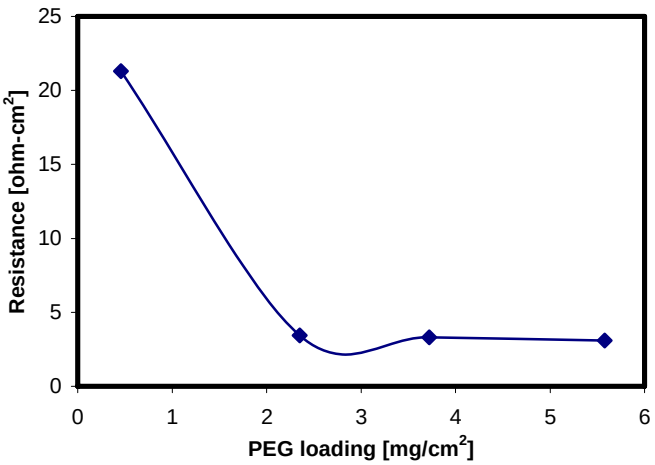

Figure 28. Electrical resistance of membranes in 0.5 M NaCl solution.

Finally, Figure 29 shows the electrical resistance of PALS membranes in 0.5 M NaCl solution. Membrane electrical resistance shows a minimum around 20 wt.% LS content. These results are in agreement with those from proton transport experiments, though the optimal LS concentration was slightly different.

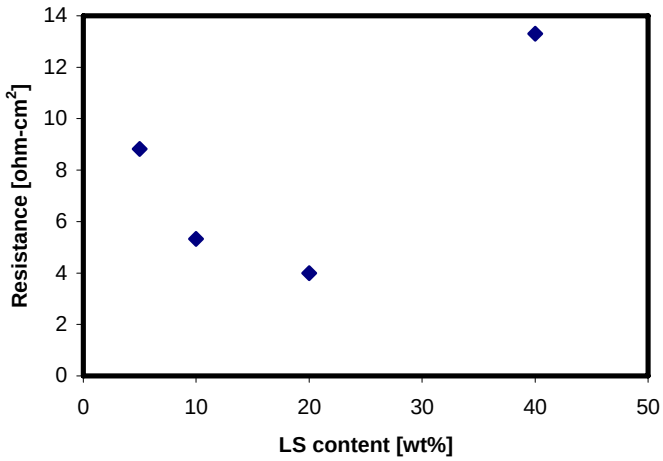

Figure 29. Electrical resistance of membranes in 0.5 M NaCl solution.

4 Conclusions

PEG and PA composite membranes were synthesized by coating PEG and PA skin layers on top of the porous PSU membranes.

PSU porous membranes were treated by thermal sulfonation, which improved their ability of proton transport. Results from transport experiments showed an increase of one order of magnitude in proton permeability after 3 h of thermal sulfonation. The IS confirmed that the PSU membrane lowered its electrical resistance by 15 times after the treatment.

Swelling and mass transport studies of PEG membranes suggested that the mass transport mechanism through the PEG skin layer depended on the water content. The most likely proton transport mechanism was dominated by hopping. The lowest mass transport resistance was found for a PEG loading of 4.65 mg/cm^2. By adjusting the support layer, we can improve the membrane selectivity of proton to methanol.

Our experimental work has confirmed that the polyamide dense layer is a good barrier for methanol. Incorporating LS into the PA matrix did not significantly increase the degree of membrane swelling. Methanol permeability correlated with the degree of swelling, while proton permeability behaved differently. The proton transport mechanism may be as follows: the sulfonic acid groups interact with the N-base of polyamide via the formation of hydrogen bonds and protonation of the basic N (polysalt). At a high LS content, polysalt formation may partially prevent the acid site from combining with proton. Moreover, protonated positive N-base may repulse proton diffusion.

If we compare optimal PEG membrane and optimal PALS membrane, the lowest electrical resistances for both kinds of membranes were around 3.0 ohm-cm^2. Corresponding methanol permeabilities were 9.38×10^{-7} cm^2/s and 2.75×10^{-7} cm^2/s for the PEG membrane and the PALS membrane, respectively. Obviously, PALS20 showed a better selectivity of proton to methanol than the PEG membrane.

We can also compare the PALS20 membranes with Nafion 117. The PALS20 membranes showed one order lower of methanol permeability than Nafion 117. However, its proton permeability was also much lower than that of Nafion 117. We suggest two ways to improve proton transport through the PALS membrane. The first one is to reduce the thickness of the PSU support. The second is to use LS with a suitable molecular weight and suitable acid groups.

There may be some concerns about membrane stability in a fuel cell operation, since the membrane may degrade due to the presence of different radical species in the cell. Specifically, species such as HO· originated from oxygen diffusion through the membrane and incomplete reduction at the fuel cell anode [35, 36]. We suggest using the real cell test in future and, if these composite membranes are not suitable for fuel cell application, they should be considered in the application of electrodialysis.

References

[1] R.J. Petersen, Composite reverse osmosis and nanofiltration membranes, J. membr. Sci. 83 (1993) 81-150

[2] J.E. Cadotte, R.J. Petersen, R.E. Larson, E.E. Erickson, A new thin film composite sea water reverse osmosis membrane, Desalination 32 (1980) 25-31

[3] R.L. Riley, R.L. Fox, C.R. Lyons, C.E. Milstead, M.W. Seroy, M. Tagami, Spiral-wound poly(ether/amide) thin film composite membrane systems, Desalination 19 (1976) 113-126

[4] C.S. Slater, R.C. Ahlert, C.G. Uchrin, Applications of reverse osmosis to complex industrial wastewater treatment, Desalination 48 (1983) 171-183

[5] B.M. Watson, C.D. Hornburg, Low-energy nanofiltration for removal of colour, organics and hardness from drinking water supplies, Desalination 72 (1989) 11-22

[6] K.J. Voorhees, S.F. Baugh, D.N. Stevenson, The thermal degradation of poly(ethylene glycol)/poly(vinyl alcohol) binder in alumina ceramics, Thermochimica Acta 274 (1996) 187-207

[7] S. Bu, Z. Jin, X. Liu, H. Du, Z. Cheng, Preparation and formation mechanism of porous TiO2 films using PEG and alcohol solvent as double-templates, Journal of Sol-Gel science and Technology 30 (2004) 239-248

[8] C. Oh, C. D. Ki, J. Y. Chang, S-G. Oh, Preparation of PEG-grafted silica particles using emulsion method, Materials Letters 59 (2005) 929-933

[9] L. Saravanan, S. Subramanian, Surface chemical studies on the competitive adsorption of poly(ethylene glycol) and ammonium poly(methacrylate) onto zirconia, Colloids and surfaces A: Physicochem. Eng. Aspects 252 (2005) 175-185

[10] Y. Xu, W. Peng, X. Liu, G. Li, A new film for the fabrication of an unmediated H2O2 biosensor, Biosensors and bioelectronics 20 (2004) 533-537

[11] Adam Heller, Electrical wiring of redox enzymes, Acc. Chem. Res., 23 (1990), 128-134

[12] H.Ju, Y.Gong and H.Zhu, Electrolyte effects on electrochemical properties of osmium complex polymer modified electrodes, Analytical Sciences, 17 (2001), 59-63

[13] L-Y. Chu, Y-J. Liang, W-M. Chen, X-J. Ju, H-D. Wang, Preparation of glucose-sensitive microcapsules with a porous

membrane and functional gates, Colloids and Surfaces B: Biointerfaces 37 (2004) 9-14

[14] Y. Song, P. Sun, L. L. Henry, B. Sun, Mechanisms of structure and performance controlled thin film composite membrane formation via interfacial polymerization process, Journal of membrane science 251 (2005) 67-79

[15] R.Garcia-Valls, M.Muñoz, M.Valiente, Selective separation of lanthanides by supported liquid membranes containing Cyanex 925 as a carrier, Analytica Chimica Acta, 387 (1999), 77-84

[16] T. Gumí, M. Oleinikova, C. Palet, M. Valiente, M.Muñoz, Facilitated transport of lead and cadmium through novel activated composite membranes containing di-(2-ethyl-hexyl) phosphoric acid as carrier, Analytica Chimica Acta, 408 (2000), 65-74

[17] D. Fengel, G. Wegener, Wood Chemistry, Ultrastructure, Reactions, Walter de Gruyter, Berlin, 1984, 157-163

[18] R. Gonzalez, E. Reguera, J.M. Figueroa, J.D. Martinez, Study of the influence of nejayote and other additives on the cohesive strength and electric properties of carbon black agglomerates, Journal of Applied Polymer Science 90 (2003) 3965-3972

[19] H.H. Tseng, M.Y. Wey, J.C. Chen, The adsorption of PAHs, BTEX, and heavy metals on surfactant-modified desulfurization sorbents in a dry scrubber, Fuel, 81 (2002) 2407-2416

[20] K.M. Askvik, S. Hetlesather, J. Sjöblom, P. Stenius, Properties of the linosulfonate-surfactant complex phase, Colloids and surfaces A: Physicochemical and engineering Aspects 182 (2001) 175-189

[21] G. Cazacu, M.C. Pascu, L. Profibre, A.I. Kowarski, M. Mihaes, C. Vasile, Lignin role in a complex polyolefin blend, Industrial Crops and Products, 20(2004) 261-273

[22] S. Baumberger, C. Lapierre, B. Monties, D. Lourdin, P. Colonna, Preparation and properties of thermally moulded and cast lignosulfonates-starch blends, Industrial Crops and Products, 6 (1997) 253-258

[23] Marcel Mulder, Basic principles of membrane technology, 2nd ed. Klumer Academic Publishers, The Netherlands, 2003

[24] P. Rao, S.V. Joshi, J.J. Trivedi, C.V. Devmurari, V.J. Shah, Structure-performance correlation of polyamide thin film composite membranes: effect of coating conditions on film formation, Journal of membrane science 211 (2003) 13-24

[25] Y. Song, F. Liu, B. Sun, Preparation, characterization, and application of thin film composite nanofiltration membranes, Journal of applied polymer science, 95 (2005) 1251-1261

[26] Moon-Sung K., C. Yong-Jin, M. Seung-Hyeon, Water-swollen cation-exchange membranes prepared using poly(vinyl alcohol)(PVA)/poly(styrene sulfoic acid-co-maleic acid) (PSfSA-MA), Journal of Membrane Science, 207 (2002), 157-170

[27] Thorsten Schultz, Su Zhou and Sundmacher, Current Status of and Recent Developments in the Direct Methanol Fuel Cell, Chem. Eng. Technol. 24 (2001) 12, 1223

[28] R. G. Schmidt, J. Brickmann, Molecular dynamics simulation study of a hydronium ion in liquid water with implementation of the proton transfer by means of a hopping mechanism, Solid State Ionics 77 (1995) 3-9

[29] J.R. Fried, Polymer Science and Technology, Englewood Cliffs, New Jersey.1995, ISBN 0-13-685561-X

[30] J. Ennari, I. Neelov, F. Sundholm, Estimation of the ion conductivity of a PEO-based polyelectrolyte system by molecular modeling, Polymer 42 (2001) 8043-8050

[31] X. Zhang, L.P. Filho, C. Torras, R.Garcia Valls, Experimental and computational study of proton and methanol permeability through composite membranes, Journal of power sources, 145 (2005) 223

[32] Jochen Kerres , Andreas Ullrich, Frank Meier, Thomas Haring, Synthesis and characterization of novel acid–base polymer blends for application in membrane fuel cells, Solid State Ionics 125 (1999) 243–249

[33] W. Cui, J. Kerres, G. Eigenberger, Development and characterization of ion-exchange polymer blend membranes, Separation and Purification Technology 14 (1998) 145–154

[34] J. Benavente, X. Zhang, R. Garcia Valls, Modification of polysulfone membranes with poly(ethylene glycol) and lignosulfate: electrical characterization by impedance

spectroscopy measurements, Journal of Colloid and Interface Science 285 (2005) 273-280

[35] A. Panchenko, H. Dilger, E. Möller, T. Sixt, E. Roduner, In situ EPR investigation of polymer electrolyte membrane degradation in fuel cell applications, Journal of Power Sources 127 (2004) 325–330

[36] Jingrong Yu, Baolian Yi, Danmin Xing, Fuqiang Liu, Zhigang Shao, Yongzhu Fu, Degradation mechanism of polystyrene sulfonic acid membrane and application of its composite membranes in fuel cells, Journal of Power Sources 4937 (2002) 1–6

Chapter 4

Hybrid lignosulfonate membranes (I): morphological characterization and mass transport

1 Introduction

Many attempts at developing proton-conducting membranes have focused on hybrid membranes made of polymer blends consisting of rigid, hydrophobic polymer and hydrophilic polymer attached with acid groups [1-8]. The hydrophobic polymer functions as a methanol barrier and the hydrophilic polymer functions as a proton affiliation site. Most hydrophilic polymers are sulfonated polysulfone (SPSU) or sulfonated poly(etheretherketone) (SPEEK). The sulfonation process modifies the hydrophobic polymers by introducing the sulfonic acid groups to the polymer backbones. The sulfonation degree can be controlled by changing the acid concentration, sulfonation time and temperature in order to generate a moderate sulfonated polymer. Too much of the sulfonic acid groups will cause high membrane swelling, which leads to undesired methanol permeability or methanol crossover [9, 10].

Rather than modifying polymers by a sulfonation process, our approach is to apply lignosulfonate (LS) in the preparation of hybrid membranes. LS is a high crosslinked polymer containing sulfonic acid groups obtained directly from the sulfite pulping industry. Its chemical structure has been illustrated in Chapter 3 (Figure 3).

In Chapter 3, we showed that LS is a good proton carrier. In this chapter

we have prepared hybrid membranes by blending LS with polysulfone (PSU). PSU is a chemical and mechanical stable polymer that acts as a methanol barrier. Blending PSU with LS in different proportion should generate membranes with good selectivity of proton over methanol. Moreover, the membrane preparation procedure is simple and industrially friendly, and LS hybrid membranes are much cheaper than other membranes.

2 Experimental

2.1 Preparation of PSU-LS hybrid membranes

PSU (Mw. 35,000) was purchased from Aldrich and LS (Mw. 7,000) was given by Borregaard Lignotech, Spain. The casting solution was prepared by dissolving LS and PSU in N,N-Dimethylformamide (DMF) at different temperatures. The casting solution was spread by a coating machine onto a glass surface in a controlled thickness film. The wet film formed a solid membrane after it was immersed into a precipitation bath or a nonsolvent bath.

Membrane properties can be changed in many ways. In this work we have considered five influential factors: the PSU concentration in the casting solution, the LS concentration in the dry membrane, the temperature of the casting solution, the temperature of the precipitation bath and the composition of the precipitation bath.

Finally, we obtained two categories of membranes that were named according to the PSU concentration in the casting solution: PSU10LS membranes (10 wt.% PSU in the casting solution) and PSU15LS membranes (15 wt.% PSU in the casting solution).

2.2 Membrane characterization

LS membranes were characterized by attenuated reflectance infra-red (ATR-IR), contact angle measurement (CA), scanning electron microscopy (SEM) and atomic force microscopy (AFM). The membrane morphologies in the SEM pictures were analyzed by IFME® software [11]. Mass transport ability, i. e. proton and methanol permeabilities, through LS membranes were determined by transport experiments. All the characterization details are described in Chapter 2.

3 Results and Discussion of PSU10LS hybrid membranes

3.1 The effect of the temperature of the casting solution

Three series of PSU10LS membranes (Table 1) were prepared by mixing LS with 10 wt.% PSU at different temperatures (20 °C, 33 °C, 48 °C and 61 °C) and then precipitated in a water bath at 20 °C.

Table 1. List of PSU10LS membranes

Membrane	LS content in the dry membrane [wt. %]	LS content in the casting solution [wt. %]
LS9	9.1	1
LS17	16.7	2
LS23	23.1	3

Membranes were tested in the transport cells to determine the optimal temperature of the casting solution according to the proton permeability. The results are shown in Figure 1.

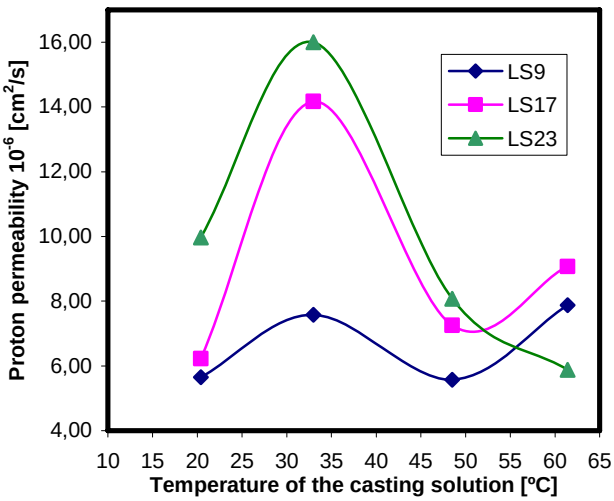

Figure 1. The effect of the temperature of the casting solution on proton permeability for LS9, LS17 and LS23.

Clearly, a casting solution temperature of around 33 °C generated membranes with the highest proton permeability.

3.2 The effect of the precipitation temperature

Having fixed the temperature of the casting solution at 35 °C, membranes LS9, LS17 and LS23 were prepared by precipitating in a water bath at different temperatures. Their proton and methanol permeabilities are presented in Figure 2 and Figure 3, respectively.

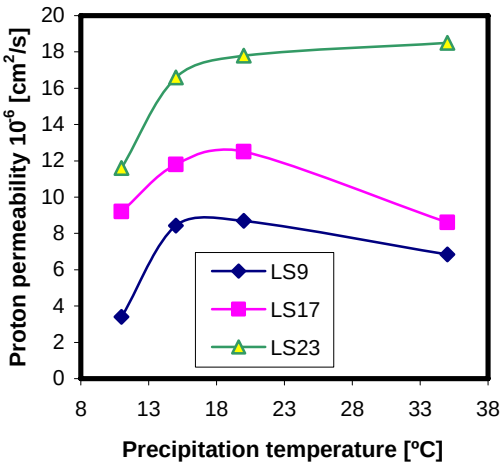

Figure 2. The effect of precipitation temperature on proton permeability.

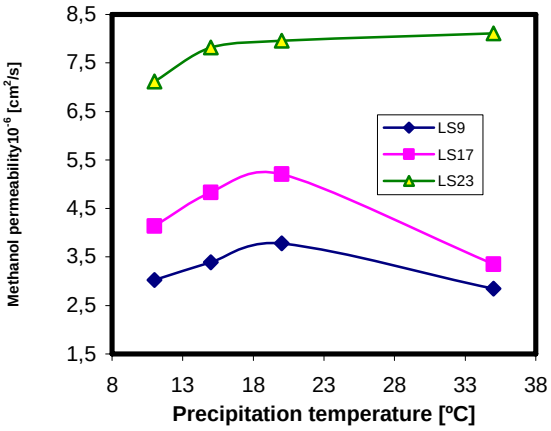

Figure 3. The effect of precipitation temperature on methanol permeability.

We noticed that when the precipitation temperatures were around 20 ºC, the membranes exhibited relatively high proton and methanol permeabilities. Clearly, for the permeability of an acid membrane is closely related to its proton permeability since either the proton or the methanol is transported together with solvating water [12-16].

3.3 The effect of LS content

In Figures 1–3, we observed that a higher LS content showed higher proton and methanol permeabilities. To show the effects of LS content on membrane morphology, we present Figure 4 to illustrate the morphological changes of membranes cast at 35 ºC and precipitated at 20 ºC.

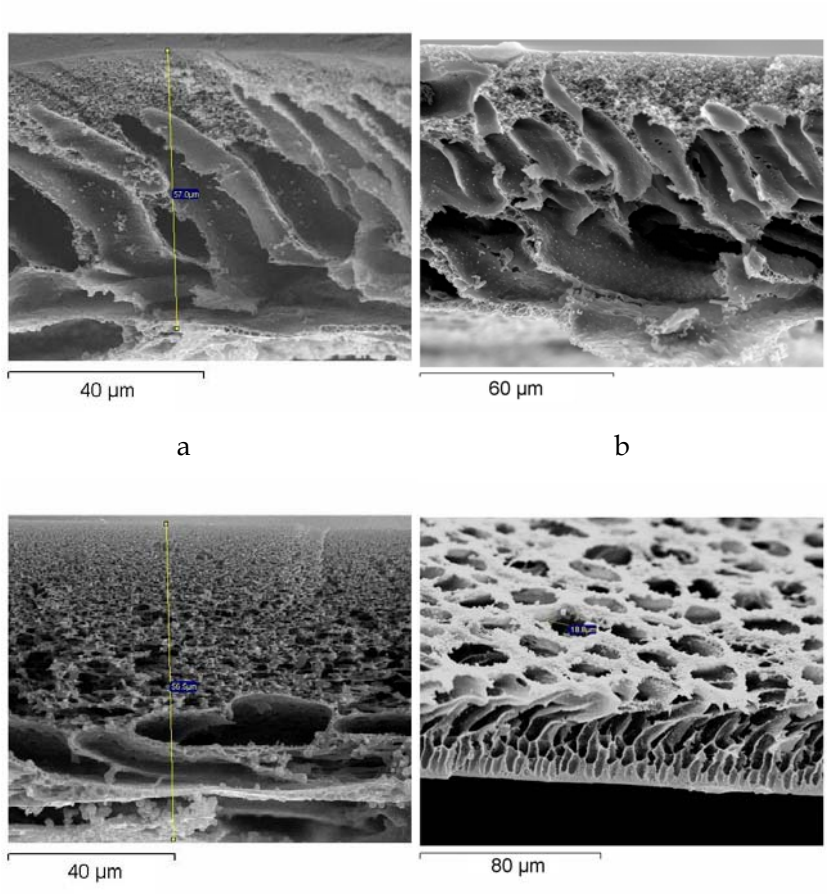

Figure 4. SEM cross-section images (a: LS9; b: LS17; c: LS23; d: PSU10).

If we compare image 4.a with image 4.d, we can see that the channel structure of the LS9 membrane was similar to that of the PSU10 membrane. From images 4.b and 4.c, we can see that, as more LS was dispersed in the PSU network, the membrane morphology changed from an open porous structure to a closed porous structure. In particular, the LS 23 membrane exhibited a denser structure with closed micropores on the top layer and macrovoids near the sublayer, and channels no longer existed. The membrane with the closed porous structures had a higher diffusion resistance than the one with the open porous structure, i.e. LS23 should have a higher resistance to proton transport than LS9. The results of transport experiments (Figure 2), however, showed that LS23 exhibited higher proton permeability than LS9. This indicates that, at a high LS content, acid groups ($-SO_3^-$) had a greater effect on proton transport than the membrane morphology did.

3.4 The effect of the composition of the precipitation bath

So far we have determined the optimal temperatures of the casting solution and precipitation bath. We have also found that the LS23 membrane had the highest proton permeability under all conditions. With the best membrane obtained so far (LS23), we then studied the effect of the composition of the precipitation bath at a precipitation temperature of 20 ^oC.

LS23-1 was precipitated in pure iso-propanol (IPA) solution, LS23-2 was precipitated in 50 wt.% IPA and 50 wt.% H_2O solution (IPAW), and LS23-3 was precipitated in 70 wt.% IPA and 30 wt.% DMF solution (IPAD).

Figures 5.a to 5.c correspond to the cross-section SEM images of LS23-1, LS23-2 and LS23-3.

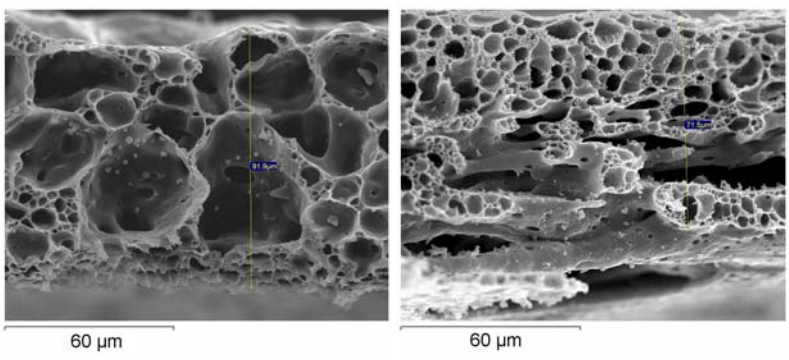

a b

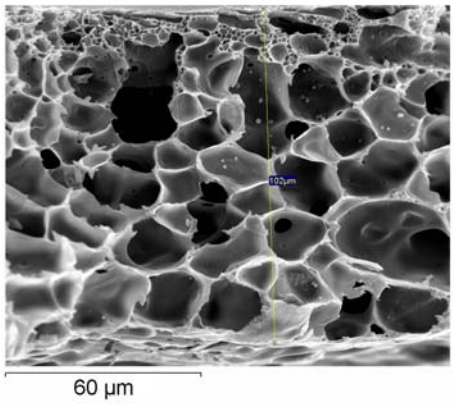

c

Figure 5. SEM cross-section images (a: LS23-1; b: LS23-2; c: LS23-3).

Different compositions of precipitation solution induced different membrane morphologies. The IPA solution generated the thinnest membrane LS23-1, which had the largest pores or macrovoids. LS23-2 had a more symmetrical structure, with elongated macrovoids in the sublayer. LS23-3 was the thickest membrane and had relatively large pores and fewer macrovoids.

The morphological differences influenced the mass transport ability of the membranes. As we can see in Figure 6, the LS23-2 membrane, which was precipitated in IPAW solution, showed the best proton permeability, and LS23-1, which was precipitated in pure IPA, showed the lowest proton permeability. Compared to the LS23 membrane precipitated in water bath, which had a proton permeability of 1.78×10^{-5} cm^2/s, the proton permeability of LS23 membranes precipitated in other solutions was dramatically lower. This suggests that the presence of water in the precipitation bath helped to obtain membranes with better proton transport abilities, perhaps because the structure provided less resistance or because the water helped to arrange the $-SO_3^-$ groups towards the polymer/air and polymer/polymer interface, thus facilitating proton transport along the pore walls and through the polymer.

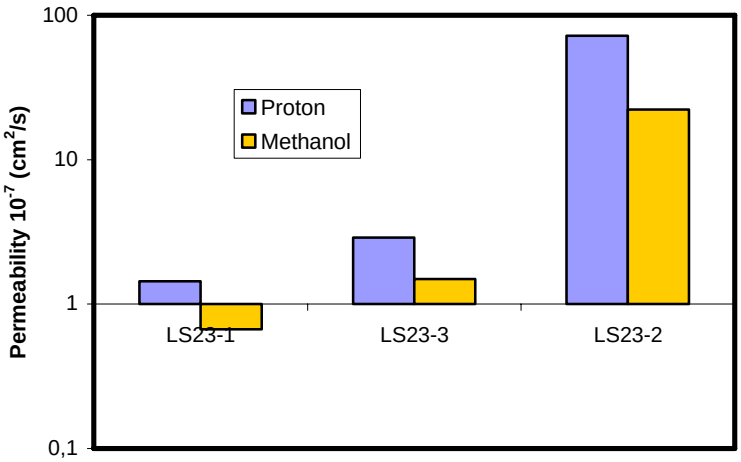

Figure 6. Logarithmic plot of proton and methanol permeabilities through LS23 membranes precipitated at different baths.

4 Results and discussion of PSU15LS hybrid membranes

Four series of PSU15LS membranes (Table 2) were prepared by mixing 15 wt.% PSU with LS at different temperatures (20 °C, 33 °C, 48 °C and 61 °C) and then precipitated in a water bath at 20 °C.

Table 2. List of PSU15LS hybrid membranes

Membrane	LS content in the dry membrane [wt. %]	LS content in the casting solution [wt. %]
LS6	6.3	1
LS12	11.7	2
LS17	16.7	3
LS21	21.1	4

Compared to the PSU10LS membranes prepared under the same conditions, the PSU15LS membranes were thicker and showed better apparent mechanical properties.

4.1 Attenuated Total Reflectance Infra-red spectra (ATR-IR)

Figure 7 shows the IR spectra of PSU and LS membranes. Compared to the spectra of the PSU blank membrane, the PSU-LS spectra showed new absorption peaks at 3451-3100 cm^{-1} and 1700-1600 cm^{-1} that were assigned to O-H stretching vibration and C=O stretching vibration, respectively. These refer to the phenolic hydroxyl groups and carbonyl groups of LS [17]. These IR absorption bands revealed that LS was incorporated into the PSU network.

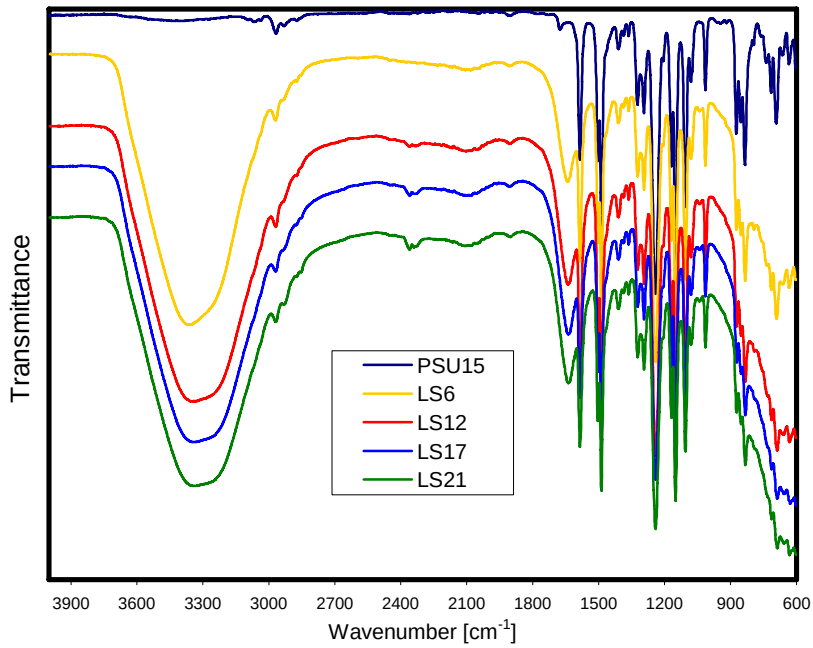

Figure 7. IR spectra of PSU and PSU15LS membranes.

4.2 The effect of the temperature of the casting solution

We conducted proton transport experiments to determine the optimal temperature of the casting solution for each series of membranes. The

results are shown in Figure 8.

Membranes obtained with the casting solution at 33 °C showed the highest proton permeability. This implied that, around 33 °C, PSU and LS might form a more homogeneous blend. Also, a higher LS content enhanced proton permeability because there were more $-SO_3^-$ groups in the membrane. However, as it was difficult to obtain LS21 membranes without defects, we stopped trying to prepare it in further studies.

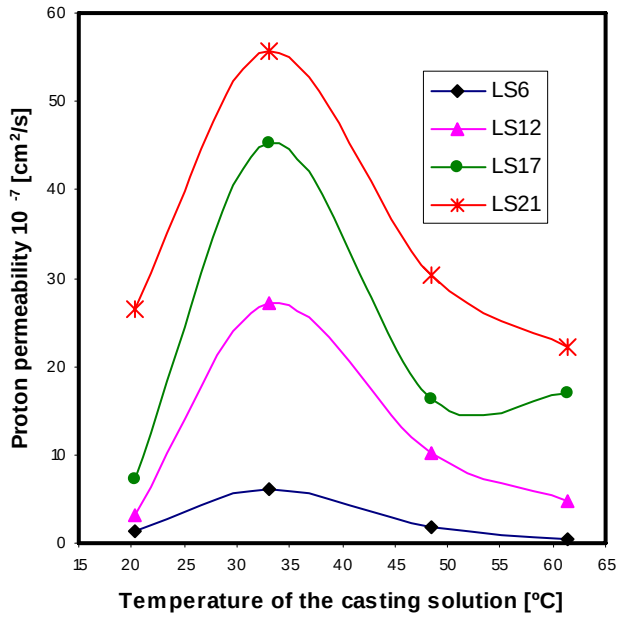

Figure 8. The effect of the temperature of the casting solution on proton permeability through the LS6, LS12, LS17 and LS21 membranes.

4.3 The effect of the precipitation temperature and LS content

4.3.1 Membrane cross-section morphologies by SEM

To examine how the precipitation temperature and LS content affect membrane morphology, we obtained membrane cross-section morphologies by SEM. The images are shown in Figures 9–11.

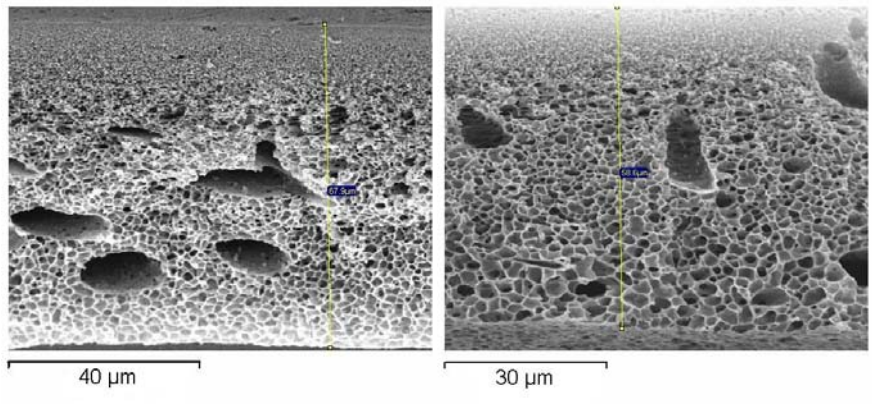

a b

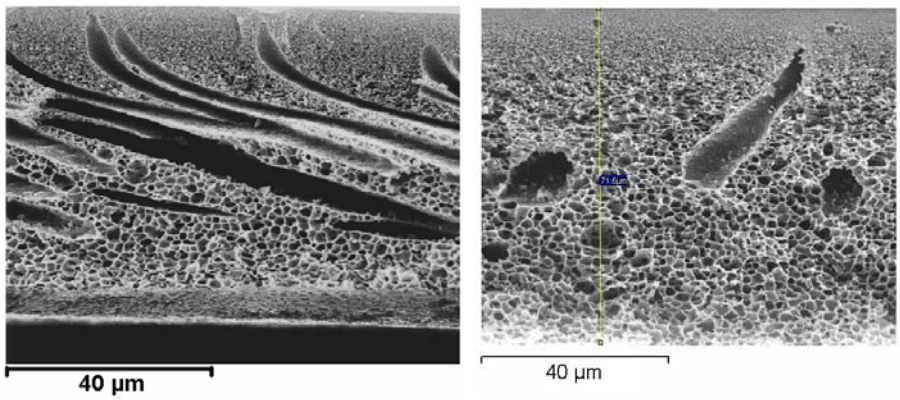

c d

Figure 9. SEM cross-section images of LS 6 membranes (a: 11 ºC; b: 15 ºC; c: 20 ºC; d: 35 ºC).

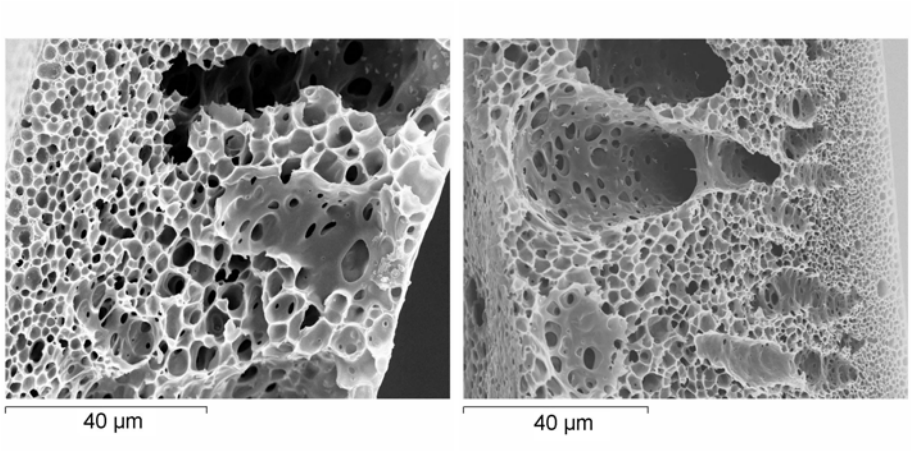

a b

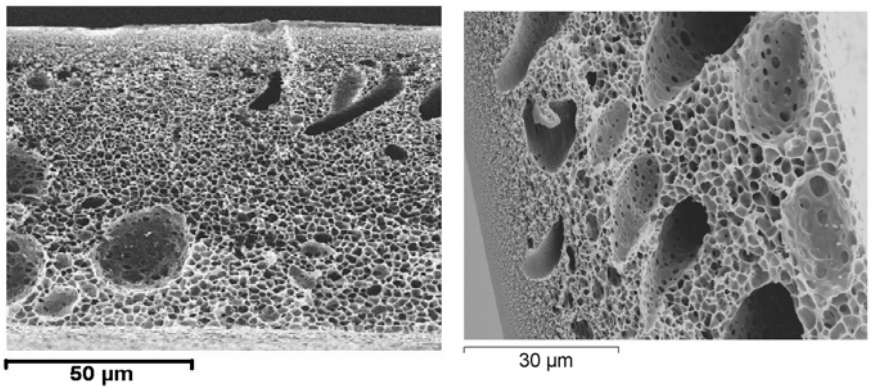

c d

Figure 10. SEM cross-section images of LS 12 membranes (a: 11 °C; b: 15 °C; c: 20 °C; d: 35 °C).

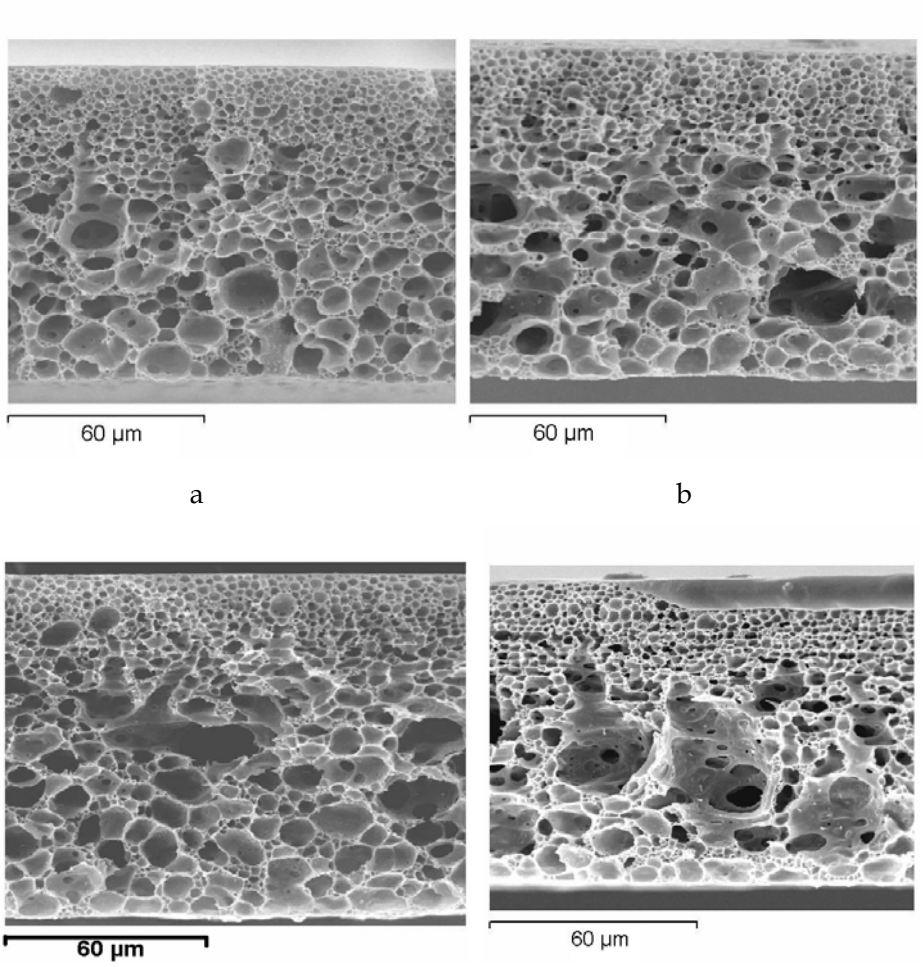

Figure 11. SEM cross-section images of LS 17 membranes (a: 11 ^{o}C; b: 15 ^{o}C; c: 20 ^{o}C; d: 35 ^{o}C).

These SEM pictures highlight two facts. First, a higher precipitation temperature induced more macrovoids and the macrovoids appeared to be closer to the top layer. Second, a higher LS content induced larger pores and fewer macrovoids in the membranes.

Membrane formation is a liquid-liquid demixing process, and instantaneous demixing favors macrovoid formation [18]. A high precipitation temperature accelerated the solvent-nonsolvent diffusion,

which speeded up the demixing process and led to the presence of more macrovoids close to the film/bath surface.

It is controversial whether increasing the LS concentration produced membranes with fewer macrovoids. As we know, LS is soluble in water and, as we saw in the preparation of the casting solution, reduces the miscibility between PSU and DMF. LS therefore showed its nonsolvent effects in the casting solution. These should accelerate the demixing process and generate more macrovoids [19]. However, we must consider the kinetic hindrance due to the rheological effects. During the experiment we found that, obviously, LS increased the viscosity of the casting solution since it is a good dispersant and has a high molecular weight. The rheological effects therefore reduced the solvent-nonsolvent exchange rate and delayed demixing took place. A similar study on PVP-DMF-PSU system in the literature [20] showed that, at a low polyvinyl pyrrolidone (PVP) content, the system was dominated by a thermodynamic driving force, which increased the demixing process. At a high PVP content, however, they observed the same rheological effects as we did and concluded that the kinetic driving force dominated and suppressed the formation of macrovoids. We believe that when the LS content in the membrane was low (LS6 and LS12 membranes), the demixing process was thermodynamically controlled so that more macrovoids formed as the precipitation temperature increased. With a high LS content (LS17 membranes), however, kinetic hindrance dominated the demixing process so that the membrane morphologies were characterized as having fewer macrovoids and the precipitation temperature had less influence.

The cross-section images of LS12 and LS17 were analyzed by the IFME program to show their asymmetric properties. The results are shown in Table 3.

Table 3. Asymmetry analysis for LS12 and LS17 membranes at several precipitation temperatures

	LS12				LS17			
	11 °C	15 °C	20 °C	35 °C	11 °C	15 °C	20 °C	35 °C
Asymmetry %	9	11	13	15	7	10	10	16

Membranes with a homogeneous pore distribution and fewer macrovoids had low values of asymmetry. Table 3 shows that membrane tended to be more asymmetrical when it was precipitated at a high temperature and tended to be more symmetrical with a high LS content.

4.3.2 Contact angle measurement

Membrane surface hydrophilicity was analyzed by contact angle measurements. The results are listed in Table 4.

Table 4. Contact angles of membranes precipitated at different temperatures

	Contact angle [°]		
Precipitation temperature [°C]	LS6	LS12	LS17
11	63.38	62.27	56.82
15	58.94	55.70	60.07
20	61.99	65.94	60.11
35	62.52	59.16	58.63

In general, Table 4 shows that the precipitation temperature of membranes generated at 15 °C had low contact angles, i.e. membranes precipitated at 15 °C were more hydrophilic than the others. We also noticed that the membranes with more LS had lower contact angles because, as more sulfonic acid groups were incorporated, the membranes became more hydrophilic. Mass transport ability through membranes should increase as the hydrophilicity increases.

4.3.3 Membrane mass transport ability

LS6, LS12 and LS17 membranes were prepared from the casting solutions at 35 °C and precipitated in a water bath at different temperatures. The proton and methanol permeabilities are presented in Figures 12 and 13, respectively.

The proton permeabilities obtained with the LS6 and LS12 membranes behaved in the same way with respect to the precipitation temperature. At

a precipitation temperature of 15 ºC, we obtained membranes with the highest proton permeabilities.

Proton permeability obtained with the LS17 membranes behaved differently from that obtained with the LS6 and LS12 membranes, increasing as the precipitation temperature increased. Again we found that the LS content improved the proton permeability through the membrane, although there was an exception for LS17 precipitated at 11 ºC, whose proton permeability was not obviously higher than that of LS12 prepared under the same conditions. We also observed the same trend for the methanol permeability in Figure 13. As, for the acid membranes, proton and methanol are transported with the solvating water, when proton permeability is high, the corresponding methanol permeability is also high. These results perfectly matched those from our analysis of membrane morphology and hydrophilicity.

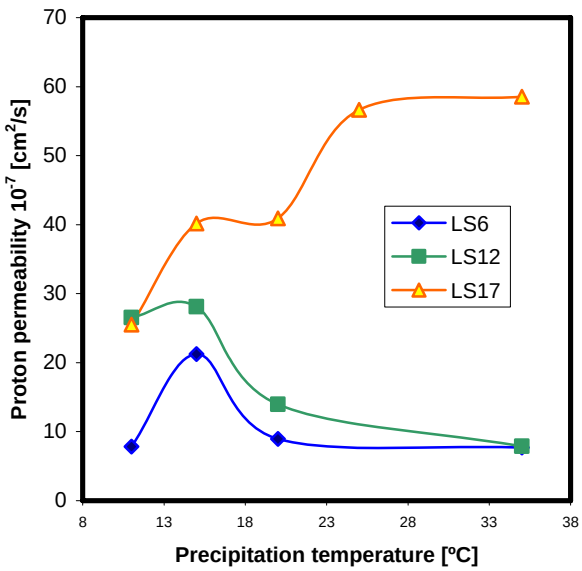

Figure 12. Effect of precipitation temperature on proton permeability for membranes LS6, LS12 and LS17.

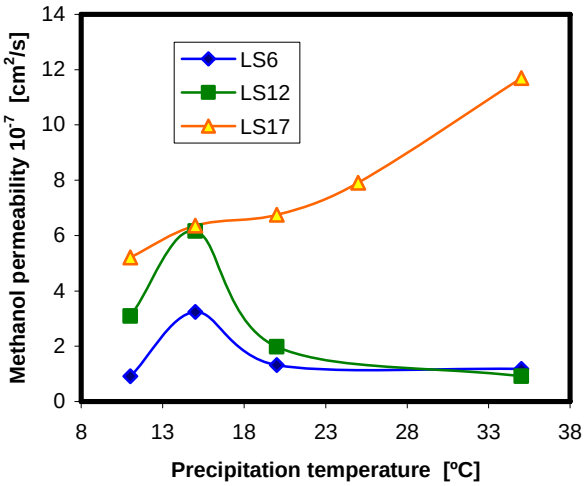

Figure 13. Effect of precipitation temperature on methanol permeability for membranes LS6, LS12 and LS17.

We selected several membranes and calculated their selectivity of proton to methanol according to Eq. (7) in Chapter 2. Figure 14 compares the results for the LS membranes with those for the Nafion 117 membrane. The LS membranes selected showed equal or even higher proton selectivity than Nafion 117.

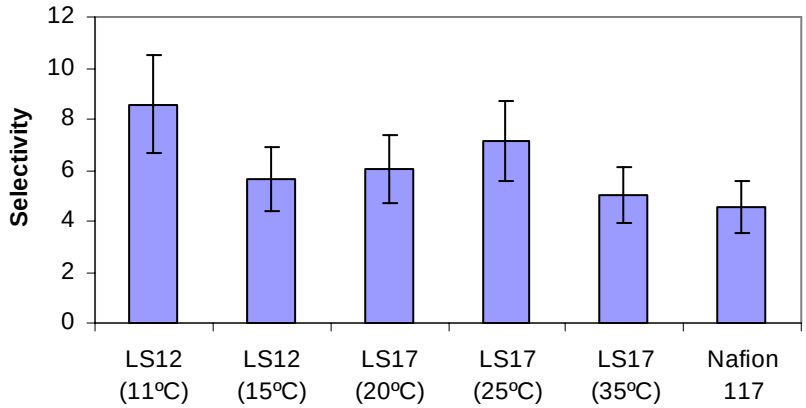

Figure 14. Selectivity values of proton over methanol for selected LS membranes and Nafion 117.

4.3.4 Membrane surface morphologies by AFM

AFM was used to determine membrane surface morphology. The tested membranes presented spherical nodules, nodule aggregates and supernodules. Nodules are partly fused spherical particles with a diameter of approximately 25-200 nm [21 - 24].

Clearly, different precipitation temperatures induced different arrangements of nodule and nodule aggregates on the film/bath surface of the LS6 membranes. At 11 ^{o}C (Figure 15), the nodules were of a different size, randomly distributed and arranged in a relatively compact form. At 15 ^{o}C (Figure 16), the nodules grew larger were shaped like water droplets. From their phase information images, we can see that the nodules were homogeneous in size and showed an ordered distribution. At 20 ^{o}C (Figure 17), nodule aggregates rather than nodules were present on the membrane surface. Clearly, at 35 ^{o}C (Figure 18), the nodules further aggregated into cluster-like domains of supernodules and the spaces between the domains were wider. This resulted in a floating islands arrangement with individual nodule visible at the edge of the cluster.

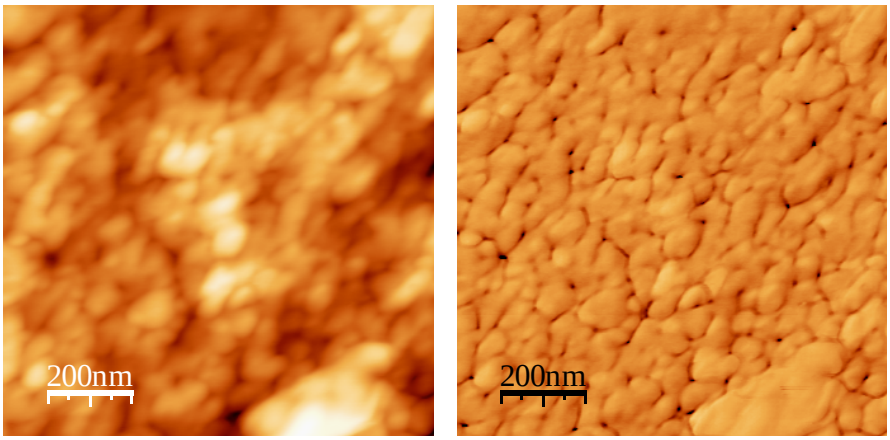

Figure 15. Topology and phase image of LS6 membrane precipitated at 11 ^{o}C.

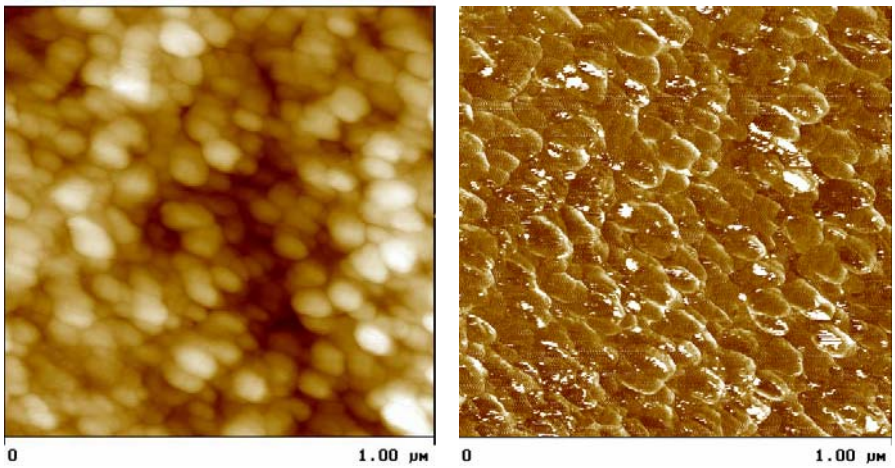

Figure 16. Topology and phase image of the LS6 membrane precipitated at 15 ºC.

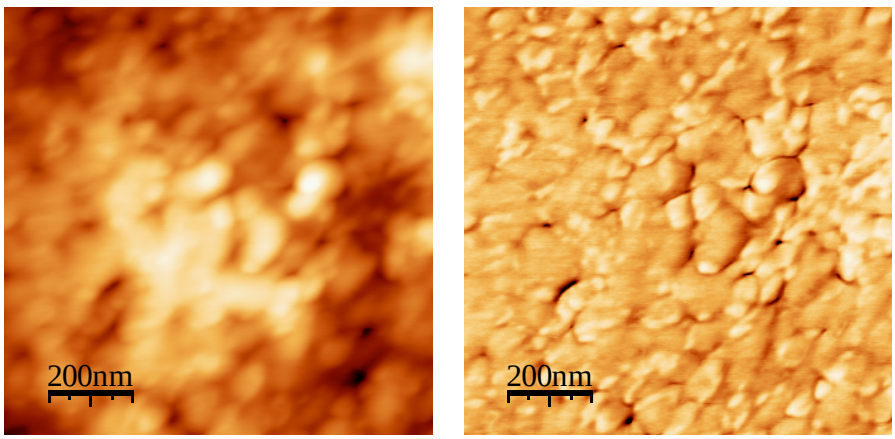

Figure 17. Topology and phase image of the LS6 membrane precipitated at 20 ºC.

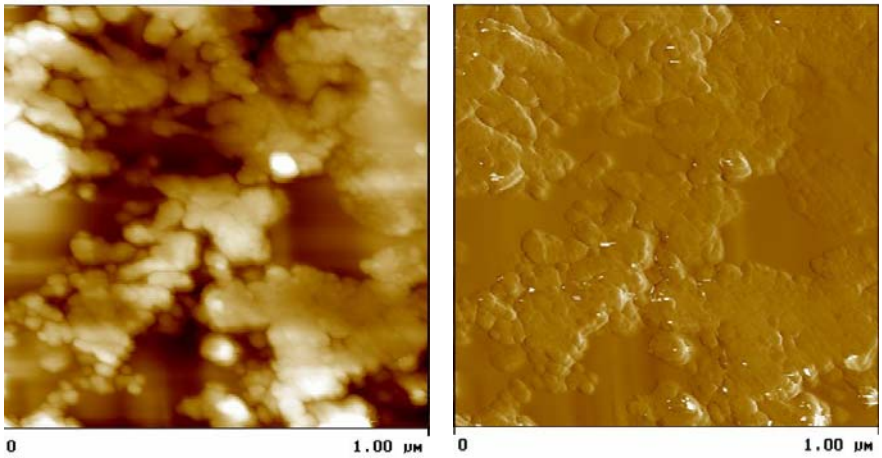

Figure 18. Topology and phase image of the LS6 membrane precipitated at 35 °C.

For LS12 membranes, we found that the effect of the precipitation temperatures on membrane topology was similar. At 15 °C (Figure 20), the topology showed an ordered compact nodular arrangement. At 20 °C (Figure 21), the nodules further aggregated and formed a looser structure between the nodules and the nodule aggregates. At 35 °C (Figure 22), the image was very similar to that of the LS6 membrane. The cluster-like supernodules were formed and distributed randomly.

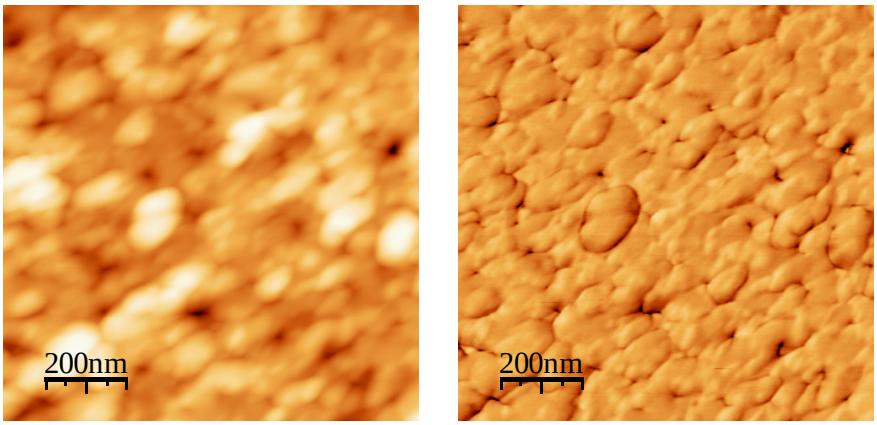

Figure 19. Topology and phase image of the LS12 membrane precipitated at 11 °C.

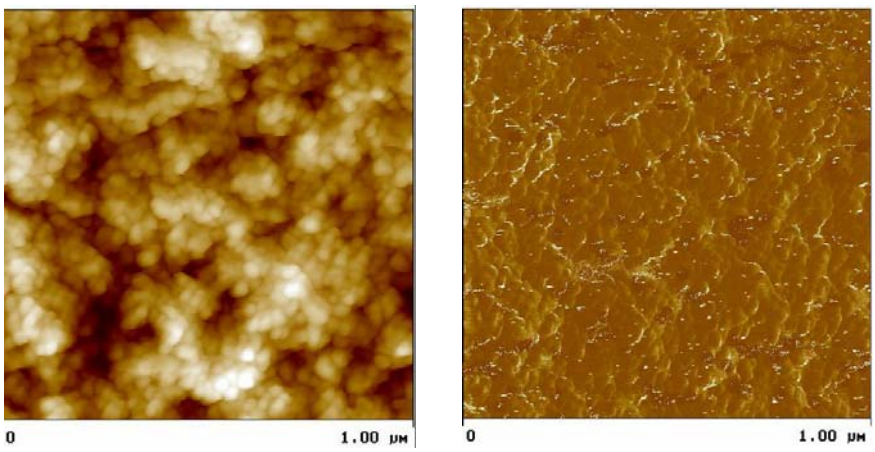

Figure 20. Topology and phase image of the LS12 membrane precipitated at 15 ºC.

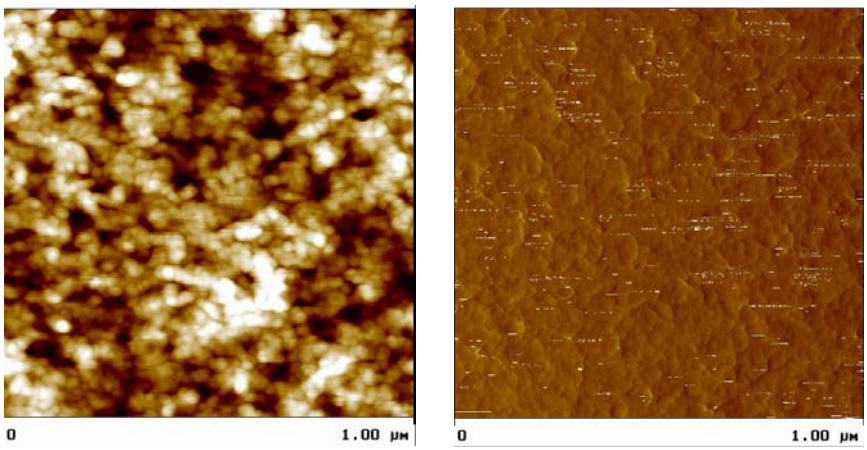

Figure 21. Topology and phase image of the LS12 membrane precipitated at 20 ºC.

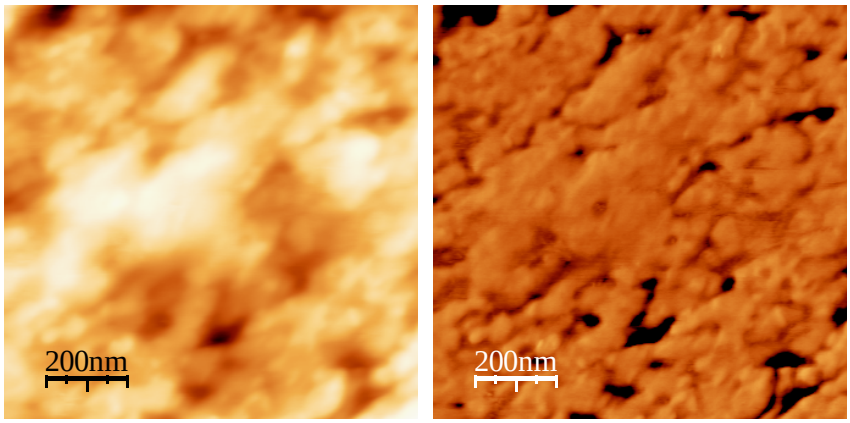

Figure 22. Topology and phase image of the LS12 membrane precipitated at 35 °C.

At the same time, we also studied the three-dimensional (3-D) images of the LS membranes. These images provided information about the global view of the membrane surfaces.

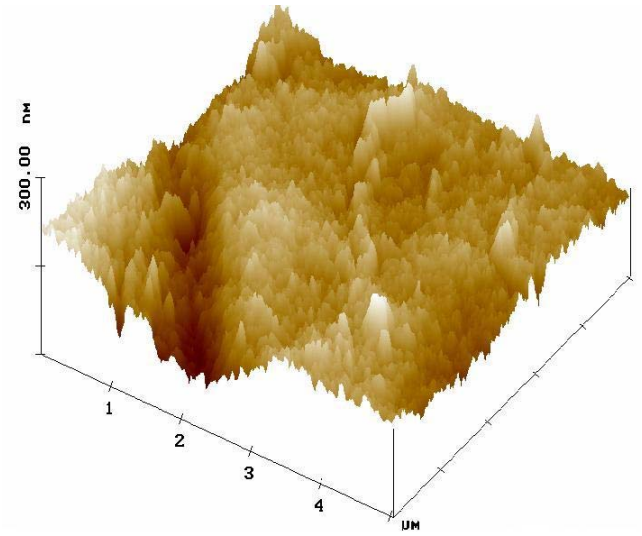

Figure 23. 3-D image of the LS6 membrane precipitated at 11 °C.

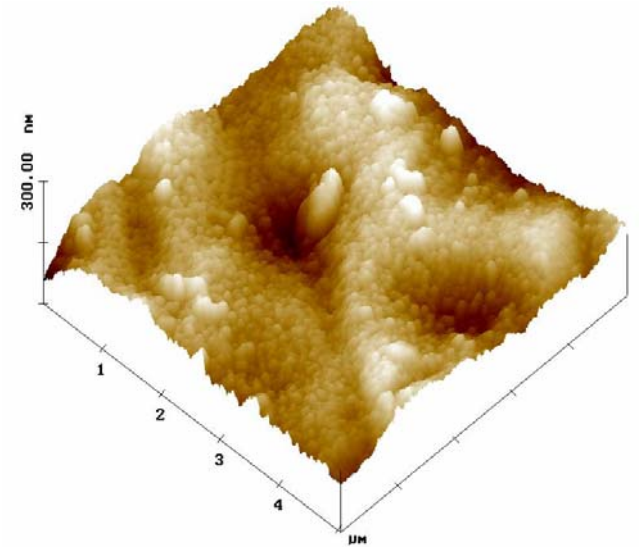

Figure 24. 3-D image of the LS6 membrane precipitated at 15 ºC.

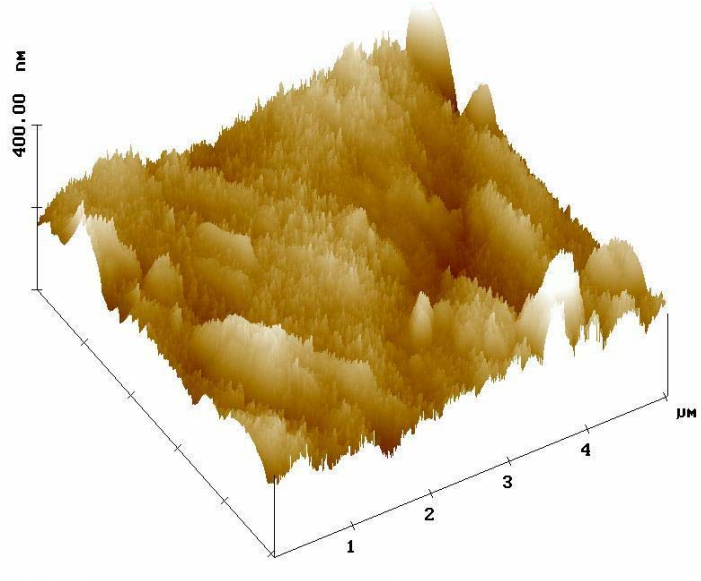

Figure 25. 3-D image of the LS6 membrane precipitated at 20 ºC.

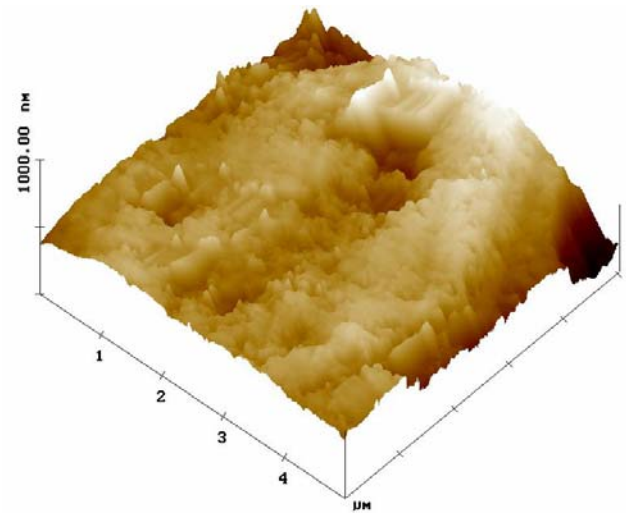

Figure 26. 3-D image of the LS6 membrane precipitated at 35 °C.

The above 3-D images are of LS6 membranes at different precipitation temperatures. The LS6 membranes at 11 °C had randomly distributed peaks of different heights due to the small and different nodule size. At 15 °C, the membrane surface had a relatively uniform nodular structure with a clear boundary, which means that the nodules were larger (around 120 nm) and homogeneous distributed. The nodule is considered to be the polymer chain deposited in a more orientated way [25, 26]. When the temperature increased to 20 °C, a large number of fine peaks with relative uniform height were present on the membrane surface, which probably because of the decreased nodule size. The nodules still maintained a relatively homogeneous distribution even though in some regions they aggregated and formed cluster-like domains. At 35 °C, the surface flattened out and no clear nodules were observed. This flattening of the surface may have been due to the surface tension and the restraining effect of contiguous nodule aggregates and supernodules [25].

Three-dimensional images were also obtained for the LS12 membranes. At 11 °C, the surface seemed flatter and smoother, which may suggest larger nodules and a relatively homogenous distribution. At 15 °C, we observed peaks instead of nodular structures on the membrane surface. When we compared this with the LS6 membrane at the same temperature, we deduced that the nodule size decreased as the LS content increased in the membrane. At 20 °C, the surface was full of fine homogeneous peaks,

which means that the nodules were smaller and homogeneously distributed, though nodule aggregates appeared occasionally. Finally, at 35 ºC, the flattened surface suggested the nodule aggregates and supernodules.

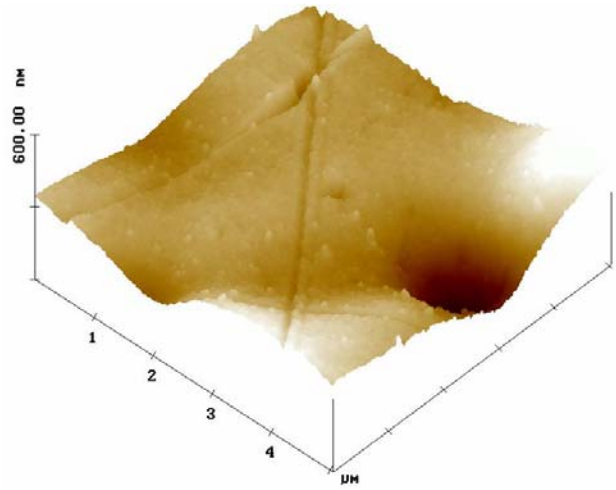

Figure 27. 3-D image of the LS12 membrane precipitated at 11 ºC.

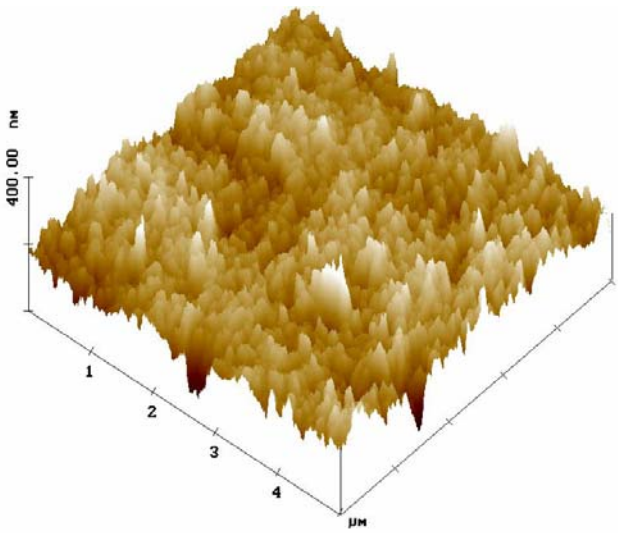

Figure 28. 3-D image of the LS12 membrane precipitated at 15 ºC.

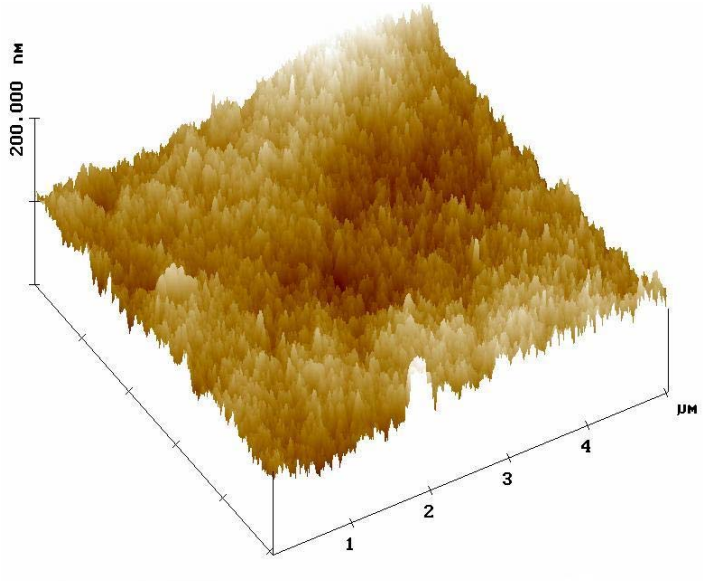

Figure 29. 3-D image of the LS12 membrane precipitated at 20 °C.

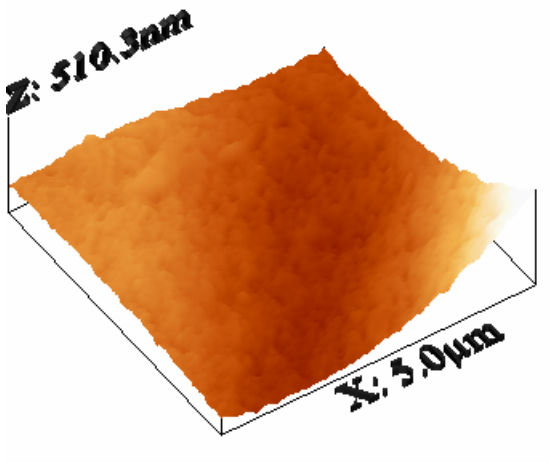

Figure 30. 3-D image of the LS12 membrane precipitated at 35 °C.

In general, for the LS6 and LS12 membranes, as the precipitation temperature increased, the size of the nodules of the LS6 and LS12 membranes first increased then decreased, their distribution became ordered and then disordered, the nodule or nodule arrangement was compact and then became looser, and the individual nodules tended to

aggregate into supernodules at high precipitation temperatures. The specific temperature (15 ^{o}C) was the turning point for the morphology change, which is closely related to the hydrophilicity of the membrane surface and helps to achieve high proton and methanol permeabilities.

When we observed the surface morphology of the LS17 membranes at different precipitation temperatures (Figures 31–38), we found that temperature did not significantly affect membrane topology and that all the membrane surfaces presented small nodule aggregates and few interstices. The 3-D images show that the membrane surfaces were quite regular, with low peaks or nodule aggregates, which suggests that a high LS content, rather than temperature, mainly influenced the LS17 membrane morphology.

To understand how the precipitation temperature and LS content influenced membrane morphology, we must begin with the demixing process. When studying the solvent-nonsolvent exchange, Ambrosone et al. [27] suggested that in the case of skin layer formation, more solvent flowed out of the solution than nonsolvent flowed into the solution, which led to an increase in polymer concentration at the interface. In section 4.3.1 we reported that LS can enhance the demixing but that it can also cause kinetic hindrance for the demixing. We conclude that the formation of the LS6 and LS12 membranes was thermodynamially controlled, so the precipitation temperature greatly influenced the membrane morphology. For the LS17 membranes, on the other hand, kinetic hindrance was dominant. Kesting [25] suggested that, before and after phase inversion, nucleation and growth of polymer-rich particles into progressively larger particle aggregates took place. These particles corresponded to nodules or nodule aggregates.

With regard to the formation of the LS6 and LS12 membranes, therefore, when the precipitation temperature increased, the kinetic hindrance started to decrease and the solvent-nonsolvent exchange rate increased under thermodynamic control. This increased the polymer concentration at the interface and formed polymer-rich phase nuclei. The nuclei then grew and formed larger nodules and nodule aggregates. At the same time, more nonsolvent entered the interface and formed interstices, which corresponded to a low-polymer-density region or pores [25, 26]. The membrane morphologies at 15 ^{o}C suggested the existence of a relatively homogeneous local polymer solution and a moderate solvent-nonsolvent exchange rate, probably because the kinetic hindrance and thermodynamic control reached equilibrium. Under this equilibrium, the nuclei grew to more uniform-sized nodules and the nodules were distributed in order.

With regard to the formation of the LS17 membrane, kinetic hindrance dominated the demixing process, so the solvent-nonsolvent exchange rate did not increase as the precipitation temperature increased. Since the polymer concentration at the interface hardly changed, the LS17 membranes showed similar nodule aggregate morphologies at different precipitation temperatures. As less nonsolvent entered the polymer network than with the LS6 and LS12 membranes, fewer interstices formed between the nodule aggregates.

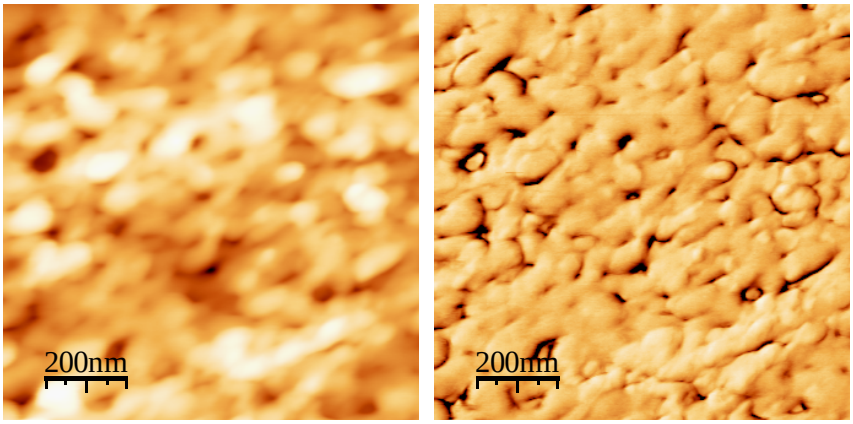

Figure 31. Topology and phase image of LS17 membranes precipitated at 11 °C.

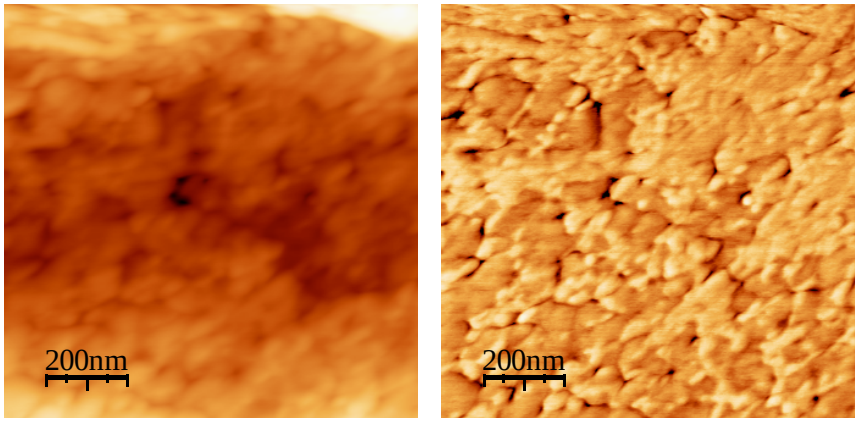

Figure 32. Topology and phase image of LS17 membranes precipitated at 15 °C.

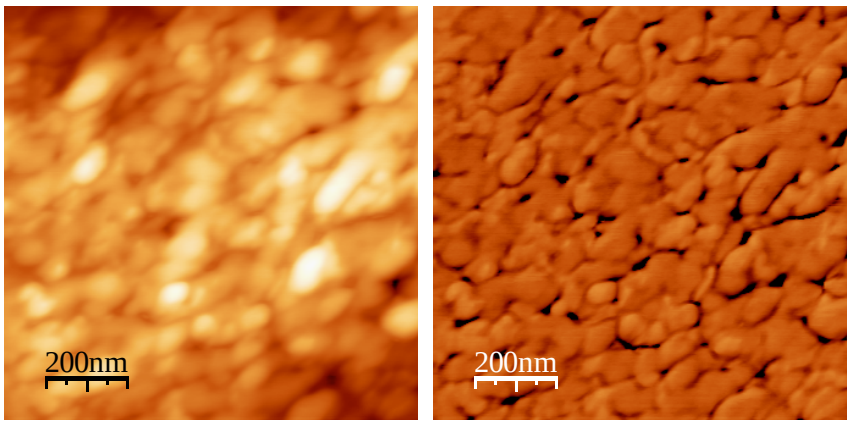

Figure 33. Topology and phase image of LS17 membranes precipitated at 20 ºC.

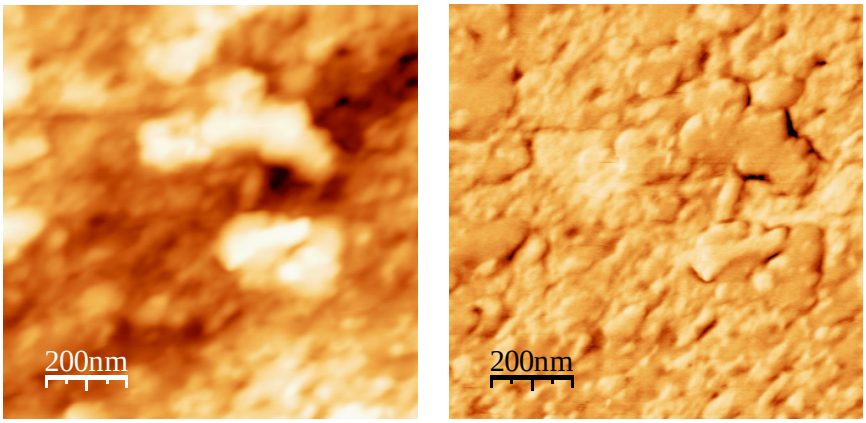

Figure 34. Topology and phase image of LS17 membranes precipitated at 35 ºC.

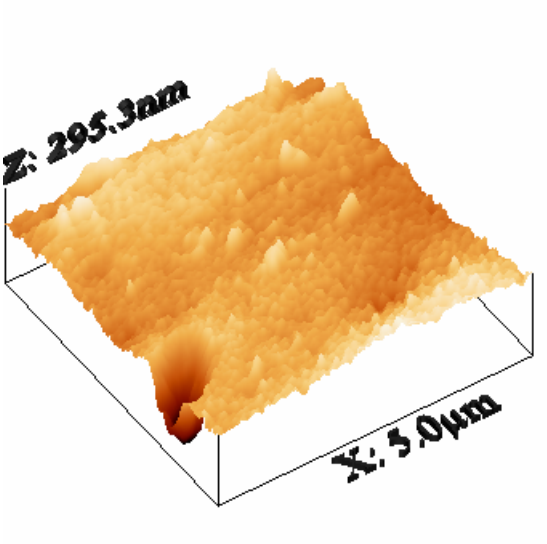

Figure 35. 3-D image of the LS17 membrane precipitated at 11 °C.

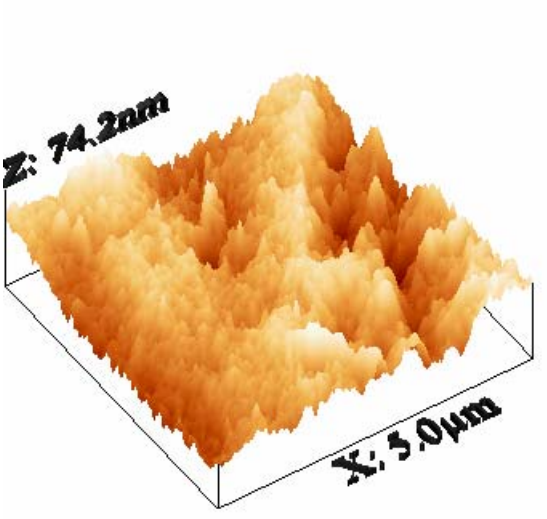

Figure 36. 3-D image of the LS17 membrane precipitated at 15 °C.

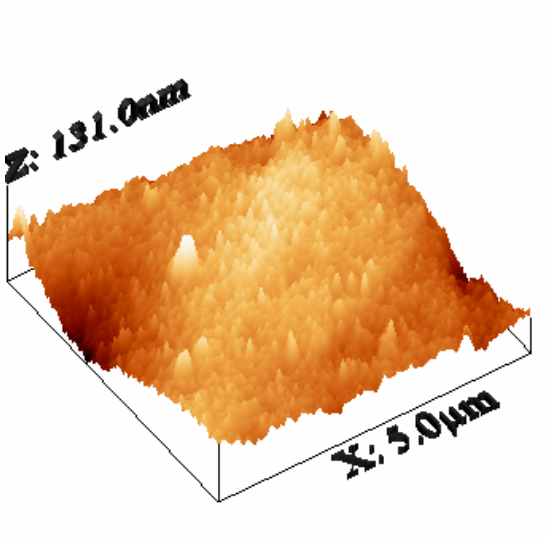

Figure 37. 3-D image of the LS17 membrane precipitated at 20 ºC.

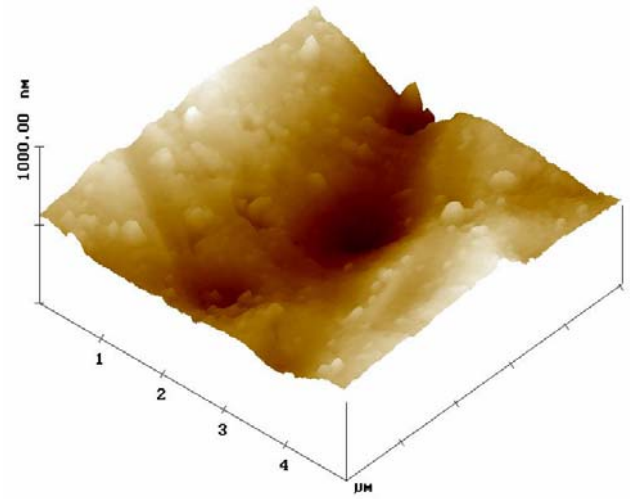

Figure 38. 3-D image of the LS17 membrane precipitated at 35 ºC.

The roughness of the membrane surfaces was also analyzed using SPIP software. The results are shown in Figure 39.

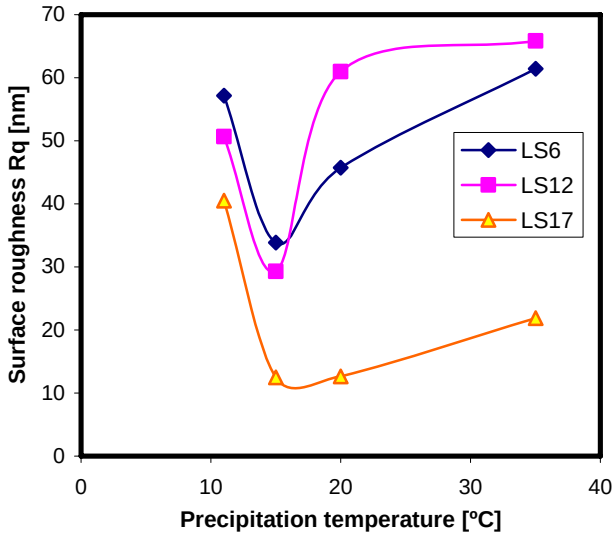

Figure 39. Effect of precipitation temperature on the roughness of the membrane surface.

The roughness of the surfaces of the LS6 and LS12 membranes, precipitated at 15 ºC, was the lowest of all membranes with the same LS content. Almost all the surfaces of the LS17 membranes were less rough than those of membranes with lower LS contents. This suggests that when the nodules and nodule aggregates were homogeneously distributed and there were fewer interstices, the roughness of the membrane surface was lower.

4.4 Effect of the composition of the precipitation solution

Two LS17 membranes (LS17-1 and LS17-2) were obtained by precipitating in pure IPA solution and 50%IPA/50%H_2O solution (IPAW), respectively. Their cross-section morphologies are shown in Figure 40. Image 40.a shows the morphology of the LS17 membrane precipitated in IPA. We can see that it is different from that of the other membranes. There were two distinct regions: the sublayer of the membrane showed a round and closed porous structure with some macrovoids, while the top layer of the membrane (image 40.b) showed flattened and closed pores, suggesting that the pores had not been completely formed during the demixing process, perhaps because the delayed demixing process tended to form a dense layer that was not completed. The LS17 membrane precipitated in

IPAW solution (image 40.c) was twice as thick and had more macrovoids than the LS17 membrane precipitated in IPA. This could be because of the greater affiliation between DMF and IPAW and because instantaneous demixing took place.

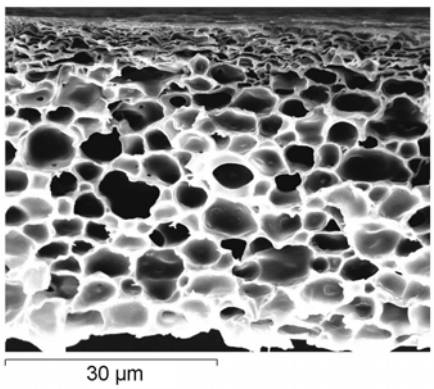

a

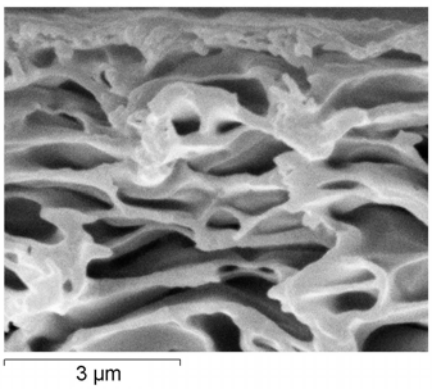

b

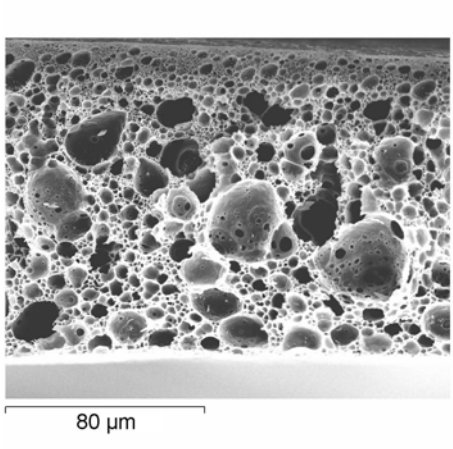

c

Figure 40. SEM cross-section images of LS17 membranes precipitated at different baths (a: IPA; b: enlarged images of top layer of image a; c: IPA/H_2O).

These different structures also influenced mass transport ability, as we can

see in Table 5. LS17-1 showed lower proton and methanol permeabilities than LS17-2, probably due to the denser top layer of the LS17-1 membrane and the less resistant structure (i.e. there were more macrovoids) of LS17-2 membrane.

Table 5. Proton and methanol permeabilities of the LS17-1 and LS17-2 membranes

	Membranes	
Permeability 10^{-8} [cm^2/s]	LS17-1	LS17-2
Proton	5.92	11.35
Methanol	0.76	3.88

AFM revealed the surface morphology of these two membranes (see Figures 41 and 42).

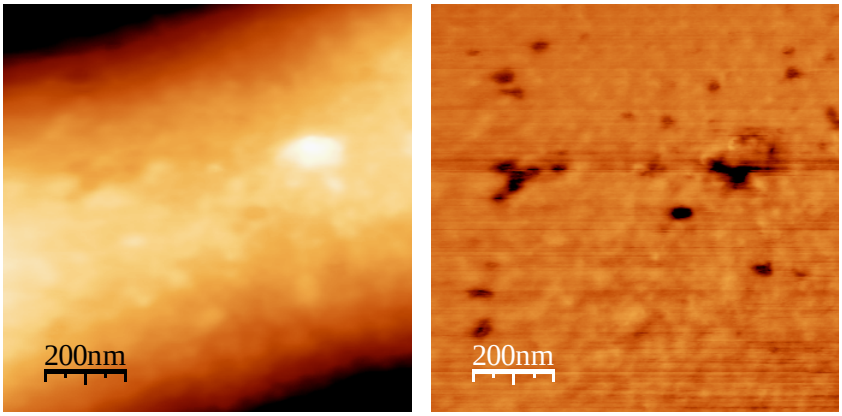

a b

Figure 41. Topology and phase images of the LS17-1 membrane precipitated in IPA.

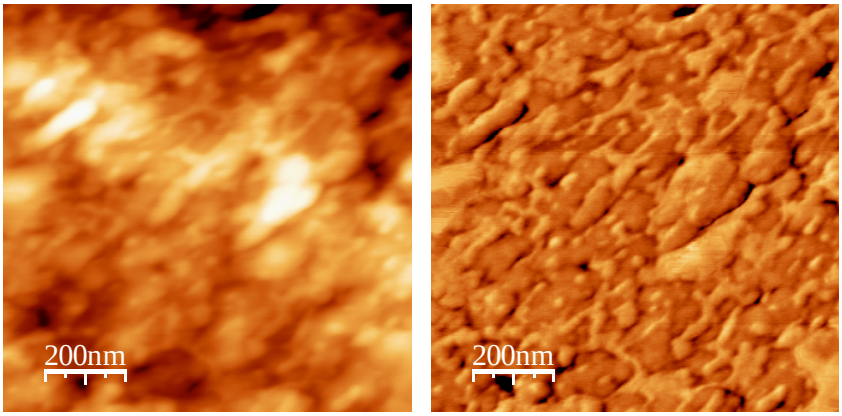

a b

Figure 42. Topology and phase images of the LS17-2 membrane precipitated in IPAW.

Unlike the LS17 membrane precipitated in water, the LS17 membranes precipitated in IPA and IPAW presented a random distribution of nodule aggregates and supernodules. The roughness R_q for LS17-1 was 107.51 nm and for LS17-2 it was 30.49 nm, which confirmed that roughness was closely related to nodule distribution.

4.5 Correlation of membrane morphology with its transport ability

Interestingly, the surface roughness (see Figure 39) and contact angles (see Table 4) of the membrane were generally inversely proportional to mass transport ability (see Figures 9 and 10).

SEM and AFM suggested that a precipitation temperature of 15 ^{o}C generated membranes of a relatively larger and uniform nodule size and that the nodules and nodule aggregates were distributed in a more orientated way. A higher LS content tended to form larger and more regular aggregates without excess interstices. Transport experiments showed that membranes generated at 15 ^{o}C (the LS6 and LS12 membranes) showed the highest proton and methanol transport abilities and that a higher LS content (LS17 membranes) led to greater permeation.

The arrangement of the macromolecules within the nodule may therefore be a determining factor for mass transport, since the macromolecule concentration decides the nodule size and the way the macromolecules are deposited could influence the nodule shape and aggregation

arrangement. A membrane with large and regularly distributed nodules or nodule aggregates on the skin layer (also called the selective layer) should lead to high permeation.

5 Conclusions

A higher PSU concentration in the casting solution generated denser LS hybrid membranes that proved to be better methanol barriers.

The optimal temperature of the casting solution was 35 ^{o}C according to the high proton permeability.

When the LS concentration in the casting solution was less than 3 wt.%, a higher precipitation temperature led to more asymmetrical membranes with smaller pores. Also, the membrane surface was rougher and had more randomly distributed nodule aggregates. These characteristics correlated with a lower mass transport ability. The optimal precipitation temperature was 15 ^{o}C. This temperature generated membranes with a unique surface morphology and the highest mass transport ability. We believe that the precipitation temperature played a more important role than LS content in membrane morphology and transport ability.

When the LS concentration in the casting solution was 3 wt.%, the membranes had fewer macrovoids in the cross-section and regularly distributed nodule aggregates on the surface or top layer. We believe that the kinetic hindrance of LS made the greatest contribution to the membrane morphology and high proton and methanol permeabilities, while the precipitation temperature had a secondary influence.

We suggest that the arrangement of the macromolecules within the nodule is a determining factor for the mass transport.

Compared to Nafion 117, the LS membranes showed the same level proton permeability (1.0×10^{-6} to 6.0×10^{-6} cm^2/s) and less methanol crossover ($<1.2\times10^{-6}$ cm^2/s), which suggests that they can be applied in DMFCs.

Future research should test other properties of LS membranes, such as their thermal and mechanical properties and long-term stability.

References

[1] A. Glüsen, D. Stolten Membranen für Polymerelektrolyt Brennstoffzellen, Chemie Ingenieur Technik 75 (2003) 1591-1597

[2] C.W. Lin, R. Thangamuthu, C.J. Yang, Proton-conducting membranes with high selectivity from phosphotungstic acid-doped poly(vinyl alcohol) for DMFC applications, Journal of Membrane Science 253 (2005) 23

[3] Jinhwan Kim, Bokyung Kim, Bumsuk Jung, Proton conductivities and methanol permeabilities of membranes made from partially sulfonated polystyrene-block-poly(ethylene-ran-butylene)-block-polystyrene copolymers, Journal of Membrane Science 207 (2002) 129–137

[4] F.G. Wilhelm, I.G.M. Pünt, N.F.A. van der Vegt, H. Strathmann, M. Wessling Cation permeable membranes from blends of sulfonated poly(ether ether ketone) and poly(ether sulfone), Journal of Membrane Science 199 (2002) 167–176

[5] Carmen Manea, Marcel Mulder, Characterization of polymer blends of polyethersulfone/sulfonated polysulfone and polyethersulfone/sulfonated polyetheretherketone for direct methanol fuel cell applications, Journal of membrane Science 206 (2002) 443–453

[6] J. Kerres, A. Ullrich, F. Meier, T. Häring Synthesis and characterization of novel acid-base polymer blends for application in membrane fuel cells, Solid State Ionics 125 (1999) 243-249

[7] J.-M. Bae, I. Honma, M. Murata, T. Yamamoto, M. Rikukawa, N. Ogata Properties of selected sulfonated polymers as proton-conducting electrolytes for polymer electrolyte fuel cells, Solid State Ionics 147 (2002) 189-194

[8] D. J. Jones, J. Rozière Recent advances in the functionalisation of polybenzimidazole and polyetherketone for fuel cell applications, Journal of Membrane Science 185 (2001) 41-58

[9] J. Kim, B. Kim, B.Jung, Journal of Membrane Science, 207 (2002) 129-137

[10] N. Carretta, V. Tricoli, E. Picchioni, Journal of Membrane Science, 166 (2000) 189-197

[11] Carles Torras-Font and Ricard Garcia-Valls, A new tool to interpret membrane photographs made by scanning electronic microscopy: the IFME© software, Journal of Membrane Science 233(2004)119-127

[12] Thorsten Schultz, Su Zhou, and Kai Sundmacher, Current Status of and Recent developments in the Direct Methanol Fuel Cell, Chem. Eng. Technol. 24 (2001) 12

[13] Anne-Laure Rollet, Gérard Gebel, Jean-Pierre Simonin, Pierre Turq, A SANS Determination of the Influence of External Conditions on the Nanostructure of Nafion Membrane, Journal of Polymer Science: Part B: Polymer Physics 39 (2001) 548-558

[14] M. Eikerling, A. A. Kornyshev, A. M. Kuznetsov, J. Ulstrup, S. Walbran Mechanisms of Proton Conductance in Polymer Electrolyte Membranes, J. Phys. Chem. B 105 (2001) 3646-3662

[15] M. Eikerling, Y. I. Kharkats, A. A. Kornyshev, Y. M. Volfkovich Phenomenological Theory of Electro-osmotic Effect and Water Management in Polymer Electrolyte Proton-Conducting Membranes J. electrochem. Soc. 145 (1998) 2684-2699

[16] Heinzel, V.M. Barragan, A review of the state-of-the-art of the methanol crossover in direct methanol fuel cells, J. power Sources, 84 (1999) 70-74

[17] D. Fengel, G. Wegener, Wood Chemistry, Ultrastructure, Reactions, Walter de Gruyter, Berlin, 1984, pp157-163

[18] P. van de Witte, p.j. Dijkstra, J.W.A. van den Berg, J. Feijen, Phase separation processes in polymer solutions in relation to membrane formation, Journal of Membrane Science 117 (1996) 1-31

[19] Marcel Mulder, Basic principles of Membrane Technology, second ed., Kluwer Academic publishers, 2003,

[20] Kune-Woo Lee, Bum-Kyoung Seo, Suk-Tae Nam, Myeong-.Tm Han, Trade-off between thermodynamic enhancement and kinetic hindrance during phase inversion in the preparation of polysulfone membranes, Desalination 159 (2003) 289-296

[21] A. Lehmani, S. Durand-Vidal, P. Turq, Surface morphology of Nafion 117 membrane by tapping mode atomic force microscope, Journal of Applied Polymer Science 68 (1998) 503

[22] Jin Liu, Huanting Wang, Shaoan Cheng, Kwong-Yu Chan, Nafion-polyfurfuryl alcohol nanocomposite membranes for direct methanol fuel cells, Journal of Membrane Science 246 (2005) 95-101

[23] R. M. Boom, I.M. Wienk, T. Van den Boomgaard and C.A. Smolders, Microstructures in phase inversion membranes: Part 2. The role of the polymeric additive, Journal of Membrane Science 73 (1992) 277

[24] M. Panar, H.H. Hoehn and R.R. Hebert, The nature of asymmetry in reverse osmosis membranes, Macromolecules 6 (1973) 777

[25] R.E. Kesting, The four tiers of structure in integrally skinned phase inversion membranes and their relevance to the various separation regimes, Journal of Applied Polymer Science 41 (1990) 2739-2752

[26] K.C. Khulbe, B. Kruczek, G. Chowdhury, S. Gagne and T. Matsuura, Surface morphology of homogeneous and asymmetric membranes made from Poly(phenylene oxide) by tapping mode atomic force microscope, Journal of Applied Polymer Science 59 (1996) 1151-1158

[27] L. Ambrosone, G. Guarino, R. Sartorio, V. Vitagliano, Diffusion in the system Poly(vinylidene fluoride)-water-dimethylformamide at 20 ^{o}C. Implication for the membrane casting process, Journal of Membrane Science, 45 (1989) 299

Chapter 5

Hybrid lignosulfonate membrane (II): electrochemical characterization and fuel cell performance

1 Introduction

In Chapter 4, we have discussed the preparation and mass transport ability of the hybrid lignosulfonate (LS) membranes. If LS membranes are to apply in the fuel cell system, their proton conductivities under various conditions are key parameters to determine the applicability in a direct methanol fuel cell (DMFC).

In this Chapter, we measured the proton conductivity of LS membranes by impedance spectroscopy under several conditions. Then LS membranes with acceptable proton conductivity were tried to fabricate the membrane electrode assemblies (MEAs). MEA is the basic electrical unit of a single DMFC. It can be prepared by several ways:

The traditional method is to prepare electrodes by spraying catalytic active material onto the diffusion backings, and then the proton exchange membrane is sandwiched between the anode and cathode by hot-pressing. Gottesfeld etc. [1, 2] prepared MEAs by transferring a catalyst layer from polytetrafluoroethylene (PTFE) to the proton exchange membrane. Another approach is to coat both side of the membrane with catalyst suspension (catalyst ink) to form a three-layer MEA [3]. Gülzow et al. [4], using a dry-sprayer for the catalytic coating of the backing or the

membrane, combined with a rolling step to bond and fix the functional layers.

For each new type of proton exchange membranes, many attempts should be carried out to find the most suitable method to fabricate MEA. LS membranes are completely new, they are porous, thinner, and more hydrophobic compared to other dense membranes – PFSA membranes. In this Chapter, we found out the way to fabricate MEA from LS membranes, but it still requires more sophisticated investigation on MEA fabrication to lead to a better performance in a DMFC test rig.

2 Membrane characterization

2.1 Lignosulfonate membranes

LS membranes were prepared as described in Chapter 4. Preparation conditions were: the temperature of the casting solution 35 ^{o}C, the precipitation bath temperature 11 ^{o}C, PSU content in the casting solution 15 wt%. The physical and chemical properties of LS membranes are listed in Table 1.

Table 1. Membrane properties

Membrane	LS content in the dry membrane [wt. %]	Casting conditions		Dry membrane density [g/cm^3]	Average membrane thickness [μm]	Theoretical gravimetric IEC [meq/g]	Theoretical volumetric IEC [meq/cm^3]
		LS content in the casting solution [wt. %]	Precipitation bath solution				
LS6	6.25	1	Water	0.2731	86	0.054	0.0148
LS12	11.70	2	Water	0.2593	89	0.102	0.0264
LS17	16.70	3	Water	0.2143	110	0.144	0.0309
LS17/IPA	16.70	3	IPA	0.3063	77	0.144	0.0438
LS17/IPAW	16.70	3	50%IPA/Water	0.1833	155	0.144	0.0265
Nafion 117	-	-	-	1.98	178	0.909	1.8

The theoretical gravimetric IEC (meq/g) was calculated as

$$IEC_{gravimetric} = \frac{LS_{content} \times Acid_{content}}{M_{acid}} \times 1000 \qquad (1)$$

where, $LS_{content}$ refers to the LS content in the dry membrane, $Acid_{content}$ refers to the sulfonic acid groups content (8.4 wt.%) which was provided by Lignotech Borregaard, M_{acid} refers to the molecular weight of the sulfonic acid.

The theoretical volumetric IEC (meq/cm^3) was calculated as

$$IEC_{volumetric} = IEC_{grametric} \times Density_{drymembrane} \quad (2)$$

From Table 1, we see that LS content and precipitation bath composition influence on the resulting membrane density. When the precipitation bath was deionized water, a high LS content reduced the membrane density. When the precipitation bath solution was isopropanol (IPA), the membrane has higher density. Membranes precipitated in a 50% IPA/water bath solution (IPAW), happened to be more porous. The gravimetric, and particularly the volumetric, IEC were much lower than the standard material Nafion 117.

2.2 Water uptake measurement

Membrane samples were cut to the size of 42 mm × 42 mm and weighed after 2 h in a 130 ^oC oven. Then, membrane samples were put into a water bath at 60 ^oC and 80 ^oC for 2 h and the bath was allowed to cool to room temperature. The membrane was immediately weighed and measured after the membrane surface had been wiped dry with filter paper. Finally, the water uptake was calculated by

$$uptake(\%) = \frac{W_{wet} - W_{dry}}{W_{dry}} \times 100 \quad (3)$$

We used Nafion 1135 as a reference because it was as thick as the LS membranes. The results are listed in Table 2. Since no dimensional change was observed for all the tested LS-membranes after the swelling experiments, we can conclude that LS membranes took water into its pores other than dimensional swelling, which was due to its porous property and rigid and hydrophobic PSU chains. Nafion 1135 swelled by 8-10% in each direction, because of the more flexible backbone of the

Nafion polymer. Higher temperatures increased the water uptake for LS membranes and Nafion 1135. This and the fact that even the swollen LS membranes have densities of less than 1 g/cm^3 indicates that some pores are not accessible at 60 °C but become accessible at 80 °C while other pores are not accessible even at 80 °C.

The membrane density is related to the water uptake capacity. Low density membranes contain more pores, which results in high water uptake.

Table 2. Membrane water uptake at different temperatures

Membrane	Water uptake [%]	
	60 °C	80 °C
LS6	131.76	156.62
LS12	162.71	185.44
LS17	245.03	282.95
LS17/IPA	89.18	93.03
LS17/IPAW	313.55	321.98
Nafion 1135	23.67	31.45

2.3 Membrane protonation

Membrane samples were put into 3.0 M H_2SO_4 solution at 60 °C for 1 h. Then, they were rinsed with deionized water, and put into deionized water at 80 °C for 1 h. Finally, the protonated membranes were rinsed with deionized water and stored in deionized water.

2.4 Proton conductivity measurement

Two cells were used to measure the membrane conductivity. Cell 1, a four-point probe conductivity measuring cell [5] made of Teflon, was used to measure the conductivity under different humidities and temperatures.

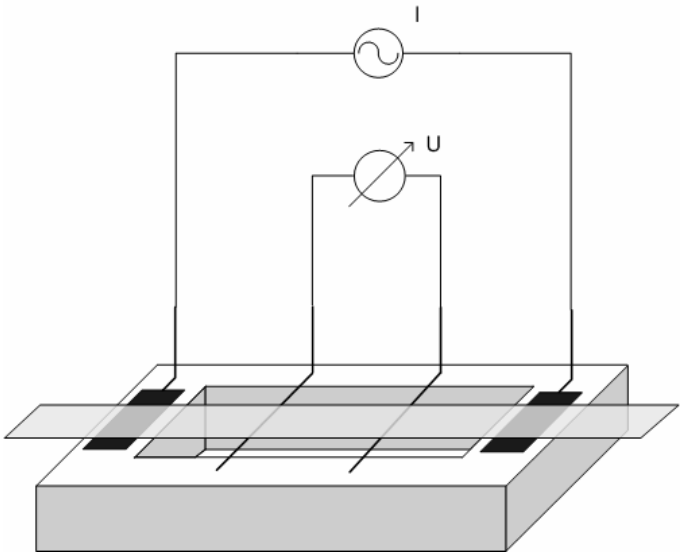

Figure 1. 4-Electrode AC-Impedance measurement cell.

It consisted of two platinum current-carrying electrodes (distance 3 cm) and two platinum potential-sensing electrodes (distance 1 cm). The cell was placed in a home built environmental chamber which allowed the cell temperature and relative humidity to be controlled independently [6].

Cell 2 is shown in Figure 1 and has the same structure as cell 1. The distance between the potential-sensing electrodes is 2 cm and the distance between the current-carrying electrodes is 4 cm. The cell was placed in a water bath and the conductivity was measured at different temperatures.

The testing sample was a piece of membrane about 10 cm long and 1 cm wide and was fixed in the cell. The membrane resistance was measured by Impedance Spectroscopy (Potentiostat / Galvanostat model 273A, EG&G Princeton Applied Research). The frequency swept from 65535 Hz to 100 Hz. The data were analyzed by Z plot software.

The conductivity was calculated using

$$\sigma = \frac{d}{RS_c} \qquad (4)$$

where σ, d, R, Sc refer, respectively, to proton conductivity (S/cm), the potential-sensing electrode distance (cm), the membrane resistance (Ω) and the membrane cross-section area (cm^2).

We tested the conductivities of LS12 and LS17 membranes using cell 1 under different humidities and temperatures. The results are presented in

Figure 2 and Figure 3. Membrane conductivity increases as the humidity and temperature increase.

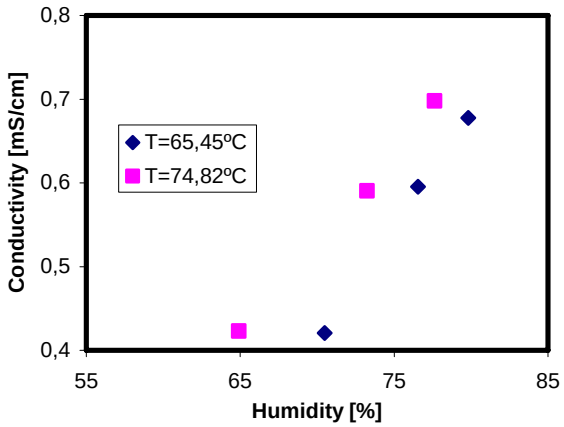

Figure 2. The effect of humidity on the proton conductivity of a protonated LS12 membrane at different temperatures.

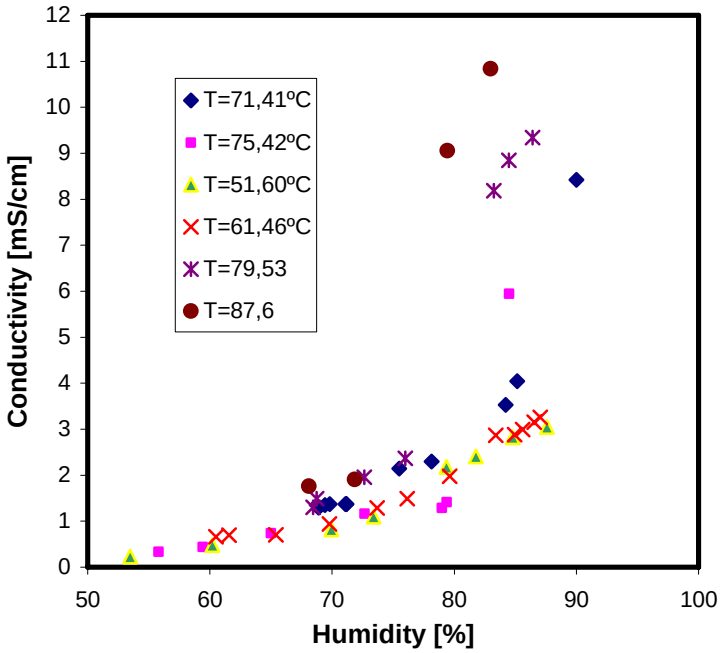

Figure 3. The effect of humidity on the proton conductivity of a protonated LS17 membrane at different temperatures.

After immersing the membrane in the water bath, we measured membrane conductivity over time by using cell 2. Figure 4 shows that membrane conductivity improved slightly with the equilibration time in water. After two hours, membrane conductivity reached a plateau. This suggested that the conductivity of LS membranes depends on the water uptake, which agrees with the conductivities measured under different humidities.

If comparing the conductivity values obtained from vapor and liquid water phase, we found that the proton conductivity was much lower in the vapor phase than that in the liquid phase. This could be due to the difficulty of condensing water vapor within the micropores of the membrane [7, 8].

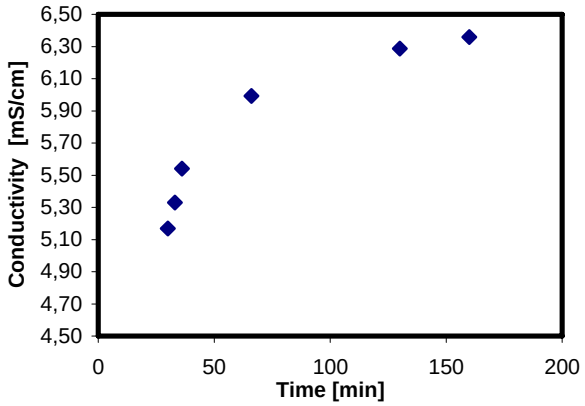

Figure 4. The effect of water uptake time on membrane conductivity at 40 ^{o}C.

Figure 5 shows the conductivities of LS membranes and Nafion 117 measured by cell 2 at different temperatures. Higher temperatures led to higher conductivities for all the membranes. It is also clear that Nafion 117 showed higher conductivity than LS membranes because its IEC was higher. Likewise, LS membranes with higher IEC showed increased conductivity. Therefore, increasing the LS content in the membrane will improve membrane conductivity.

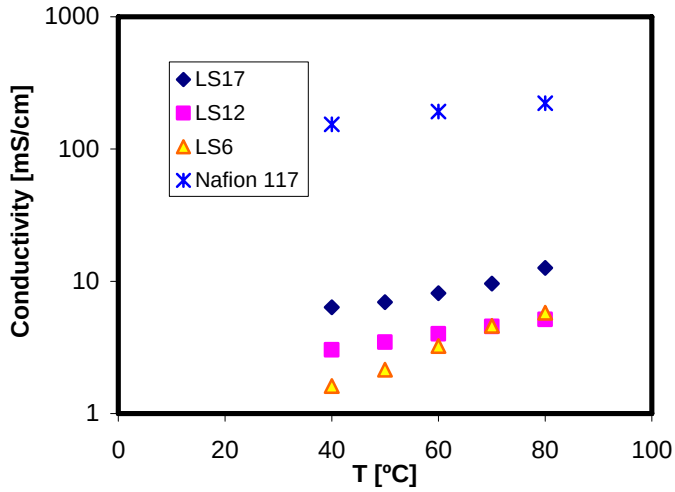

Figure 5. Logarithmic plot of proton conductivity of LS membranes and Nafion 117 at different temperatures.

LS membrane conductivity also depends on the precipitation bath solution (Figure 6). At the same LS content, the conductivity of the membranes precipitated in a water bath was higher than the conductivity of those precipitated in other solutions, which was coherent with the conclusion drawn from Chapter 4.

As we observed when measuring the water uptake with IPA as the precipitation bath solution, the membrane was denser and took up much less water, which resulted in lower conductivity. However, LS17/IPAW showed lower conductivity than LS17 although LS17/IPAW took more water than LS17. Obviously the IEC, water uptake and precipitation solvent all play a role in membrane conductivity. It should be pointed out that the conductivity of the LS17 membrane is fifteen times lower than that of Nafion, while the volumetric acid group density is sixty times lower. The general expectation is that conductivity should be reduced more than the acid group density, because even if only a few acid groups are removed, some conduction pathways will be broken. This leads us to conclude that by choosing the right precipitation solvent, the acid groups can be directed into a very favorable steric arrangement.

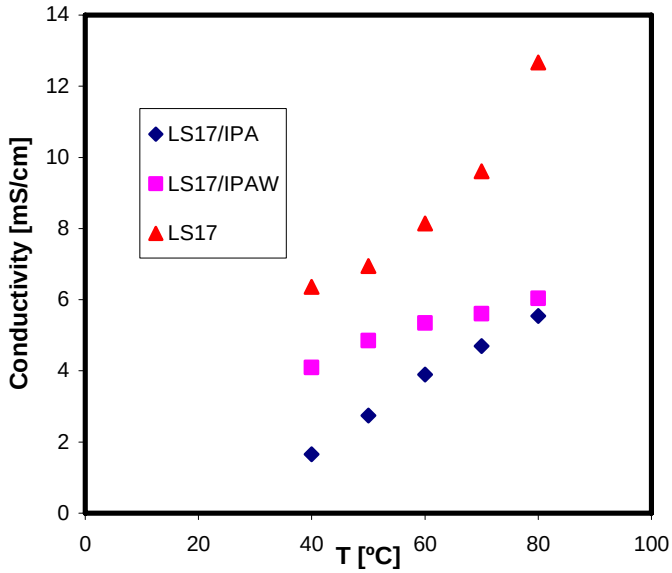

Figure 6. The effect of the precipitation bath solution on membrane conductivity.

3 Fabrication of the membrane electrode assemblies (MEAs)

3.1 Catalyst inks preparation

The catalyst ink for the cathode was prepared by proportionally mixing 57.2% Pt/C (Johnson Matthey Hispec 9100) with deionized water, 5% Nafion solution (Fluka Chemika) and isopropanol (IPA). The catalyst ink for anode was prepared by proportionally mixing 40% PtRu/C (Heraeus) with deionized water, 5% Nafion solution and IPA. The suspension was mixed by ultrasound for 10 min at room temperature. The suspension was then further mixed by ultraturrax (High shear rotor-stator system).

A study [9] suggested that optimal Nafion ionomer in the anode catalyst ink was about 30-40 wt.%, but in our study the optimization was not performed at this stage.

3.2 Gas diffusion electrodes preparation

Gas diffusion electrodes (GDE) were prepared by spraying catalyst ink on top of the diffusion layer which was made by depositing carbon black

with 40% PTFE on the carbon cloth (Vulcan XC 72, Cabot Corp.). Then, the electrode was dried at 60 ºC for 2 h. The electrode area was 45 mm × 45 mm. Before use, some GDEs were sprayed with 5% Nafion solution and then dried at 60 ºC. Nafion loading was about 1 mg/cm^2. This Nafion layer on top of the electrode was to obtain a good contact between the electrodes and the membrane.

Figure 7 and Figure 8 show the SEM-EDS images of anode and cathode. EDS determined the Ruthenium and Platinum particles throughout the electrodes so we can see the catalysts distribution.

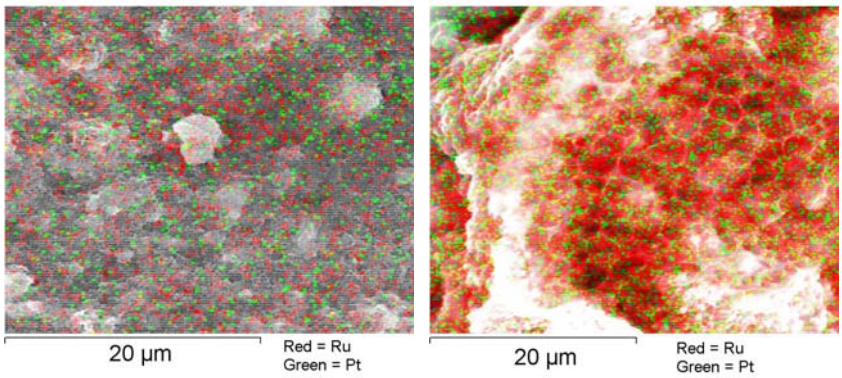

Figure 7. SEM-EDS images of anodes.

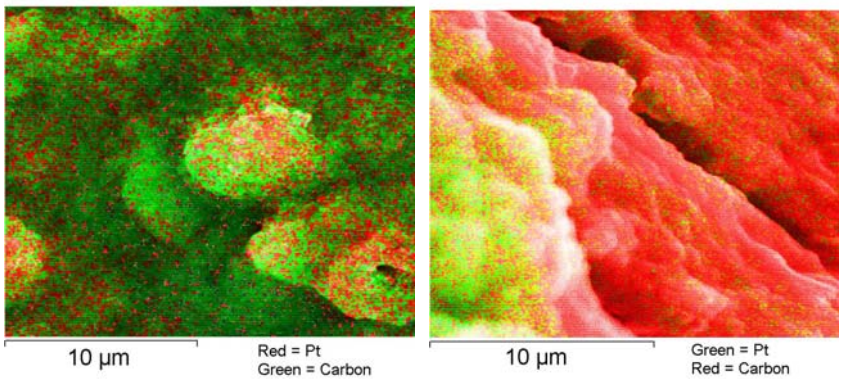

Figure 8. SEM-EDS images of cathodes.

We observe from Figure 7 that binary catalysts Pt/Ru were dispersed homogeneously on top of the diffusion layer, Pt particles formed some aggregates and these aggregates were dispersed among Ru particles.

Cathodes images show that Pt particles were not distributed very homogeneous on top of the diffusion layer. This suggested that the catalyst ink formula for the cathode should be adjusted to get homogeneous distribution of Pt.

Both electrode surfaces were quite rough.

3.3 Hot-pressing technique

The MEA was fabricated by placing the GDEs and the membrane between two steel plates. 0.5 kN/cm^2 pressure was exerted to the steel plates at 130 ^{o}C for 3 min. Then the MEA was allowed to cool down to the room temperature between the plates without pressing.

Several attempts were tried to prepare an MEA from pretreated LS17 membrane and GDEs with or without extra Nafion solution sprayed on top.

In the first occasion, without Nafion spraying on top of GDEs, the anode was in contact with the film/glass surface of the dry membrane, and the cathode was in contact with the film/bath surface of the dry membrane. The GDEs did not stick onto the membrane. When pressing the same GDEs with wet membrane, the anode stuck to the membrane, while the cathode did not. It is suspected that since LS membranes are hydrophobic in general, then dry membrane had very low affinity with hydrophilic GDEs. We tried the hot-pressing in the reverse order. It is, the anode facing to the film/bath surface of the membrane, and the cathode facing to the film/glass surface of the membrane. The results showed that the cathode stuck to the membrane while the anode did not. It is clearly demonstrated that the film/glass surface of the membrane has stronger interaction with electrodes than the film/bath surface of the membrane. One reason for this could be the hydrophilicity of the membrane surfaces, which was presented in Table 3.

Table 3. Contact angles of LS12 and LS17 membranes

Membrane	Contact angle [^{o}]	
	Film/glass surface	Film/bath surface
LS12	54.4	62.3
LS17	52.1	56.8

LS12 and LS17 showed more hydrophobicity of their film/bath surfaces and more hydrophilicity of their film/glass surfaces.

In the second occasion, GDEs were sprayed with Nafion solution. By pressing, MEAs were formed tightly. It is proved that the contact between electrodes and the membrane were improved and Nafion played as the adhesive. However, single cell measurement showed zero open cell voltage (OCV) because pin holes formed during the pressing process, which led to gas permeation from the cathode to the anode.

In order to know the membrane morphology change during the hot-pressing process, we pressed the LS17 membrane under the same condition. We observed that the membrane thickness has reduced over 57% and its area dimension has slightly extended. Confocal laser scanning microscopy (Leica TCS SP2) was used to characterize its morphology change after the pressing (Figure 9).

From uncompressed LS17 image (Figure 9.a), we can clearly observe the pores and macrovoids on the membrane cross section. After the hot-pressing, the compressed LS17 membrane became denser. From Figure 9.b, micro pores could not be observed while the flattened macrovoids are still present.

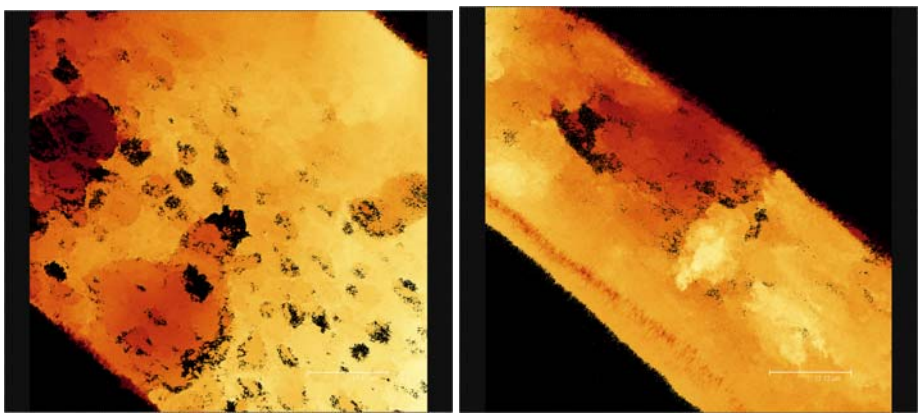

a b

Figure 9. Membrane morphology by confocal laser scanning microscopy (a: Uncompressed LS17 height information, b: Compressed LS17 height information).

SEM images (Figure 10) showed clearly the membrane morphology changes before and after the pressing. Uncompressed LS17 showed round pores, while the compressed LS17 showed deformed flattened pores. And

from Figure 10.c we also see some cracks along the pore walls which implied that during the pressing process, the pores were slightly broken.

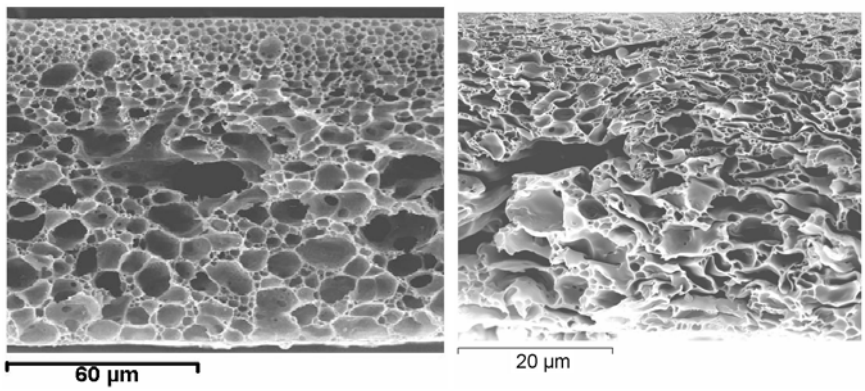

a b

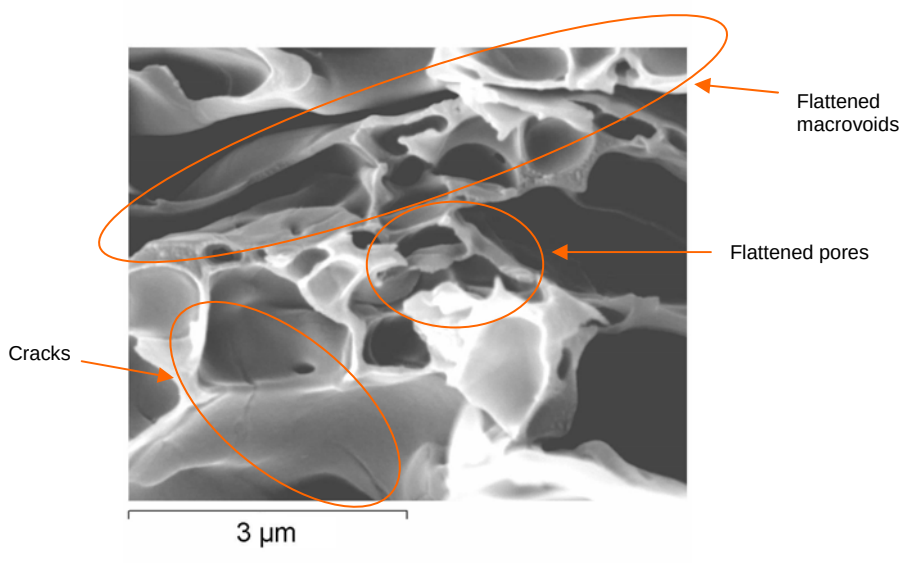

c

Figure 10. SEM cross-section images (a: uncompressed LS17, b: compressed LS17, c: enlarged image of compressed LS17).

Because the density of the compressed membrane doubled, the volumetric density of sulfonic acid group also doubled. Hence, the compressed membrane showed higher conductivity than the uncompressed one from

the results of conductivity measurement as shown in Figure 11, which indicated that few cracks did not break the proton transport paths.

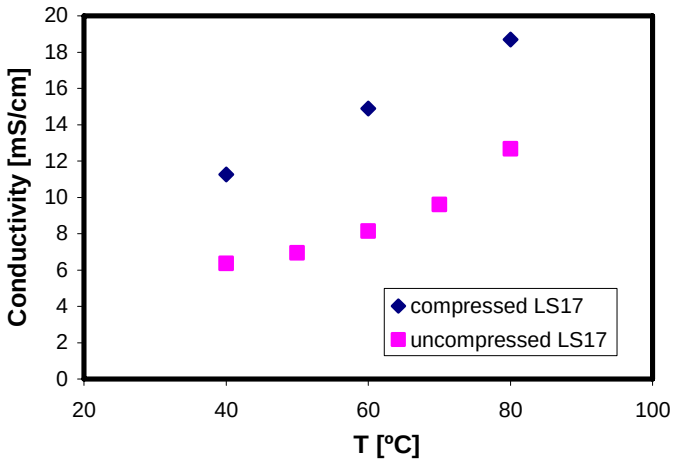

Figure 11. Hot-pressing influence on membrane conductivity.

3.4 Direct knife-coating of membrane with catalyst layers

The coating ink was prepared as the catalyst ink stated above with adjusted proportion. The membrane was covered by 3 layers of Tesa transparent tape (approx. 160 μm) except for the coating area (45 mm × 45 mm). The coating ink was poured onto one side of membrane and was cast upon it by a coating knife. After the catalyst layer was air dried, Tesa tape was removed from the membrane. Then, the membrane with catalyst layer was further dried at 60 ºC for 2 h.

When coating ink was poured upon a wet membrane surface and then let dry at room temperature, the catalyst layer cracked into many pieces. By this process, MEAs were not formed.

When coating ink was poured upon a dry membrane surface, immediately the membrane was swelling in the presence of IPA. When it dried, a discontinuous catalyst layer formed on top of membrane, but it could not be used as MEA. There exist two solutions for the problem. One is to make membranes resistible to IPA, the other is to prepare coating ink with aqueous solution.

3.5 Direct MEA formation in the test cell

MEA was formed by directly placing GDEs, the pre-treated membrane and the sealing materials in a single measure cell. During operation, the GDEs would stick to the membrane surface and thus the MEA was formed in situ.

Some membranes were pretreated by spraying 5% Nafion solution on both sides, and then it was dried at 130 ^{o}C. Very thin Nafion dense layers formed on the surfaces of the LS membrane. Nafion loading was around 2 mg/cm^2. The Nafion layers on the membrane would help to improve contact between the membrane and the electrodes. Furthermore, the Nafion dense layers sealed the surface of the LS membrane and significantly reduced the risk of pin-holes.

Several MEAs were formed by placing GDEs without Nafion sprayed and blank LS17 or Nafion-coated LS17. The results are presented as following:

1. GDEs with Blank LS17: at 80 ^{o}C, the open cell voltage (OCV) was 0.7 V, and methanol permeation was 94 mA/cm^2.

2. GDEs with Nafion-coated LS17: at 80 ^{o}C, the OCV was 0.726 V. Methanol permeation was 83 mA/cm^2.

It can be noticed that the Nafion dense layer slightly reduced the methanol permeation and hence slightly increased the OCV. However, the above two cells did not give U-I performance when current was applied. It demonstrated that catalyst layer did not have enough contact with membrane surfaces. Then, we chose Nafion-sprayed GDEs and Nafion-coated LS membranes to form MEAs although Nafion applied on top of a catalyst may reduce the active catalyst surface area [10].

In this way, several MEAs were formed and listed in Table 4.

Table 4. MEA properties

MEA	Membrane	Anode catalyst loading [mg/cm^2]	Cathode catalyst loading [mg/cm^2]
1	Nafion 117	2.70	2.01
2	LS17	1.77	2.38
3	LS17	2.76	2.11
4	LS17	2.60	2.02
5	LS12	1.78	2.30

3.6 Single cell performance and methanol permeability

MEA1 – MEA5 were characterized in a test rig with a single titanium cell. The flow-field had a grid-structure. The channels were 1.0 mm deep, 1.0 mm wide and spaced 1.0 mm from each other. The electrode area was 20 cm^2. The anode compartment was fed with 1.0 M methanol under 1.0 bar pressure, and the cathode compartment was fed with air under 1.5 bar pressure. The flow rates were 664 ml_N/min of air at the cathode and 249 ml/h of methanol solution at the anode. The operation temperature was 80 ^oC.

Methanol permeating to the cathode was mostly oxidized directly on the cathode. In order to ensure complete conversion of permeated methanol to CO2, a catalytic converter was placed in the cathode exhaust. Then, the total CO2 in the cathode exhaust was measured by an IR-detector. The amount of CO2 enabled the amount of permeated methanol to be calculated and from this the current density that could have been generated was calculated (loss-current) [11]. Then the corresponding methanol permeability (P , cm^2/s) was calculated as

$$J_{methanol} = \frac{i}{6F} \tag{5}$$

$$P = \frac{J \times l}{C_{methanol}} \tag{6}$$

where, F is Faraday constant, i (A/cm^2) is the current density, $J_{methanol}$ ($mol/(cm^2 s)$) is the crossed methanol flux , l (cm) is the membrane thickness, $C_{methanol}$ (mol/cm^3) is the methanol concentration of the anode, which was consider as 1.0×10^{-3} mol/cm^3 in our case.

Figure 12 shows the loss-current density due to methanol crossover for MEAs based on LS membranes and Nafion 117.

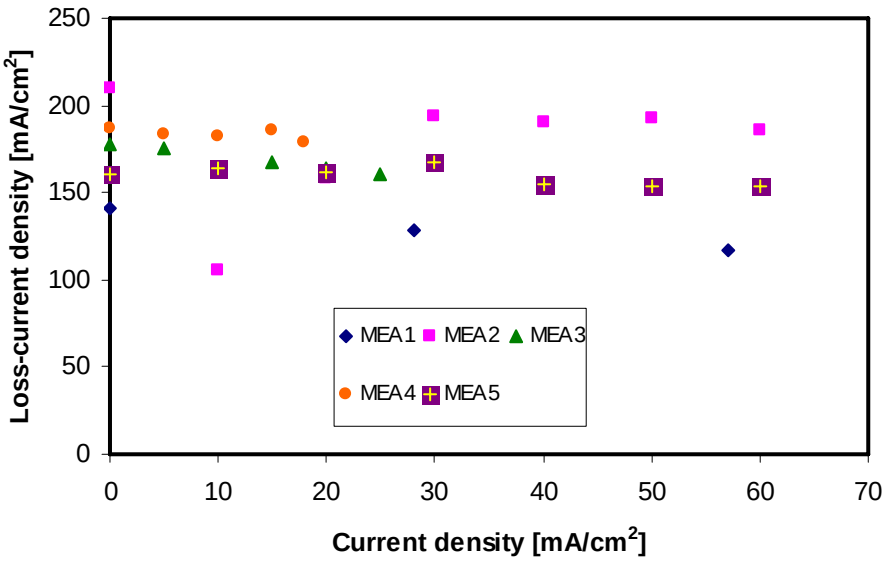

Figure 12. Loss-current density of MEA1 - MEA5.

The loss-current densities for MEA1, MEA2 and MEA3 were about 210 mA/cm², 160 mA/cm² and 140 mA/cm², respectively. A high loss-current density means high methanol permeation. Using equation (5) and equation (6), we calculated the methanol permeabilities of three MEAs based on the loss-current density obtained at open cell condition. The methanol permeability of MEA3 based on the Nafion 117 membrane was 4.90×10^{-6} cm²/s, and that of MEA1 based on the LS17 membrane was 3.98×10^{-6} cm²/s and that of MEA2 based on the LS12 membrane was 2.45×10^{-6} cm²/s. It was clear that MEAs based on the LS membranes showed lower methanol permeabilities comparing to the MEA based on Nafion 117. From this result we can also conclude that our lignosulfonate membranes can separate the anode and cathode reactants effectively. The porous structure is a closed pore structure as shown elsewhere [12]. Therefore the method taken during MEA-preparation to avoid pinholes as described above make these membranes very good separators in spite of their low density.

Cell performance for MEA1 showed in Figure 13. At 300 mV, the current density is about 214 mA/cm². The maximum power reached is about 68 mW/cm².

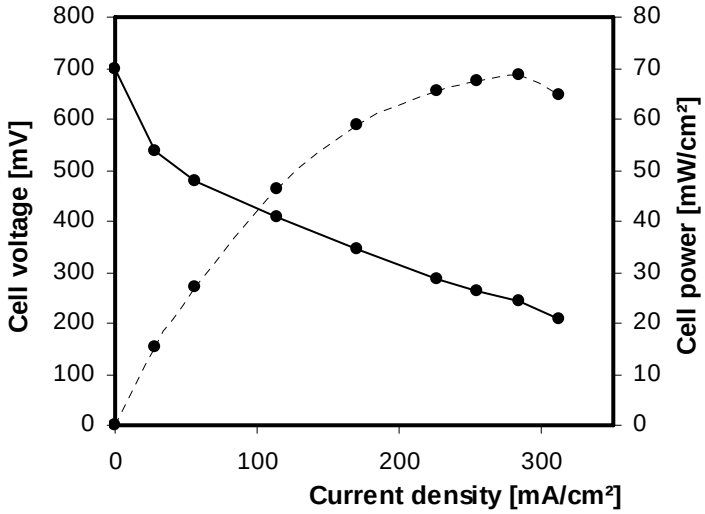

Figure 13. Cell performance of MEA1.

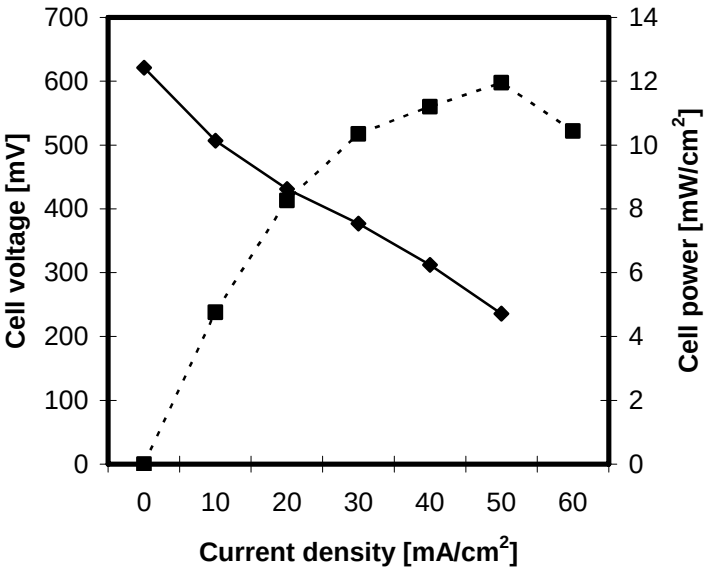

Figure 14. Cell performance of MEA2.

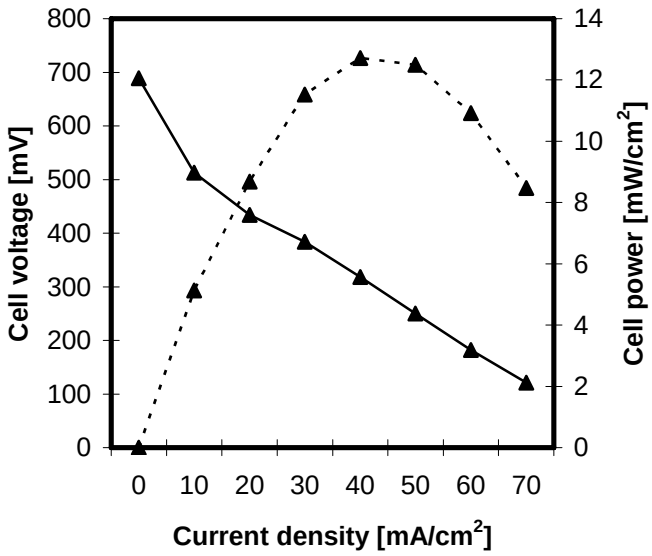

Figure 15. Cell performance of MEA5.

MEA2 and MEA5 (Figure 14 and Figure 15) show very similar performances in spite of the difference in membrane conductivity. This may be an indication of non-perfect proton transfer between Nafion-based catalyst layers and the LS-based membrane. At 300 mV, the average current density reached for MEA2 and MEA5 was around 42 mA/cm^2. The maximum power obtained for both cases was of 12 mW/cm^2, which was 5 times lower than Nafion based MEA1. This is because the conductivity of Nafion 117 is better than that of LS membranes and also Nafion has better contact with GDEs.

We detached MEA2 in order to know better the contact between the electrodes and the membranes after the test. SEM images of the fresh membranes and detached electrodes are presented in Figure 16 and Figure 17.

Figure 16 shows the film/bath surface of LS17 was denser with few nanopores, while the film/glass surface of LS17 was more porous with micropores.

Figure 17 shows the detached anode and cathode from MEA2. The anode (Figure 17.b) appears surprisingly to be a porous structure on top of the catalyst layer, which demonstrated that during operation some region of the anode stuck tightly onto the film/glass surface of the membrane and chemically the PSU/LS blend was bonded to the catalyst layer including

Nafion layer. The cathode (Figure 17.a) does not present the porous structure because the film/bath surface is less porous, but the cathode surface seems to be smoother than the fresh prepared one (Figure 8). However, still large regions of the electrodes did not present such close contact with the membrane surfaces. Therefore, we think the low cell performance is mainly because of the bad contact when the membrane conductivities are not in big difference.

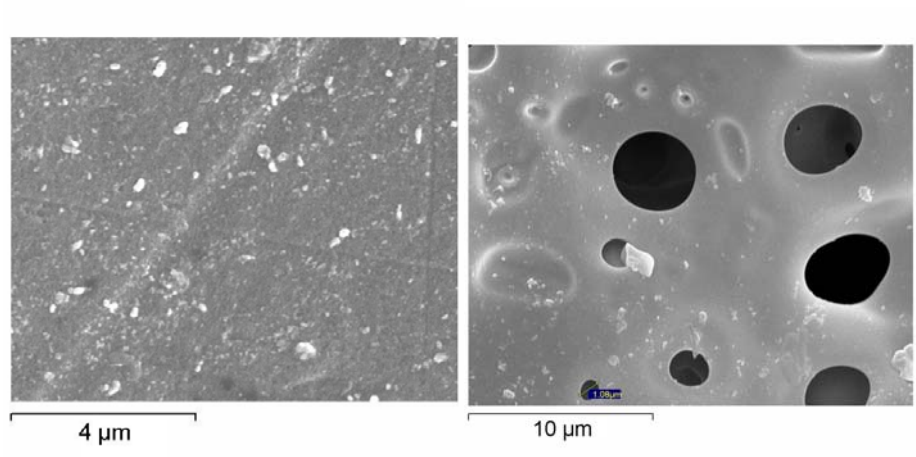

a b

Figure 16. LS17 membrane surface before MEA (a: the film/bath surface, b: the film/glass surface).

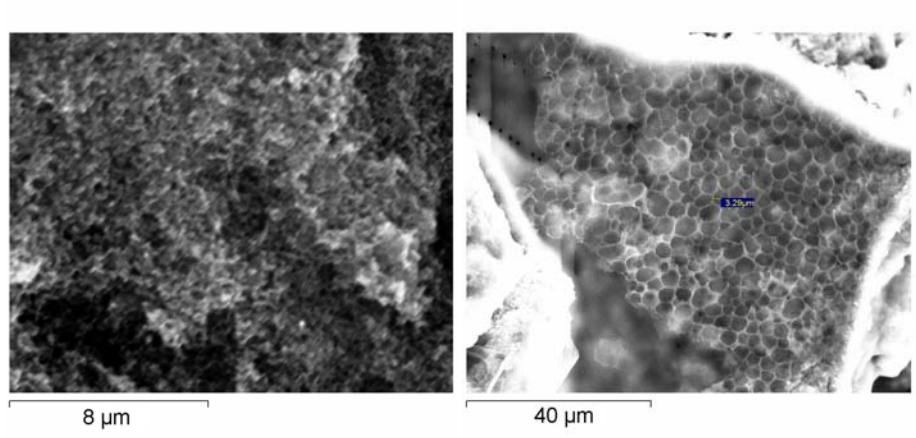

a b

Figure 17. Detached electrode surfaces (a: the cathode, b: the anode).

MEA 3 and MEA 4 (Figure 18 and Figure 19) showed reduced cell performance comparing to MEA2 although all of them were based on LS17. It may result from conductivity difference of membranes from different batches and also from the manual spray technique which resulted in inhomogeneous catalyst distribution as we concluded from the SEM-EDS images of the GDEs. Another reason may be the bad contact between the electrodes and the membranes as discussed above.

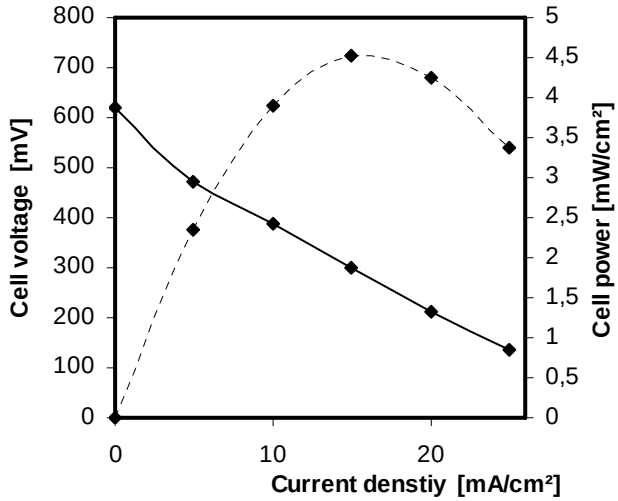

Figure 18. Cell performance of MEA3.

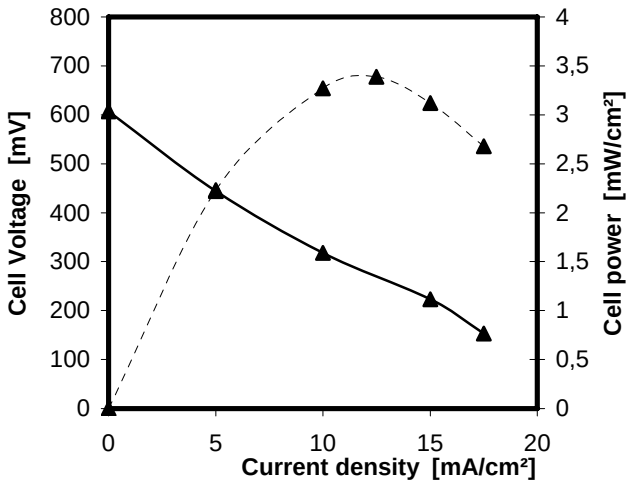

Figure 19. Cell performance of MEA4.

Although we did not test the life time of the LS-membrane-based MEA, MEAs have operated for over 60 h and have shown stable cell performance. This demonstrated that LS membranes are stable during the real cell test. Since membranes made of other aliphatic polymers have also been successfully tested under fuel cell conditions [13], it is reasonable to assume that Lignosulfonate membranes are sufficiently stable under DMFC conditions.

4 Conclusions

This research has focused on the electrical and electrochemical characterization of lignosulfonate membranes for Direct Methanol Fuel Cells and MEAs based on them. Our swelling experiments showed that porous LS membranes took up water into their pores but did not swell in water. Their dimensional stability in water is an advantage to be used in the DMFC. Impedance analysis showed that LS membranes were more resistant than Nafion 117, which is mainly because of their low IEC. In fact, considering the low IEC, the proton conductivity is remarkably high, so the lignosulfonate in the blend must have a steric distribution which is favorable for proton transport.

MEAs were successfully formed in the single cell build-up. The current density at 300 mV was about 42 mA/cm^2, which was 5 times lower than that of MEA based on Nafion 117. Membrane resistance plays a crucial role in cell performance. The methanol permeability of LS-based MEA was lower than that of Nafion 117-based MEA. LS-based MEA was stable for 60 hours in the test condition.

As a new type of membrane for DMFC, LS membranes still require further investigation if they are to perform as well as the more expensive Nafion membranes. Especially the membrane preparation process has to be improved in order to obtain membranes with higher IEC and higher conductivity. In spite of the high porosity and high water uptake these membranes show very low methanol permeability, making them highly promising candidates for further development. MEA preparation should also be investigated in the future if cell performance is to be improved.

References

[1] M.S. Wilson, S. Gottesfeld, High performance catalyzed membranes of ultra-low platinum loadings for polymer electrolyte fuel cells, J. Electrochem. Soc. 139 (1992) L28

[2] G. Rosenthal, U. Kunz., U. Hoffmann, On the question of MEA preparation for DMFCs A. Lindermeir, Journal of Power Sources 129 (2004) 180–187

[3] R. Mosdale, P. Stevens, New electrodes for hydrogen/oxygen solid polymer electrolyte fuel cell, Solid state Ionics 61 (1993) 251

[4] E. Gülzow, T. Kaz, R. Reissner, H. Sander, L. Schilling, M. v. Bradke, Study of membrane electrode assemblies for direct methanol fuel cells, J. Power Sources 105 (2002) 261–266.

[5] Yoshitsugu Sone, Per Ekdunge, Daniel Simonsson Proton Conductivity of Nafion -117 as Measured by a Four-Electrode AC Impedance Method, Journal of the Electrochemical Society 143 (1996) 1254-1259

[6] Morten Schonert, Mike Veldhuisen, personal communication 2004

[7] T.A. Zawodzinski Jr., C. Derouin, S. Radzinski, R.J. Sherman, V.T. Smith, T.E. Springer, S. Gottesfeld, J. Electrochem. Soc. 140 (1993) 1041.

[8] J.T. Hinatsu, M. Mizuhata, H. Takenaka, J. Electrochem. Soc. 141 (1994) 1493.

[9] Young-Hwan Chu, Yong Gun Shul, Won Choon Choi, Seong Ihl Woo, Hak-Soo Han, Evaluation of the Nafion effect on the activity of Pt–Ru electrocatalysts for the electro-oxidation of methanol, Journal of Power Sources 118 (2003) 334–341

[10] M.S. McGovern, E.C. Garnett, C. Rice, R.I. Masel, A. Wieckowski, Effects of Nafion as a binding agent for unsupported nanoparticle catalysts, Journal of Power Sources 115 (2003) 35–39

[11] H. Dohle, J. Divisek, J. Mergel, H.F. Oetjen, C. Zingler, D. Stolten, Recent development of the measurement of the methanol permeation in a direct methanol fuel cell, Journal of power sources 105 (2002) 274-282

[12] X. Zhang, J. Benavente and R. Garcia Valls, lignin-based membranes for electrolyte transference, Journal of power sources 145 (2005) 292

[13] P. D. Beattie, F. P. Orfino, V. I. Basura, K. Zychowska, J. Ding, C. Chuy, J. Schmeisser, S. Holdcroft, Ionic conductivity of proton exchange membranes, Journal of Electroanalytical chemistry 503 (2001) 45

Conclusion

We have successfully completed the three objectives of the thesis.

1. Several novel proton exchange membranes were prepared through different techniques. In general, PEG composite membranes, PA composite membranes and LS hybrid membranes showed lower methanol permeability than Nafion 117. Optimal LS hybrid membranes (with very low IEC) showed acceptable conductivities as we expected which were 10 – 20 mS/cm, which suggested LS was incorporated into the membrane with sterical favourite for proton transport. LS proved to be a good proton conducting material, which indicate an economic and efficient way to prepare proton exchange membranes.
2. SEM and AFM were used as the main characterization methods to reveal the correlation of membrane morphology with its transport ability. The results suggested that the PEG composite membrane proton transport is dominated by the hopping mechanism, whereas the PA composite membrane proton transport is dominated by the acid – base (polysalt) mechanism. The lowest mass transport resistance was found for PEG loading of 4.65 mg/cm^2. When 20 wt.% of LS was trapped in the PA skin layer, the resulted membrane showed better selectivity of proton to methanol. The hopping mechanism also is for LS membranes. The optimal temperature of the casting solution was 35 ^{o}C, the optimal precipitation temperature was 15 ^{o}C. High LS content in the dry membrane yielded high proton conductivity.

The future work should focus on the membrane proton conductivity. We suggest using some other host polymers such as heterocyclic polymers which may be more compatible with LS so that the resulted membrane will have higher IEC. In this case, the acid-base mechanism will improve the proton selectivity.

3. MEAs based on novel LS membranes were successfully formed in the single cell build-up. The current density at 300 mV was about 42 mA/cm2, which was 5 times lower than that of MEA based on Nafion 117 membrane. The methanol permeability of LS-based MEA was lower than that of Nafion 117-based MEA. LS-based MEA was stable for 60 hours in the test condition. From these preliminary results we concluded that the LS porous membranes could be used in direct methanol cells.

   To improve the contact between the membrane and the electrodes, further optimization of MEA conditions is required.

Appendix A

"Experimental and Computational Study of Proton and Methanol Permeability through Composite Membranes", Journal of Power Sources, 145 (2005) 223

Corresponds to Chapter 3.

Available online at www.sciencedirect.com
SCIENCE DIRECT®
Journal of Power Sources 145 (2005) 223–230
JOURNAL OF POWER SOURCES
www.elsevier.com/locate/jpowsour

Experimental and computational study of proton and methanol permeabilities through composite membranes

Xiao Zhang, Luizildo Pitol Filho, Carles Torras, Ricard Garcia-Valls *

Departament d'Enginyeria Química, Escola Tècnica Superior d'Enginyeria Química, Universitat Rovira i Virgili, Av. Països Catalans 26, 43007 Tarragona, Spain

Accepted 28 January 2005
Available online 23 May 2005

Abstract

To design direct methanol fuel cells, proton permeability and methanol crossover have to be evaluated. A study of the transport of methanol and protons through composite membranes of poly(ethylene glycol) (PEG) and polysulfone (PSf) was performed and permeabilities of these components were determined. PSF was treated with dilute sulfuric acid to enhance hydrophilicity. PEG was found to be a good material for the active layer, because it contains −OH hydrophilic groups which combine with hydrated protons. A composite membrane made of 15 wt.% PSf and 40–50 wt.% PEG showed a lower methanol crossover (1.0E−06 $cm^2\ s^{-1}$) than the commercial reference NAFION® 117. Maximal proton conductivity is also lower than NAFION® 117. A mathematical deterministic model, considering transport by diffusion through the composite membrane and equilibrium at the membrane–reservoir interfaces, was derived. However, the PEG layer did not present any pores and diffusion in the dense membrane was estimated using a transport probability. On the other hand, the porous PSf layer required an effective diffusivity that is a function of physical properties such as porosity and tortuosity. The contribution made by each mass transfer phenomenon to the total permeation was calculated by an association of mass transfer resistances.

Keywords: Composite membranes; Permeability; Mathematical model

1. Introduction

Fuel cells, composed of an anode, a membrane and a cathode, can be used to generate energy by oxidation of either hydrogen or methanol. To take maximum advantage of the fuel, a membrane is needed to conduct protons and avoid methanol crossover.

The most representative kinds of fuel cells are the proton-exchange membrane fuel cell (PEMFC) and the direct methanol fuel cell (DMFC), which use proton-conducting membranes [1]. DMFC is more interesting than PEMFC, because its theoretical potential is higher [2], and because it allows simple liquid handling. Also, as PEMFC operation is based on the supply of hydrogen, the management of water generated is very important. This is not an issue with DMFC, which already has a liquid phase. On the porous anode, electrochemical oxidation of the methanol occurs to produce carbon dioxide, protons and electrons. The protons diffuse through the membrane to the cathode side, where they react with the oxygen to produce water.

The most used membranes for DMFC are the perfluorinated sulfonated NAFION® membranes of DuPont, due to their chemical stability, high conductivity and high permeability to protons. However, these membranes also allow methanol to permeate, which reduces the efficiency of the electrochemical process, increases fuel consumption and damages the own cells. This phenomenon is known as *methanol crossover*. Several authors have reported the factors behind it, including cell temperature, cathode pressure, methanol concentration and catalyst morphology [3,4].

Many alternative membranes for DMFC are under investigation in the following four aspects: the primary structure of the polymer, the morphology of the polymer, the nature of the

* Corresponding author. Tel.: +34 977 55 96 11; fax: +34 977 55 85 44.
E-mail address: ricard.garcia@urv.net (R. Garcia-Valls).

0378-7753/$ – see front matter © 2005 Elsevier B.V. All rights reserved.
doi:10.1016/j.jpowsour.2005.01.074

Nomenclature

A	membrane area (cm^2)
C	concentration ($gmol\ cm^{-3}$)
d	pore diameter (cm)
D	diffusivity ($cm^2\ s^{-1}$)
e	elementary charge
k_B	Boltzmann's constant
k_j	mass transfer coefficient on the membrane–reservoir j interface ($cm\ s^{-1}$)
L	membrane thickness (cm)
p	number of pores of different diameters
P	permeability ($cm\ min^{-1}$)
Q	volumetric permeate flow ($cm^3\ min^{-1}$)
S	selectivity for proton transport
t	time (s)
T	temperature (K)
V_j	volume of reservoir j (cm^3)
x	axial position (cm)
z	non-dimensional axial position ($cm\ cm^{-1}$)
Z	total ionic strength ($ion\ m^{-3}$)

Greek symbols

α_j	mass transfer at reservoir j–membrane interface
ε	porosity
θ	non-dimensional time
μ	time factor
π_j	mass transfer number at reservoir j–membrane interface
τ^2	tortuosity
φ	non-dimensional concentration
Ψ	transport probability on dense layer

Subscripts

0	initial, for concentrations, or infinite dilution diffusion coefficient
c	calculated through simulations
D	diffusive
e	experimental
f	feed
H^+	proton
L	liquid
MeOH	methanol
PEG	poly(ethylene glycol) layer
PSf	polysulfone layer
s	stripping

acid group, and the nature of the medium within the polymer matrix [5]. Other membranes have been tested and results of these tests have been compared to those with NAFION® [6–8]. A better ratio between conductivity and methanol permeability has been reported. Much attention is given to polysulfone (PSf), poly(ether ketones) and poly(benzimidazole). PSf is the simplest of these polymers and the morphologies of its membranes have been well characterized. Sulfonation is an efficient way to activate polysulfone in proton permeability. There are two methods for obtaining proton-selective PSf membranes: one is to introduce anionic moieties into a performed solid membrane [9]. The other is to introduce anionic moieties into a polymer as a kind of modification, then to dissolve of the polymer and cast it into a film [10]. The second method is more complicated from an industrial point of view, and the sulfonated polysulfone itself cannot perform as a membrane with enough physical strength. The first method is industrially easier. The treatment is with sulfuric acid, and this does not change the physical strength of a performed polysulfone membrane.

To reduce the methanol crossover, the dense layer may serve as a barrier for methanol, and at the same time may facilitate the proton transport. PEG is a kind of polymer that is widely used in many fields. For example, it is used as a lubricant and as a preservative for conserving archaeological materials, because it is reasonably inexpensive and compatible with many organic materials. In biosensors, PEG is presented as "hydrogel" [11] to immobilize enzyme or protein on the carbon electrode surface and transport electrons. PEG is therefore used as a proton-selective layer.

For the reasons outlined above, the asymmetric PSf membrane was chosen as support and treated by thermal sulfonation to improve its proton conductivity. A PEG dense layer was then produced on top of PSf support.

Despite the interest in DMFCs, only a little effort is being made to propose mathematical modelling comprising the mass transfer mechanism through the membrane [6,12]. Most studies apply an empirical adjustment to the membrane and predict the electrochemical potential generated. Traditionally, diffusivities through membranes are determined without taking into account mass transfer coefficients at the membrane–reservoir interfaces. In the case of composite membranes, a global coefficient is calculated, and the different layers are not mathematically treated separately.

We have measured the permeability of protons and methanol in membranes comprising a dense layer of poly(ethylene glycol) (PEG) and a porous layer of polysulfone (PSf). The equilibrium cell comprised a feed reservoir, the composite membrane, and a stripping reservoir. Our results are expressed in terms of diffusivity. We fed our data to a mathematical model that considered transport by diffusion through the membrane and equilibrium at the feed–membrane and membrane–stripping interfaces. We then determined diffusivity for each layer was then determined using mass transfer resistances.

2. Methods

The system used in this study comprised a feed reservoir, a composite membrane and a stripping reservoir. The PEG layer of the composite membrane faced the feed reser-

voir, and the PSf layer faced the stripping reservoir. A solution of known pH or methanol concentration is fed into the feed reservoir and the protons or methanol molecules permeate through the membrane, reaching the stripping reservoir, where the concentration is measured. It is possible then to calculate permeability for the components studied. To study permeability with this equilibrium-diffusion model, we need to:

- prepare the membrane and collect the experimental data,
- determine the experimental diffusivity,
- determine the proton, methanol and membrane properties, such as the molar volume of each component, and the porosity and tortuosity of the membrane,
- determine the proton and methanol diffusivities by correlations with the literature,
- develop an equilibrium model, to obtain transient data on concentration for each reservoir,
- associate mass transfer resistances, to evaluate the effect of each transport coefficient on experimental diffusivity, and
- calculate the selectivity of proton transport at the membrane–reservoirs interfaces and through the membrane.

2.1. Preparation of the membranes and experimental data

A polysulfone casting solution was prepared by dissolving 15 wt.% PSf (MW: 16,000, Aldrich) in *N*,*N*-dimethylformamide (DMF) with vigorous agitation for 12 h at room temperature. The solutions were cast onto a glass plate using a 200 μm thick casting knife, then precipitated in 15 wt.% DMF solution and/or water. The PSf membranes were then taken from the bath and rinsed with distilled water. The PSf membranes obtained were kept at 80 °C in 0.25 M H_2SO_4 aqueous solution for 3, 24 and 72 h. Excess acid on the surface was removed by a short rinse of water. The membranes were then placed in an oven at 80 °C for 1 h. These thermally treated membranes were then soaked in distilled water and rinsed daily until the pH of the rinsed water was neutral.

Usually sulfonation process requires using strong acids. However, in the present work the degree of sulfonation is not under investigation. The treatment of the PSf with dilute sulfuric acid aims enhancing proton permeability by increasing hydrophilicity of the membrane. Indeed, preliminary experiments using blank PSf membranes (not treated with H_2SO_4) provided a proton diffusivity of 10^{-12} $cm^2\,s^{-1}$. On the other hand, after sulfonation, proton diffusivity increased to 10^{-11} $cm^2\,s^{-1}$.

Wax-like PEG (MW 1000, from Aldrich) was dissolved in methanol at several concentrations (5, 10, 20, 30, 40, 50, 60, 70 and 80 wt.%). The solution was deposited onto the top surface of support PSf membranes. The PEG-covered PSf membranes were placed in an oven to cross-link at 80 °C for 30 and 60 min, and the composite membranes were then stored in water before use. For biosensors, often PEG film is dried overnight at room temperature to cross-link [13]. In the case studied here the PEG film was dried at 80 °C to avoid the membrane to peel off in DMF solutions.

Experiments to evaluate proton and methanol permeability were carried out by using a testing cell, consisting of two reservoirs separated by a composite membrane with a dense layer of poly(ethylene glycol) and a porous layer of polysulfone. The transversal area of tested membranes was 8.51 cm^2 and both reservoirs (that of the feed solution and that of the stripping solution) had a volume of 200 cm^3. To measure proton permeability the feed reservoir was filled with a solution of HCl 1.0 M. Also, to evaluate methanol crossover a 1.0 M solution of methanol was used. Experimental data were the initial feed concentration C_f (methanol concentration, in M, or pH) and the initial stripping concentration C_0. The stripping concentration was also plotted against time.

The permeability coefficient P (cm min^{-1}) was calculated according to Eq. (1):

$$-\ln\frac{C_f}{C_0} = \frac{QP}{V_f}t \tag{1}$$

Permeability was then multiplied to membrane thickness (95 μm) to obtain diffusivity ($cm^2\,s^{-1}$). Proton conductivity was obtained by using the Nernst–Einstein equation [14] as follows:

$$\sigma = \frac{DZe^2}{k_B T} \tag{2}$$

2.2. Determination of porosity and tortuosity

Important properties in mass transfer through porous media are porosity and tortuosity. In the case of tortuosity, diffusion is more difficult when the pore geometry is irregular. The diffusion mechanisms for transient and steady states are different. In the transient state, the component tends to distribute itself homogeneously for the whole solid matrix, even reaching pores that are blocked at any of the extremities. Once the system reaches steady state, there is preferential diffusion through the sections with a concentration gradient, which is the driving force for diffusion. Therefore, transport does not occur in blocked pores. To make calculations easier, we decided to determine tortuosity for the steady state, by a model that considers a porous medium as an association of pores of different diameters [15]. If we consider pores to be spheres, steady-state tortuosity may be written as in Eq. (3):

$$\tau^2 = \sum_{i=1}^{p} \frac{1}{d_i} \frac{\sum_{i=1}^{p} d_i^3}{\left(\sum_{i=1}^{p} d_i\right)^2} \tag{3}$$

After comparing effective diffusivity and binary diffusivity coefficients for various compounds, some authors [16] have reported that expression for tortuosity should be a function of the transported molecule structure, since cyclic and acyclic compounds have different preferential paths within

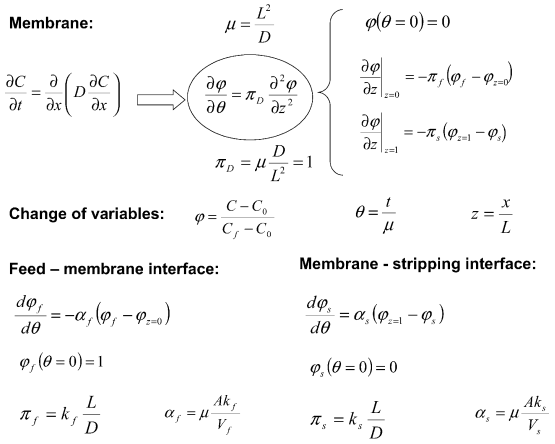

Fig. 1. Equations for the feed–membrane–stripping equilibrium model.

the porous media. In our study, however, the size of transported molecules is small enough to assume there are no significant differences in transport.

By digitally treating data from scanning electron microscopy, the pore size distribution of the polysulfone (PSf) layer [17] can be evaluated. Then, tortuosity can be calculated by applying Eq. (3). Porosity, on the other hand, is the ratio of the total volume of pores to the volume of the membrane.

2.3. Feed–membrane–stripping equilibrium model

As a first approach, the system can be modelled just by considering the diffusive transport through the membrane, which is made up of a single polymeric layer. Fig. 1 shows the model equations, which consist of a partial differential equation, describing the change in concentration through the membrane, and an ordinary differential equation of each reservoir.

Our experimental data are the initial feed concentration and the stripping concentration varying on time. Data are collected and converted into stripping non-dimensional concentrations according to time. By comparing both stripping concentrations (simulated and experimental), it is possible to find the μ parameter, which relates the thickness of the membrane to the diffusivity.

We can reduce the complexity of the numeric system, which is made up of one partial differential equation (PDE) and two ordinary differential equations (ODEs), by applying finite differences. The decision on how many elements are necessary to do the simulations is based on calculated errors and required calculation time. For a hypothetic situation in which the volumes of the membrane and both reservoirs are equal, the equilibrium concentration should be one third of the initial concentration at the feed reservoir. Choosing 25 ODEs may be then justified, since a very accurate solution can then be provided (less than 1.5% error) in a short simulation time (less than 6 min), when the simulations are performed in a Pentium IV of 2.66 GHz with 256 MB RAM for 10,000 time iterations.

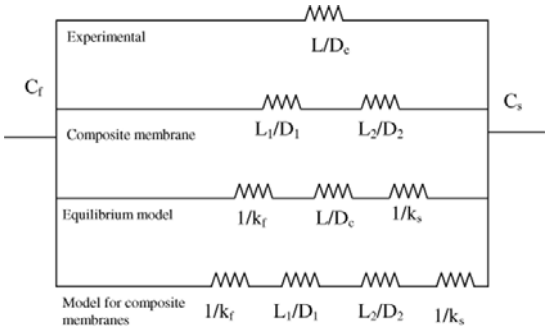

Fig. 2. Association of mass transfer resistances.

2.4. Association of mass transfer resistances

Mass transfer may be seen as a series of resistances, as in Fig. 2. Experimental diffusivity can be evaluated using a single parameter model. According to this approach, a composite membrane should have two diffusivities – one for each layer, as expressed by Eq. (4):

$$\frac{L}{D_\mathrm{e}} = \frac{L_1}{D_1} + \frac{L_2}{D_2} \tag{4}$$

The literature reports several correlations for diffusivities and describes their relative advantages and disadvantages. To calculate diffusivities in liquids, the Wilke–Chang equation [18,19] provides acceptable data, while proton diffusivity can be determined from the Nernst–Haskell [19] equation, which is more suitable to transport of ions. To apply the Wilke–Chang equation we needed to calculate the molar volumes, which were determined according to the Le Bas rule. However, liquid diffusivity must be corrected, depending on the medium considered. For a composite membrane, one proposal is

$$D = \begin{cases} D_\mathrm{L}\Psi \rightarrow 0 < z \leq L_\mathrm{PEG}, \\ D_\mathrm{L}\dfrac{\varepsilon}{\tau^2} \rightarrow L_\mathrm{PEG} < z \leq L \end{cases} \tag{5}$$

When transport occurs through the poly(ethylene glycol) (PEG) layer, liquid diffusivity is multiplied to the probability of the molecule passing through the molecules. In the porous polysulfone (PSf) layer, effective diffusivity is the product of liquid diffusivity and the ratio of porosity to tortuosity. Both porosity and tortuosity, on the other hand, can be estimated by analysing the membrane with electron microscopy.

One way to find transport probability may be to assume an association of resistances for the composite membrane, as shown in Fig. 2. Using Eq. (5), experimental diffusivity can

Table 1
Equations used to determine proton selectivity

Membrane or layer	Proton selectivity
Membrane, experimental	(8) $S_e = \frac{D_{e,H^+}}{D_{e,MeOH}}$
Membrane, calculated	(9) $S_c = \frac{D_{c,H^+}}{D_{c,MeOH}}$
PEG layer	(10) $S_{PEG} = \frac{D_{L,H^+}\Psi_{H^+}}{D_{L,MeOH}\Psi_{MeOH}}$

be rewritten as in Eq. (6):

$$\frac{L}{D_c} = \frac{1}{D_L}\left[\frac{L_{PEG}}{\Psi} + \frac{L - L_{PEG}}{\varepsilon}\tau^2\right] \quad (6)$$

Therefore, if we accept that the solutions are dilute, we can establish a relationship between the experimental data and the simulation parameters, i.e. the transport probability and coefficients (Eq. (7)):

$$\frac{L}{D_e} = \frac{1}{k_s} + \frac{1}{k_f} + \frac{1}{D_L}\left[\frac{L_{PEG}}{\Psi} + \frac{L - L_{PEG}}{\varepsilon}\tau^2\right] \quad (7)$$

The mass transfer coefficients should be properly correlated to the chemical structure of the membrane, since they are interpreted as interaction parameters. However, for the first approach, we will assume the film mass transfer theory. According to this theory, the interfacial mass transfer coefficients are directly proportional to diffusivity and inversely proportional to boundary layer thickness [20].

2.5. Selectivity for proton transport

Once the experimental and calculated diffusivities and the mass transfer coefficients are obtained, the selectivity can be calculated for proton transport at the membrane–reservoirs interfaces and through the membrane. Table 1 lists the procedures for determining selectivities. Eqs. (8)–(10) in this table can be used to analyse each transport process separately and evaluate selectivity for different membrane compositions.

3. Results and discussion

In this section we present our experimental results and the data obtained from simulations.

3.1. Physico-chemical properties

By analysing the membrane using electron microscopy and the equations in Section 2, we determined porosity and tortuosity for the polysulfone layer. Table 2 lists the average data for the membranes, the thickness of both layers, expressed in micrometers and the diffusivities calculated from Wilke–Chang (for methanol) or from Nernst–Haskell (for protons, in this case considered as HCl molecules) theories. Although thickness of PEG layer may vary according to the PEG content in the casting solution, we assumed an average value of 1 μm for all membranes. Tortuosity shows that the membrane structure was well represented by a sequence of straight channels, because the value was not far from 1.0.

Table 2
Physico-chemical and geometric data

Property	Value
L (μm)	95.00
L_{PEG} (μm)	1.00
A (cm^2)	8.51
ε	0.13
τ^2	1.04
D_{MeOH} (cm^2 s^{-1})	1.70E−05
D_{H^+} (cm^2 s^{-1})	3.33E−05

3.2. Experimental data

The membranes were placed in the equilibrium cell between the feed and the stripping reservoirs, and the concentration (for methanol crossover experiments) or pH (for proton permeability experiments) was measured. Initial feed pH in all experiments was 0.12.

We made preliminary experiments using NAFION® 117. Methanol crossover of 2.54E−06 cm^2 s^{-1} was obtained, in perfect agreement with values available in the literature [21]. Proton diffusivity was 9.54E−06 cm^2 s^{-1}. Therefore, by using Nernst–Einstein equation, diffusivity was converted to proton conductivity (71.80 mS cm^{-1}).

Composite membranes used had a polysulfone (PSf) (15% PSf–water) porous layer covered by a PEG layer. Diffusivities are presented in the Fig. 3. Proton permeation presents a maximum for a membrane with 50 wt.% of PEG in the casting solution. On the other hand, maximal methanol crossover for composite membranes is less than a half of the value obtained using NAFION® 117. Data of proton conductivity (Fig. 4) of composite membranes may help assessing if they are appropriated for fuel cells. Proton conductivity for the composite membranes is still too low if compared to NAFION® 117.

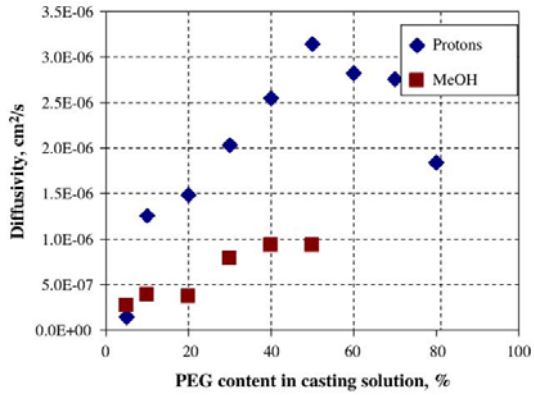

Fig. 3. Experimental diffusivities for proton and methanol.

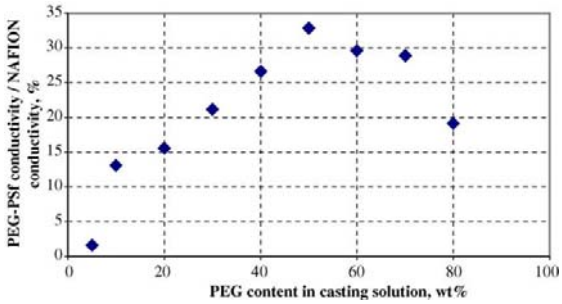

Fig. 4. Correlated proton conductivity, compared to value obtained using NAFION® 117 (71.8 mS cm^{-1}).

3.3. Determination of transport probability

From the association of mass transfer resistances we divided our experimental results for diffusivity into the several factors that contribute to its value. In this section, we analyse transport probability (see Fig. 5), which shows the change in the transport probability of protons and methanol through the dense layer, depending on the content of PEG in the casting solution.

We used the equilibrium model to calculate the transport probability from our experimental data. Simulations were performed in FORTRAN as follows:

1. Experimental concentrations were converted into non-dimensional concentrations varying (in terms of dimensional time), according to the equations presented in Section 2.
2. Interfacial mass transfer coefficients were set to 1 (case of low external mass transfer resistance).
3. Simulation was performed until the calculated non-dimensional concentrations (in terms of non-dimensional time) reached the maximum values of the experimental non-dimensional concentrations of the stripping solution.
4. Experimental and simulated non-dimensional concentrations were compared and the values of the calculated diffusivities were found.

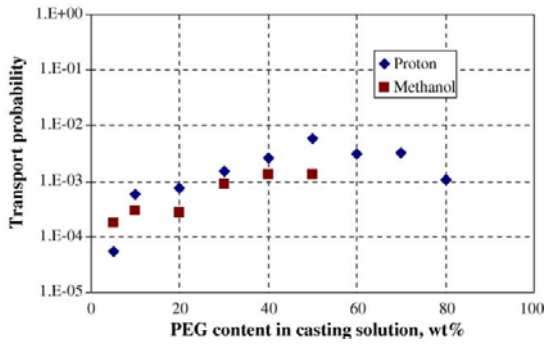

Fig. 5. Transport probabilities for protons and methanol obtained through the equilibrium model.

Table 3
Proton selectivity

w_{PEG} (wt.%)	S_e	S_c	S_{PEG}
5	0.570	0.663	0.608
10	3.210	3.289	3.877
20	4.094	4.132	5.372
30	2.542	2.554	3.227
40	2.714	2.606	3.872
50	3.349	3.232	8.807

5. The transport probabilities were calculated from the correlation between experimental and calculated diffusivities.

Fig. 5 compares the transport probabilities for protons and for methanol, determined by the equilibrium model. The PEG content in the casting solution determines the number of active sites that are responsible for the mass transfer. The transport probability for protons increased significantly when the PEG content increased from 10 to 50 wt.% and reached a maximum at this composition. Thereafter, the probability decreases, because the amount of PEG in the casting solution also helped to block any transport paths. This was because, in the dense layer, transported molecules had to pass in the free spaces between molecules. The more concentrated was the casting solution, the fewer the free spaces there were when the solvent was evaporated and the PEG layer was formed. This effect of maximum can also be seen by analysing the fit of the transport of methanol. In this case, probabilities were much lower, because:

- the molecules of methanol are much bigger than protons, so there is less space between PEG molecules is reduced for such component,
- fewer molecules of methanol are transferred by electronic effects than protons.

Transport probabilities could be estimated in a first attempt as the ratio of the molecule size to free volume in the polymer cell size. If there was a correlation between the PEG content in the casting solution and the polymer conformation, the transport probabilities of any molecule, once its molar volume had been calculated, could at least be estimated in order to design a membrane to separate one of two components or, as in the present case, to allow protons to flow and avoid methanol crossover.

As mentioned in Section 2, we can also use these results to calculate proton selectivity (see Table 3). Whether calculated directly from experimental data or indirectly by applying the equilibrium model, selectivity was maximum for a membrane with 20 wt.% of PEG in the casting solution. This property could also be calculated for the PEG layer. This was maximum for 50 wt.%, which shows that selectivity may increase if another support layer is used.

From these results, we calculated the relative resistance of each mass transfer phenomenon to the experimental diffusivity. See Fig. 6 for data on protons and Fig. 7 for data on methanol. The resistance to the permeation of pro-

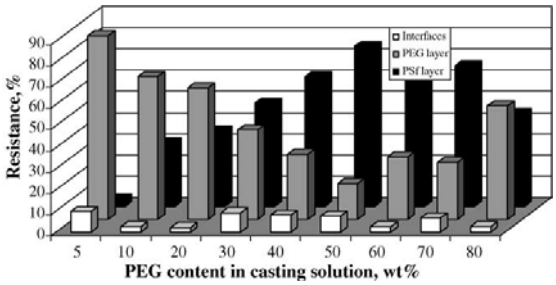

Fig. 6. Relative contribution of each mass transfer phenomenon to total resistance to permeation of protons.

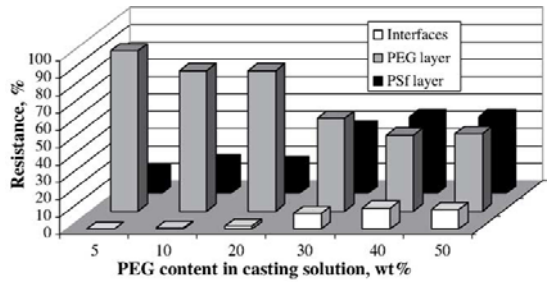

Fig. 7. Relative contribution of each mass transfer phenomenon to total resistance to permeation of methanol.

tons of the PSf layer was maximum when the PEG content in the casting solution was 50 wt.%. When we evaluated the methanol crossover, we found that the resistances of the two layers were almost equal at this composition. When membrane–reservoirs equilibrium was instantaneous, the mass transfer resistance at both interfaces could be as much as 10%, which confirms that this effect must be taken into consideration when simulating membrane permeation. It is important to evaluate mass transfer coefficients because they govern equilibrium at membrane–reservoir interfaces and also promote the transport through the membrane by increasing chemical potential. Mass transfer coefficients represent the relative affinity of the membrane for a given component and may be used to recommend optimal materials.

4. Conclusions

In this study we aim to contribute to the phenomenological knowledge of the permeation transport processes occurring in a fuel cell, by identifying the dominant mechanisms and contributions to permeability of mass transfer phenomena. The permeation of protons and methanol through composite membranes provided data for modelling. The main conclusions of this study are:

- The composite membranes tested provided a lower methanol crossover than NAFION® 117. As this happens also for proton permeation, more materials should be tested in order to manufacture a fuel cell with better performance.
- Transport probabilities for protons and methanol were maximum for the membrane whose casting solution had 50 wt.% of PEG. For higher PEG contents, there may be less free space for transport in the dense layer, so transport probability decreased.
- Overall selectivity is maximum for a membrane with 20 wt.% of PEG in the casting solution. However, this value was higher when only the PEG layer was considered, which indicates that selectivity may be enhanced if another support layer is used.
- When evaluating the resistance of the different mass transfer phenomena, the PEG layer had the lowest resistance when the casting solution had 50 wt.% of PEG. Choosing a suitable porous support may reduce total mass transfer resistance and increase overall selectivity.
- Even if we consider instantaneous membrane–reservoirs equilibrium, the interfacial mass transfer resistance may represent 12% of the total mass transfer resistance.

At the moment, this model only takes into account the diffusive processes. However, in the values of diffusivity obtained through simulations other effects, like complexation reactions or hopping, may appear. Physico-chemical interactions of the membrane with the transported species should also be considered, for example by the Enskog–Thorne theory.

Once the transport phenomena have been evaluated, we can derive a phenomenological model for the whole fuel cell, including the kinetics of methanol oxidation. Unlike those already published, this model will not treat the membrane as a black box and will not depend exclusively on experimental data. It can therefore also recommend materials for a better fuel cell performance.

References

[1] H.Y. Chang, C.W. Lin, J. Membr. Sci. 218 (2003) 295–306.
[2] C.K. Dyer, J. Power Sources 106 (2002) 31–34.
[3] A. Heinzel, V.M. Barragán, J. Power Sources 84 (1999) 70–74.
[4] K. Scott, W.M. Taama, P. Argyropoulos, K. Sundmacher, J. Power Sources 83 (1999) 204–216.
[5] T. Schulz, S. Zhou, K. Sundmacher, Chem. Eng. Technol. 24 (2001) 12, 1223.
[6] H. Dohle, J. Divisek, R. Jung, J. Power Sources 86 (2000) 469–477.
[7] B.S. Pivovar, Y. Wang, E.L. Cussler, J. Membr. Sci. 154 (1999) 155–162.
[8] K.D. Kreuer, J. Membr. Sci. 185 (2000) 29–39.
[9] M.J. Ariza, D.J. Jones, J. Roziere, Desalination 147 (2002) 183–189.
[10] C. Manea, M. Mulder, J. Membr. Sci. 206 (2002) 443–453.
[11] K. Habermüller, M. Mosbach, W. Schuhmann, J. Anal. Chem. 366 (2000) 560–568.
[12] P. Argyropoulos, K. Scott, A.K. Shukla, C. Jackson, J. Power Sources 123 (2003) 190–199.
[13] Y. Xu, W. Peng, X. Liu, G. Li, Biosens. Bioelectron. 20 (2004) 533–537.
[14] Sh. Obeidi, B. Zazoum, N.A. Stolwijk, Solid State Ionics 173 (2004) 77–82.

[15] L.T. Pinto, Um estudo do transiente da difusão gasosa em meios porosos, Doctorate Thesis in Chemical Engineering, Chemical Engineering Programme, COPPE, Universidade Federal do Rio de Janeiro, Rio de Janeiro, 1994, 197 pp.
[16] M. Sato, M. Goto, A. Kodama, T. Hirose, Sep. Sci. Technol. 33 (1998) 1283–1301.
[17] C. Torras, R. Garcia-Valls, J. Membr. Sci. 233 (2004) 119–127.
[18] W.Y. Fei, H.-J. Bart, Chem. Eng. Process. 40 (2001) 531–535.
[19] R.C. Reid, J.M. Prausnitz, T.K. Sherwood, The Properties of Gases and Liquids, McGraw-Hill, New York, 1987.
[20] C. Geankoplis, Transport Processes and Unit Operations, 3rd ed., Prentice-Hall, 1993, 921 pp.
[21] P. Mukoma, B.R. Jooste, H.C.M. Vosloo, J. Membr. Sci. 243 (2004) 293–299.

Appendix B

"Modification of Polysulfone Membranes with Polyethylene Glycol and Lignosulfate: Electrical Characterization by Impedance Spectroscopy Measurements", Journal of Colloid and Interface Science, 285 (2005) 273-280

Corresponds to Chapter 3.

Available online at www.sciencedirect.com
SCIENCE DIRECT
Journal of Colloid and Interface Science 285 (2005) 273–280
JOURNAL OF Colloid and Interface Science
www.elsevier.com/locate/jcis

Modification of polysulfone membranes with polyethylene glycol and lignosulfate: electrical characterization by impedance spectroscopy measurements

J. Benavente [a,*], X. Zhang [b], R. Garcia Valls [b]

[a] *Grupo de Caracterización Electrocinética de Membranas e Interfases, Departamento de Física Aplicada I, Facultad de Ciencias, Universidad de Málaga, E-29071 Málaga, Spain*

[b] *Grupo de Biopolímeros y Vegetales, Departamento de Ingeniería Química, Universitat Rovira i Virgili, E-43007 Tarragona, Spain*

Received 29 July 2004; accepted 15 November 2004

Available online 29 January 2005

Abstract

Two sets of composite membranes having an asymmetric sulfonated polysulfone membrane as support layer have been obtained and electrically characterized (membranes SPS–PEG and PA–LIGS). The skin layer of the membrane SPS–PEG contains different percentages of polyethylene glycol in the casting solution (5, 25, 40, and 60 wt%), while lignosulfonate was used for manufacturing PA–LIGS membranes (5, 10, 20, and 40 wt%). Membrane electrical characterization was done by means of impedance spectroscopy (IS) measurements, which were carried out with the membranes in contact with NaCl solutions at different concentrations ($10^{-3} \leqslant c(M) \leqslant 5 \times 10^{-2}$). Electrical resistance and equivalent capacitance of the different membrane samples were determined from IS plots by using equivalent circuits as models. Results show a clear decrease in the membrane electrical resistance as a result of both polysulfone sulfonation and the increase of the concentration of modifying substances, although a kind of limit concentration was obtained for both polyethylene glycol and lignosulfonate (40 and 20%, respectively). Results also show a decrease of around 90% in electrical resistance due to polysulfone sulfonation, while the value of the dielectric constant (hydrated state) clearly increases.

Keywords: Sulfonated polysulfone membranes; Polyethylene glycol; Lignosulfate; Thermal treatment; Impedance spectroscopy; Equivalent circuits

1. Introduction

Membrane separation systems are currently employed in different industrial fields, mainly those related to the use of pressure and concentration gradients (ultrafiltration, nanofiltration, or reverse osmosis and dialysis or hemodialysis, respectively), but those associated with an electrical potential gradient (electrodialysis) are also well established nowadays [1–3]. Moreover, new membrane applications such as fuel cells must be considered, due to their industrial interest importance [4]. It is clear that the structure of membranes and the materials used in such diverse kinds of separation processes, as well as the characterization techniques, have to be rather different. In fact, to predict the membrane performance under pressure differences, it is often necessary to know the mean pore size and pore size distribution, or membrane (active layer) thickness and salt rejection [5–9]. However, for processes directly related to the transport of charged species, membrane electrical parameters such as ion transport numbers, bulk and surface charge concentration, and membrane resistance (or conductivity) are parameters of major interest [10–13]. On the other hand, with respect to membrane materials, polyamide, polysulfone, and regenerated cellulose are polymers commonly used in separation under pressure and concentration gradients [1,2,7,11], while sulfonated polymers are used as cation-exchange membranes in electrolysis and electrodialysis cells [14,15].

* Corresponding author. Fax: +34-952-132382.
E-mail address: j_benavente@uma.es (J. Benavente).

0021-9797/$ – see front matter
doi:10.1016/j.jcis.2004.11.051

As a result of the need for new membranes for emerging applications, the synthesis of new materials (or the modification of some of the known polymer) must be considered, in order to improve the membrane behavior for a specific use. Sulfonated polymers have also recently gained importance as materials for fuel cell membranes, where a strong demand has arisen for polymer electrolytes [16].

The purpose of this work is the evaluation of changes in the electrical resistance of two sets of modified sulfonated polysulfone membranes. Membrane modification consists in the addition of different percentages of polyethylene glycol (PEG) or lignosulfonate (LIGS), respectively. The reasons to choose these polymers are related to the possibility of facilitating the transport of ions (particularly protons) across the membranes, which could be of interest in the application of the membranes in fuel cell systems. In this context, it should be mentioned that lignosulfonate is a highly anionic polymer consisting of a complex mixture of small to moderate-sized polymeric compounds with sulfonate groups attached to the molecule, which can affect the proton transport across lignosulfonated–polysulfone membranes, while polyethylene glycol is a polymer widely used in many fields, since it is compatible with many organic materials; it presents as a hydrogel and can be used as a proton-selective layer [17,18]. Membrane electrical resistance was determined from impedance spectroscopy (IS) measurements, which were carried out with the membranes in contact with NaCl solutions at different concentrations. IS measurements enable us to obtain information about the different sublayers of heterogeneous systems (such as those formed by membrane/electrolyte solutions) by means of the impedance plots, using equivalent circuits as models, in order to correlate the different circuit elements with the structural/transport properties of the system [19–22].

2. Theory

Impedance spectroscopy is an ac technique for electrical characterization of materials and interfaces based on impedance measurements carried out over a wide range of frequency (10^{-6}–10^{9} Hz). In fact, one of the most important features of IS comes with the development of a direct correlation between the response of a real system and an idealized model circuit composed of discrete electrical components [23].

When a linear system is perturbed by a small $v(t)$ voltage, its response, the electric current $i(t)$, is determined by a differential equation of nth order in $i(t)$, or a set of n differential equations of the first order. If $v(t)$ is a sine-wave input, the current intensity $i(t)$ is also a sine wave,

$$v(t) = V_0 \sin \omega t,$$

$$i(t) = I_0 \sin(\omega t + \phi),$$

where V_0 and I_0 are the maximum voltage and intensity; ω and ϕ are the angular frequency and the phase angle, respectively. Thus, a transfer function, the admittance function, can be defined: $Y^*(\omega) = |Y(\omega)|e^{j\phi}$. The inverse of the admittance is the impedance function: $Z^*(\omega) = [Y^*(\omega)]^{-1}$. Since both the amplitude and phase angle of the output may change with respect to the input values, the impedance is expressed as a complex number.

Phenomenologically, a resistance (R) represents the dissipative component of the dielectric response, while a capacitance (C) describes the storage component of the material. The overall admittance of a parallel (RC) circuit is given by the sum of conductance and capacitance contributions,

$$(1/Z^*) = (1/R) + (j\omega C). \tag{1}$$

The complex impedance can be separated into real and imaginary parts by algebraic rules:

$$Z_{\text{real}} = \left(R \big/ \left[1 + (\omega RC)^2\right]\right),$$

$$Z_{\text{img}} = -\left(\omega R^2 C \big/ \left[1 + (\omega RC)^2\right]\right). \tag{2}$$

Analysis of the impedance data is often carried out by the complex plane $Z^*(\omega)$ method using the Nyquist plot ($-Z_{\text{img}}$ vs Z_{real}). The equation for the parallel (RC) circuit gives rise to a semicircle in the $Z^*(\omega)$ plane such as that shown in Fig. 1a for an electrolyte solution (NaCl); the semicircle has intercepts on the Z_{real} axis at R_∞ ($\omega \to \infty$) and

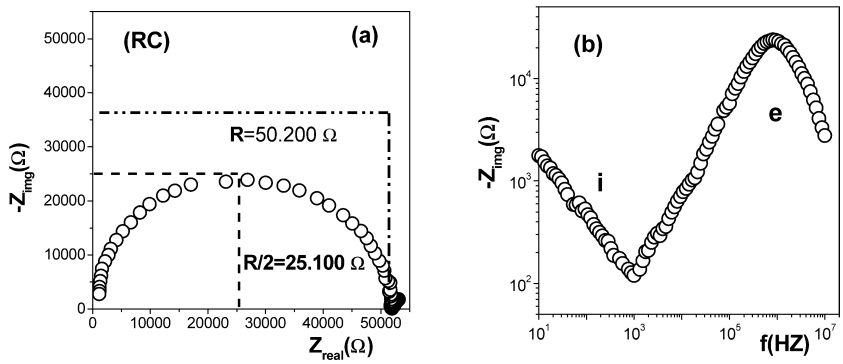

Fig. 1. Impedance plots and equivalent circuit for an electrolyte solution, $c = 0.002$ M NaCl. (a) Nyquist plot; (b) Bode plot.

R_0 ($\omega \to 0$), ($R_0 - R_\infty$) being the resistance of the system. The maximum of the semicircle equals $0.5(R_0 - R_\infty)$ and occurs at such a frequency that $\omega RC = 1$, $RC = \tau$ being the relaxation time [24]. The Bode plot ($-Z_{\text{img}}$ vs f) allows the determination of the frequency interval associated with each relaxation process. As can be seen in Fig. 1b, for an electrolyte solution a unique relaxation process at frequencies ranging between 10^5 and 10^7 Hz (with the maximum frequency around 10^6 Hz) can be observed, while at low frequencies ($10 \leqslant f$ (Hz) $\leqslant 10^3$) electrode/electrolyte interaction is observed.

Membranes in contact with electrolyte solutions are heterogeneous systems consisting of two subsystems with different dielectric properties. In such cases, two or more different semicircles can exist, which are associated with the different relaxation processes taking place in the system [24]. Moreover, complex systems present a distribution of relaxation times, and the resulting plot is a depressed semicircle; thus, a nonideal capacitor or constant phase element (CPE), which is related to bulk and interfacial inhomogeneities of the system, must be considered [25,26]. The impedance for the CPE is expressed by [24]

$$Q(\omega)^* = Y_0(j\omega)^{-n}, \tag{3}$$

where the admittance $Y_0 = R_0\tau_0^{-n}$ is a real parameter ($0 \leqslant n \leqslant 1$); in these cases, an equivalent capacitance (C^{eq}) can be determined [27]: $C^{\text{eq}} = (RY_0)^{(1/n)}/R$. When $n = 0.5$, the circuit element is called a Warburg impedance, W, and is associated with a diffusion process according to Fick's first law.

Impedance spectroscopy data allow the determination of the membrane electrical resistance and capacitance, and from these results membrane geometrical parameters can also be determined [20,28,29]. Symmetric dense membranes (or the dense active sublayers of composite membranes) can be considered as plane capacitors [20,30],

$$C = \varepsilon_0\varepsilon_r S/\Delta x_m, \tag{4}$$

where ε_0 is the permittivity of vacuum and ε_r the relative dielectric constant of the membrane; S and Δx_m are the membrane surface and thickness, respectively. The dielectric constant of a dense symmetric membrane can be estimated from the capacitance value if the membrane thickness is known [29,30]. In the case of composite membranes (two-layer systems), formed by a dense active layer and a porous and thick support, Eq. (4) allows the estimation of its thickness from capacitance results if a certain value for the dielectric constant is assumed [30].

3. Material and methods

3.1. Materials

Two sets of asymmetric composite membranes having a sulfonated polysulfone membrane as support layer have been obtained and characterize (membranes SPS–PEG and PA–LIGS). The skin or active layer of SPS–PEG membranes contain different percentages of polyethylene glycol (PEG), while lignosulfonate was used for the manufacturing of asymmetric polyamide PA–LIGS samples. Membrane preparation and thermal sulfonation process for the polysulfone support are briefly indicated in the following paragraphs, but it is extensively developed in Ref. [31].

3.1.1. Preparation of asymmetric polysulfone support membrane

Polysulfone casting solution was prepared by dissolving 15 wt% PS (M_n 16,000) purchased from Aldrich in N,N-dimethylformamide (DMF) with vigorous agitation for 12 h at room temperature. The solutions were cast onto a glass plate using a casting knife of thickness 200 mm followed by precipitation in 15 wt% DMF solution. Then the polysulfone membranes were taken from the bath and rinsed with distilled water (membrane PS). The thickness of the different samples was determined by a digital micrometer (Digimatrix Marck II) and the following average value can be taken: $\Delta x_m = (75 \pm 10)$ μm.

3.1.2. Thermal sulfonation process

The obtained PS membranes were kept in a 0.25 M H_2SO_4 aqueous solution for 3 h at 80 °C. Excess acid on the surface was removed by a short water rinse. Afterwards the membranes were put into an oven at 80 °C for 1 h. The thermally treated samples were soaked in distilled water and rinsed daily until the rinsed water reached neutral pH; this type of membrane is labeled as SPS.

Fig. 2 shows the molecular structure of sulfonated polysulfone. The presence of sulfonic acid groups (–SO_3H) improved the polysulfone hydrophilicity, which increases the solution taken-up by the membrane matrix [32], which should affect the membrane electrical resistance.

3.2. Synthesis of polyethylene glycol (PEG) membrane

Wax-like PEG (MW 1000, from Aldrich) was dissolved in methanol with different concentration of 5, 25, 40, and 60 wt%. The solution was deposited coherently onto the top surfaces of different samples of the sulfonated polysulfone support membrane. The PEG-covered asymmetric SPS composite membranes obtained were put into an oven to cross link at 80 °C for 30 min, and they were stored in water before use. These membranes will hereafter be named SPS–PEG-5, SPS–PEG-25, SPS–PEG-40, and SPS–PEG-60, respectively. A SEM micrograph of the cross

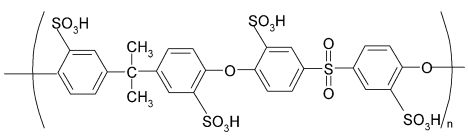

Fig. 2. Molecular structure of sulfonated polysulfone.

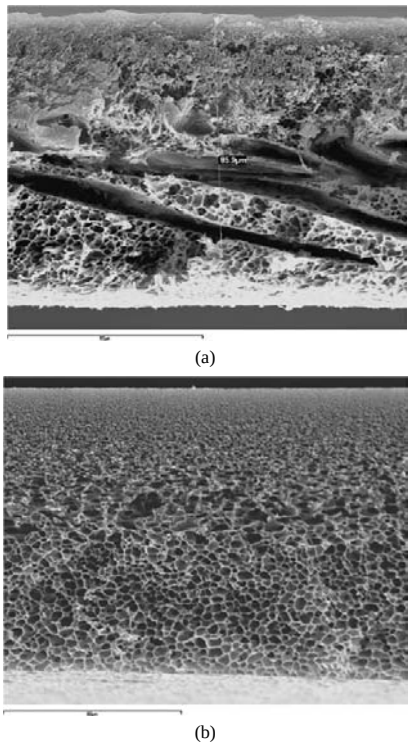

(a)

(b)

Fig. 3. Scanning electron microscopy photograph of the cross section of (a) the polyethylene glycol-supported membrane; (b) the lignosulfate polyamide-supported membrane.

section of one of the PEG-covered samples (from Ref. [31]) is shown in Fig. 3a, where the top layer containing PEG is clearly differentiated from the porous polysulfone structure.

3.3. Synthesis of polyamide containing lignosulfonate (LIGS) membrane

The skin layer of polyamide containing lignosulfonate at different concentrations (5, 10, 20, and 40 wt%) were obtained by interfacial polymerization. Thermally treated sulfonated polysulfone membranes were immersed in a 3 wt% 1,3-phenylenediamine solution, which contains water-soluble lignosulfonate (MW 7000 g/mol, acid groups 8.4 wt%). A solution of 0.15 wt% 1,3,5-triclorotricarbonyl benzene in hexane was continuously dropped onto the membrane surface, where the interfacial polymerization happened immediately. The formed polyamide composite membrane was cured at 60 °C for 30 min, followed by a complete water rinse. All the obtained polysulfone–polyamide–lignosulfonate membranes were also stored in distilled water before use. These membranes will hereafter be named PA–LIGS-5, PA–LIGS-10, PA–LIGS-20, and PA–LIGS-40, respectively. Fig. 3b shows a SEM micrograph of the membrane cross section, where the asymmetric structure with degradation in the pore size can be observed.

3.4. Impedance spectroscopy measurements

Impedance spectroscopy (IS) measurements were carried out in a test cell similar to that described elsewhere [33] and using an impedance analyzer (Solartron 1260) controlled by a computer. The membrane was tightly clamped between two glass half cells by using silicone rubber rings. In order to minimize concentration-polarization at the membrane surfaces, a magnetic stirrer was placed at the bottom of each half cell, which allows an external control of its speed rate. IS data were corrected by software as well as the influence of connecting cables and other parasite capacitances. One hundred different frequencies in the range 10–10^6 Hz, at a maximum voltage of 0.01 V, were used. Measurements were carried out at a stirring rate of 525 rpm, at six different NaCl solutions ($10^{-3} \leqslant c(M) \leqslant 5 \times 10^{-2}$ M), at room temperature $t = (25.0 \pm 0.3)$ °C and standard pH (5.8 ± 0.3); the solutions on both sides of the membrane having the same concentration. Before use, the membranes were immersed for at least 10 h in a solution of the appropriate concentration.

4. Results and discussion

Nyquist plots obtained with PS and SPS membranes in contact with a NaCl solution ($c = 0.01$ M) are shown in Figs. 4a and 4b, while Fig. 4c shows a comparison of the Bode plots obtained for both membranes. Two relaxation processes for the whole membrane/solution system were obtained, as can be clearly observed in Fig. 4c, which correspond to the membrane ($100 \leqslant f_{\max} \leqslant 1000$ Hz) and the electrolyte layers between the membrane and the electrodes ($f_{\max} \approx 3 \times 10^6$ Hz). The shift of the maximum frequency to lower values is associated to closer membrane structure [32].

The impedance plots for two SPS–PEG samples with different concentration of polyethylene glycol (5 and 25 wt%, respectively) are shown in Fig. 5, while Fig. 6 shows the experimental values obtained for two PA–LIGS samples containing 10 and 40 wt% of lignosulfate; all these data correspond to measurements carried out with the membranes in contact with a 0.002 M NaCl solution. For both sets of membrane/electrolyte solution systems two different relaxation processes were also obtained, and a similar maximum frequency was determined in all cases ($f_{\max} \approx 4000$ Hz).

The equivalent circuits for the different membrane/solution systems consists in series associations of two subcircuits: (i) a resistance in parallel with a constant-phase element for the membrane (circuit: $R_m Q_m$); (ii) a parallel association of a resistance and a capacitor for the contribution of the electrolyte solution placed between the membrane and the electrodes (circuit: $R_e C_e$). The fitting of the experimental points was carried out by means of a nonlinear program [34], which allows the determination of the different circuit parameters (electrical resistance and equivalent capacitance). It

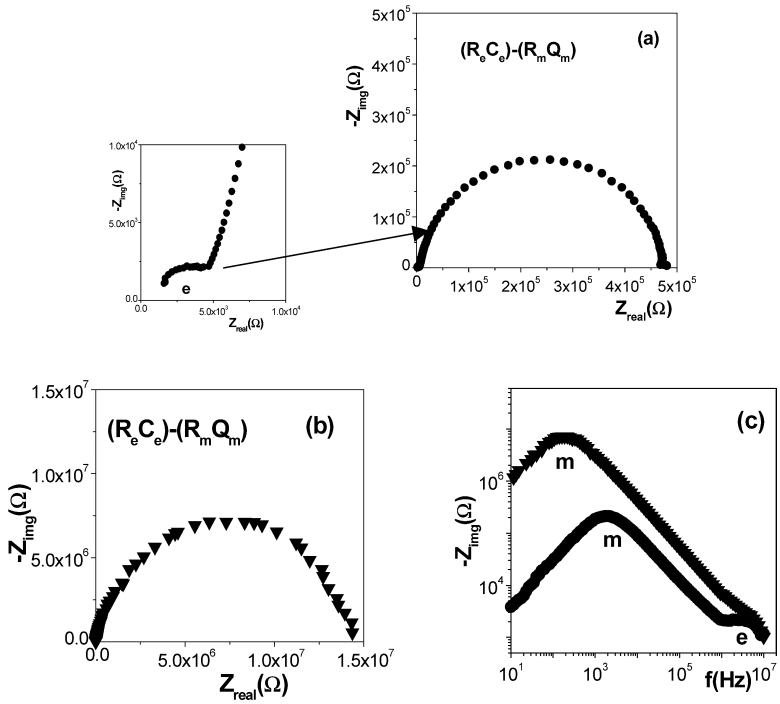

Fig. 4. Impedance plots and equivalent circuits for PS and SPS membranes in contact with a 0.01 M NaCl solution. (a) Nyquist plot for SPS sample; (b) Nyquist plot for PS sample; (c) Bode plot for SPS (●) and PS (▼) membranes.

should be pointed out the clear difference in the subcircuit assigned to the membrane (m) for the samples containing different percentages of modifying substance (see Figs. 5 and 6), while in all cases similar values were obtained for the impedance part associated with the electrolyte solution (e). It can be considered as a test of the reliability and reproducibility of the impedance spectroscopy measurements.

The variation of PS and SPS membranes electrical resistance with NaCl concentration is shown in Fig. 7a. The decrease in the values of membrane resistance when the salt concentration increases is attributed to the concentration dependence of the electrolyte solution embedded in the membrane network [21,22]. As can be observed, significant differences in the values of the electrical resistance for both samples were obtained; in fact, R_m values for the sulfonated membrane are around 15 times lower than that for the nonsulfonated polysulfone one, and the average resistance ratio for the whole range of concentration is $\langle R_m^{PS}\rangle/\langle R_m^{SPS}\rangle = 16 \pm 4$. As was previously indicated, the sulfonic groups incorporated into the sulfonated sample greatly enhance the uptake of aqueous solutions by the membrane matrix, reducing its electrical resistance. Variation of equivalent capacitance with NaCl concentration for PS and SPS membranes is shown in Fig. 7b; differences in C^{eq} values were also obtained, the values for the sulfonated sample being approximately 10 times higher than those for the nonsulfonated membrane. As can be observed, the equivalent capacitance

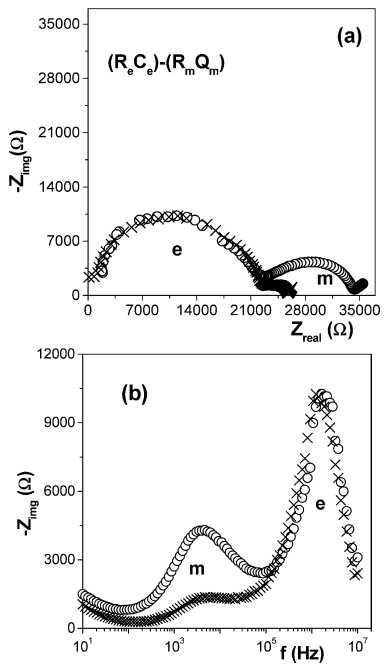

Fig. 5. Impedance plots and equivalent circuits for two SPS–PEG membranes in contact with a 0.002 M NaCl solution, (○) 5 wt% and (×) 25 wt%: (a) Nyquist plot; (b) Bode plot.

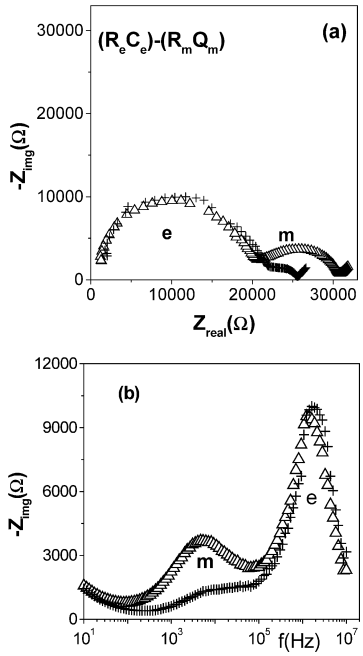

Fig. 6. Impedance plots and equivalent circuits for two PA–LIGS membranes in contact with a 0.002 M NaCl solution, (△) 10 wt% and (+) 40 wt%: (a) Nyquist plot; (b) Bode plot.

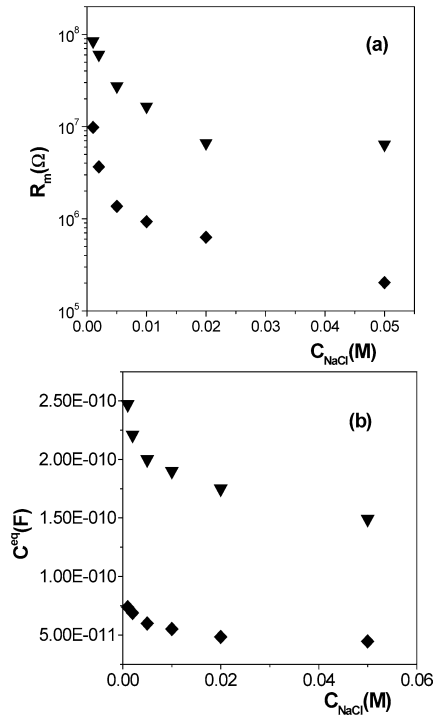

Fig. 7. Concentration dependence of (a) membrane electrical resistance and (b) membrane equivalent capacitance, for SPS (◆) and PS (▼) membranes.

Table 1
Average values for the equivalent capacitance, C^{eq}, and the empirical parameter, n, of the different membranes

Membrane	C^{eq} (F)	n
PS	$(6.1 \pm 1.1) \times 10^{-11}$	0.92 ± 0.02
SPS	$(2.0 \pm 0.4) \times 10^{-10}$	0.87 ± 0.04
SPS–PEG	$(5.1 \pm 1.3) \times 10^{-9}$	0.75 ± 0.08
PA–LIGS	$(3.2 \pm 1.2) \times 10^{-9}$	0.70 ± 0.06

of both membranes slightly decreases when the salt concentration increases, but an average value for the whole range of concentrations for C^{eq} as well as for the empirical parameter n can be determined, and the values are indicated in Table 1. According to these results, the nonsulfonated membrane practically behaves as an ideal capacitor.

Taking into account Eq. (4), the membrane dielectric constant can be estimated from capacitance values, and the following average values were obtained, $\langle \varepsilon \text{ (PS)} \rangle = (10 \pm 2)$ and $\langle \varepsilon \text{ (SPS)} \rangle = (30 \pm 6)$, which correspond to both materials in hydrate state. The higher dielectric constant obtained for the sulfonated polysulfone membrane support the improve of hydrophilicity assumed for this sample. In fact, the differences obtained in the electrical parameters for PS and SPS samples clearly show the effect of sulfonation process in the membrane electrical parameters, and they are in agreement with those previously obtained for sulfonated poly(ether sulfones) with different sulfonation degrees [30].

Variation of the electrical resistance of membranes SPS–PEG and SPS–LIGS with NaCl concentration is shown in Figs. 8a and 8b, respectively. For the samples containing the lowest amount of PEG a clear correlation between the decrease in the electrical resistance of the sample and the increase of PEG content can be observed, but small differences between SPS–PEG-40 and SPS–PEG-60 samples were obtained. According to these results, the increase of PEG concentration in the membrane up to 40% practically does not affect its electrical resistance. However, for PA–LIGS samples an optimum concentration of lignosulfate seems to exist (20 wt%) in order to obtain lower electrical resistance, as can be seem in Fig. 8b. The following sequence of values for the membrane electrical resistance of lignosulfate modified samples was obtained: PA–LIGS-5 > PA–LIGS-40 > PA–LIGS-10 > PA–LIGS-20. The increase in the electrical resistance of the samples at the higher lignosulfate content could be related to compaction of the membrane top layer.

Fig. 9 shows the variation of the equivalent capacitance of two SPS–PEG and PA–LIGS samples with different content of the modifying substances. As can be observed, C^{eq} values slightly increase when the NaCl concentration increases, and small differences depending on both the kind of sample and the concentration of modifying substance exist. However, an average value for the equivalent capacitance and the empirical parameter n for each set of membranes and the whole range of concentrations were also determined, and their val-

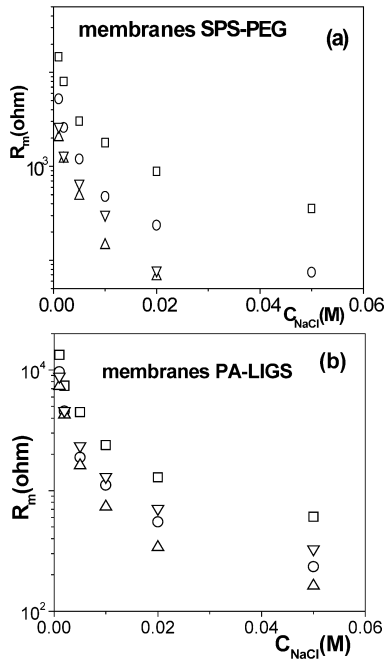

Fig. 8. (a) Membrane electrical resistance versus electrolyte concentration for SPS–PEG membranes: (□) 5, (○) 25, (▽) 40, and (△) 60%. (b) Membrane electrical resistance versus electrolyte concentration for PS–LIGS membranes: (□) 5, (○) 10, (▽) 20, and (△) 40%.

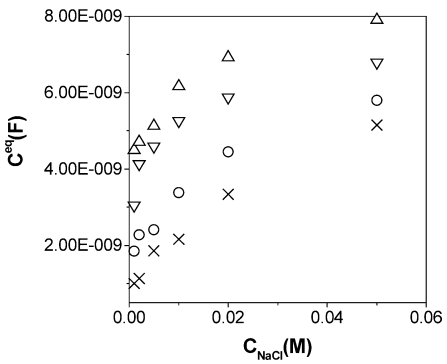

Fig. 9. Equivalent capacitance versus electrolyte concentration for two samples with different modifying substance concentration for each set of membranes: (○) SPS–PEG 5%, (△) SPS–PEG 25%, (×) PA–LIGS 10%, (▽) PA–LIGS 40%.

ues are also indicated in Table 1. These results show that the presence of modifying substances clearly increases the adsorption of charge by the membrane.

Finally, Fig. 10 shows a correlation between the percentage of modifying substance (polyethylene glycol or lignosulfonate) in the membrane and the surface electrical resistance, r_m, of the different samples at a given concentration ($c = 0.01$ M NaCl, $r_m = R_m \times S_m$, S_m = membrane area). It can be seem that the presence of polyethylene glycol

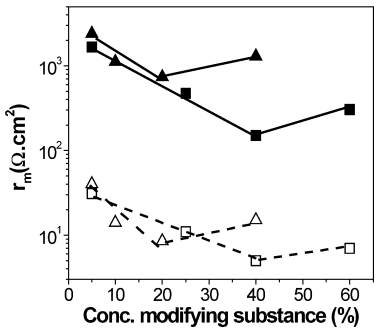

Fig. 10. Variation of the membrane surface resistance, r_m, with the concentration of modifying substance. Experimental values ($c_{NaCl} = 0.01$ M): (■) SPS–PEG, (▲) PA–LIGS; extrapolated values ($c_{NaCl} = 0.5$ M): (□) SPS–PEG, (△) PA–LIGS.

produces a reduction in the membrane electrical resistance higher than that caused by lignosulfonate at similar percentages. Particularly, for PEG concentrations higher than 25 wt% the reduction in r_m value is around 20% of that corresponding to the sample with the lowest PEG concentration (5 wt%), while for PA–LIGS samples that reduction is around 30%. For comparison, extrapolated values of the surface electrical resistance for the different samples at high concentration (0.5 M NaCl) are also shown in Fig. 10; these values were obtained by extrapolation of those indicated in Fig. 8 for the corresponding membranes. As was previously indicated, membranes with low electrical resistance are of great interest for their possible application in electrodialysis and fuel cell systems. In this context, the results obtained indicate that the SPS–PEG-40 membrane could be a candidate for application in low-resistance devices, since the value of its electrical resistance is only slightly higher than that presented by high-ion-exchange conducting membranes, but it could be improved by using a thinner support.

5. Summary

The electrical characterization of two different sets of composite membranes when they were in contact with NaCl solutions at different concentrations has been carried out. Different membrane samples were prepared by using a sulfonated polysulfon membrane as support layer and different percentages of a modifying substance, polyethylene glycol or lignosulfate, respectively.

Membrane electrical resistance and equivalent capacitance were determined from impedance data using an equivalent circuit as model, which consists in parallel association of a resistance and constant phase element. A clear reduction in the membrane electrical resistance as a result of both the polysulfone sulfonation and the incorporation of modifying substance was obtained. In this later case, an optimum concentration percentage can be estimated from electrical

results (40% for PEG-containing samples and 25% for lignosulfate ones).

References

[1] M. Mulder, Basic Principles of Membrane Technology, Kluwer, Dordrecht, 1992.
[2] M. Cheryan, Ultrafiltration Handbook, Technomic, Lancaster, PA, 1986.
[3] T. Sata, Pure Appl. Chem. 58 (1986) 1613.
[4] W. Saltronstall, Desalination 22 (1977) 229.
[5] E. Staude, Makromol. Chem. Sup. 1 (1982) 139.
[6] V. Gekas, G. Tragärdh, B. Hallström, Ultrafiltration Membrane Performance Fundamentals, KF–Sigma, 1993.
[7] K. Sakai, J. Membr. Sci. 96 (1994) 91.
[8] W.R. Bowen, H. Mukhtar, J. Membr. Sci. 112 (1996) 263.
[9] I. Masselin, X. Chasseray, M.-R. Chevalier, J.-M. Lainé, D. Lemordant, J. Membr. Sci. 172 (2000) 125.
[10] H.U. Demish, W. Pusch, J. Colloid Interface Sci. 69 (1979) 247.
[11] Y. Kimura, H.-J. Lim, T. Ijima, J. Membr. Sci. 18 (1984) 285.
[12] T. Jimbo, A. Tanioka, N. Minoura, Langmuir 14 (1998) 7112.
[13] A. Cañas, J. Benavente, J. Colloid Interface Sci. 246 (2002) 328.
[14] R. Nolte, K. Ledjeff, M. Bauer, R. Mulhaupt, J. Power Source 83 (1994) 211.
[15] E. Vallejo, G. Pourcelly, C. Gavach, R. Mercier, M. Pineri, J. Membr. Sci. 160 (1999) 127.
[16] R. Nolte, J. Membr. Sci. 83 (1993) 211.
[17] K. Reknes, in: International Symposium on Self-Compacting Concrete, Tokyo, 2001.
[18] K. Habermüller, M. Mosbach, W. Schuhmann, J. Anal. Chem. 366 (2000) 560.
[19] A. Asaka, J. Membr. Sci. 50 (1990) 71.
[20] H.G.L. Coster, K.J. Kim, K. Dahlan, J.R. Smith, C.J.D. Fell, J. Membr. Sci. 66 (1992) 19.
[21] J. Benavente, J.R. Ramos-Barrado, A. Heredia, Colloids Surf. A 140 (1998) 333.
[22] M. Oleinikova, M. Muñoz, J. Benavente, M. Valiente, Langmuir 16 (2001) 716.
[23] J. Mijovíc, F. Bellucci, Trends Polym. Sci. 4 (1996) 74.
[24] J.R. Macdonald, Impedance Spectroscopy, Wiley, New York, 1987.
[25] J. Benavente, J.R. Ramos-Barrado, S. Bruque, in: N. Kalay (Ed.), Interfacial Dynamics, Dekker, New York, 2000.
[26] Z. Kerner, T. Pajkossy, Electrochim. Acta 46 (2000) 207.
[27] A.K. Jonscher, Dielectric Relaxation in Solids, Chelsea Dielectric Press, London, 1983.
[28] A. Cañas, J. Benavente, Sep. Purif. Technol. 20 (2000) 175.
[29] J. Benavente, M.J. Ariza, A. Cañas, in: H. Hubert (Ed.), Encyclopedia of Surface and Colloid Science, Dekker, New York, 2003.
[30] J. Benavente, J.M. García, J.G. de la Campa, J. de Abajo, J. Membr. Sci. 114 (1996) 51.
[31] X. Zhang, R. Garcia Valls, J. Benavente, in: Fuel Cells Science and Technology, Munich, Germany, 2004.
[32] J. Benavente, J.M. García, R. Riley, A.E. Lozano, J. de Abajo, J. Membr. Sci. 175 (2000) 43.
[33] J. Benavente, J.R. Ramos-Barrado, A. Heredia, Colloids Surf. A 140 (1998) 333.
[34] B.A. Boukamp, Solid State Ionics 18/19 (1986) 136.

Appendix C

"Lignin-based Membranes for Electrolyte Transference", Journal of Power Sources, 145 (2005) 292

Corresponds to Chapter 4.

Available online at www.sciencedirect.com
SCIENCE DIRECT®
Journal of Power Sources 145 (2005) 292–297
JOURNAL OF POWER SOURCES
www.elsevier.com/locate/jpowsour

Short communication

Lignin-based membranes for electrolyte transference

Xiao Zhang [a], Juana Benavente [b], Ricard Garcia-Valls [a,*]

[a] *Departament d'Enginyeria Química, Escola Tècnica Superior d'Enginyeria Química, Universitat Rovira i Virgili, Av. Països Catalans 26, 43007 Tarragona, Spain*
[b] *Department of Applied Fisics, Faculty of Science, University of Málaga, Málaga, Spain*

Accepted 7 February 2005
Available online 1 June 2005

Abstract

Homogeneous PSf-LS membranes are formed by incorporating Lignosulfonate (LS) into the Polysulfone (PSf) network. LS obtained from sulfite pulping process contains sulfonic acid groups that will act as proton transport media. PSf-LS membranes were characterized by reflectance Infrared and scanning electron microscopy. LS showed significant influence on membrane morphology. Higher LS concentration caused a decrease in macrovoid formation and induced larger pores. Precipitation temperature was investigated as influencing parameter. Proton fluxes through PSf-LS membranes were measured by transport experiments. Impedance analysis confirmed that PSf-LS membranes possess ion conductivity. The selected PSf-LS membranes exhibited high selectivity for proton over methanol, which indicates their potential applicability in direct methanol fuel cell (DMFC).

Keywords: Lignosulfonate; Polymer blends; Membrane morphology; Proton conductivity; Selectivity

1. Introduction

As an alternative energy source, polymer electrolyte membrane fuel cell (PEMFC) has developed quickly since 1980s. Hydrogen fuel cell powered electric buses are already running in Canada and USA. A Japanese company has declaimed that in 2005 they are going to put into market a new type mobile phone powered by direct methanol fuel cell (DMFC). Recently, China is backing up this global event and shows its potential in the PEMFC market.

The most important part of PEMFC is the proton transport membrane. At present, there are only few commercial membranes to meet the market, i.e. Nafion® by Du Pont. Nafion is a perfluorosulfonic acid (PFSA)-based polymer. This membrane is still quite expensive. It is commonly used in hydrogen fuel cell. Nafion shows a high methanol cross-over, which limits its application in DMFC due to its consequent lowering of the efficiency, one of the factors in fuel cell implementation. Under this scenario, materials for proton transport membrane have been developed quickly. Many of them are sulfonated polymers and their blends. For example, sulfonated PSf, sulfonated PEEK, sulfonated polyimide among others. Sulfonation provides sulfonic acid groups in the polymer main chain, which improves the proton transport. Usually the sulfonation degree determines the proton transport of the membrane, high sulfonation degree results in high proton transport [1,2]. On the other hand, high sulfonation degree also increases methanol transport since methanol can be transported by electro-osmotic drag and diffusion [3]. Therefore, an optimized sulfonation degree is crucial to control the membrane property.

Instead of modifying polymers by a sulfonation process, our approach to the problem is the application of lignosulfonate (LS) in the preparation of a proton transport membrane. LS is an amorphous, polyphenolic, high cross-linked polymer containing sulfonic acid groups. Its molecular structure is showed in Fig. 1. LS is a by-product of sulfite pulping. Annually a huge amount of LS is produced all around

* Corresponding author. Tel.: +34 977 55 96 11; fax: +34 977 55 85 44.
E-mail address: ricard.garcia@urv.net (R. Garcia-Valls).

0378-7753/$ – see front matter © 2005 Elsevier B.V. All rights reserved.
doi:10.1016/j.jpowsour.2005.02.052

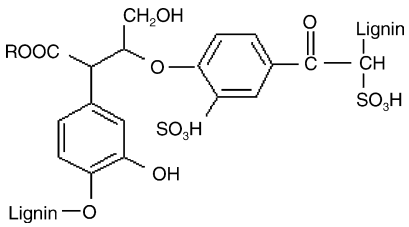

Fig. 1. Molecular structure of LS.

the world. It has application as additive [4], surfactant [5]. LS has also been reported as a component in polymer blends and showed bioactive and biocompatibility [6]. Moreover, LS has applications in blends with thermoplastics [7]. Although LS research is getting more attention, most of LS is incinerated as a waste and it is still a significant environmental burden.

Incorporating LS into PSf matrix to produce membrane provides membrane with proton-affiliated functional groups. The preparation procedure of the membrane can be simple and industry compatible. The membrane price would easily be lower than the commercially available at present. This new exploration of LS application could be of significant improvement from both the economical and environmental point of view.

2. Experimental

2.1. Preparation of PSf-LS membranes

PSf (M_w 35,000) was purchased from Aldrich and LS (7000 g mol^{-1}) was provided by Lignotech. The casting solution was prepared by dissolving LS and 15 wt.% PSf in *N*,*N*-dimethylformamide (DMF) at 35 °C. Then the coating machine spread the casting solution onto a glass surface in a controlled thickness film. The wet film was precipitated in water bath immediately.

We obtained series of PSf-LS membranes (PSf-LS1, PSf-LS2, PSf-LS3) by changing the LS concentration in the casting solution (1, 2 and 3 wt.%, respectively) and the temperature of the water bath.

The obtained membranes were light yellow color. After precipitation, they were kept in distilled water for a week and were daily rinsed before use.

2.2. Membrane characterization

PSf-LS membranes were characterized by reflectance infrared (Bruker-Tensor 27) to demonstrate the incorporation of LS in the membrane.

Cross-section images of PSf blank and PSf-LS membranes were obtained by scanning electron microscopy (SEM, JEOL JSM-6400). The membrane morphologies present in the SEM pictures were analyzed by software IFME® [8].

2.3. Transport experiments

In our research, we are using flux (J mol cm^{-2} s^{-1}) to evaluate the membrane ability for proton and methanol transport. The transport cell includes two compartments, which are separated by the tested membrane [9]. In the case of proton transport, the initial feed was 1.0 M HCl aqueous solution and the stripping was 1.0 M NaCl aqueous solution. The pH value of stripping was measured every 2 s by a Crison Compact Titrator. In the case of methanol transport, the initial feed was 1.0 M methanol aqueous solution and stripping was deionized water. The methanol in the stripping was detected versus time by HPLC (Agilent 1100), using a XDB-C8 column.

Eq. (1) describes permeability coefficient (p, cm^3 cm^{-2} s^{-1}) [10]:

$$-\ln\frac{C_f}{C_0} = \frac{Ap}{V_f}t \tag{1}$$

where C_0 (mol l^{-1}) is the initial concentration of feed, C_f (mol l^{-1}) is the feed concentration calculated through the stripping solution at time t (s). V_f is the feed volume (ml) and A the actual membrane area (cm^2). From Eq. (1) we observe the linear relationship between $-\ln(C_f/C_0)$ and time. The slope of the corresponding plot determines the value of p.

Under steady-state condition, proton and methanol flux were calculated by Fick's First Law:

$$J = \frac{P\Delta C}{l} \tag{2}$$

where, l (cm) is the membrane thickness. ΔC is the concentration difference between the initial feed and the final stripping. In our condition, C_0 is much greater than the final stripping concentration, so we consider $\Delta C \approx C_0$.

P is the permeability (cm^2 s^{-1}), which is defined as:

$$P = pl \tag{3}$$

Then the flux is related to the permeability coefficient:

$$J = pC_0 \tag{4}$$

Selectivity α of proton over methanol is a comprehensive evaluation of membranes and is calculated by Eq. (5):

$$\alpha = \frac{J_{H^+}}{J_{\text{Methanol}}} \tag{5}$$

2.4. Impedance spectroscopy

In order to check that the results from transport experiments reflected the intrinsic conductivity of tested membranes, we also measured proton conductivity of some selected hydrated membranes by using impedance spectrometry (Solartron 1260). The cell has two compartments with volume of 10 cm^3 each, the electrode used was Ag/AgCl. Membranes were examined at maximum voltage of 10 mV with the contact solution of 0.1 M NaCl.

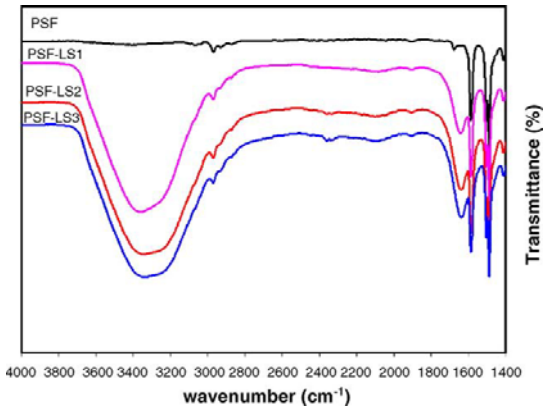

Fig. 2. IR spectra of PSf and PSf-LS membranes.

3. Results and discussion

3.1. Reflectance Infrared spectra

Fig. 2 shows the IR spectra of PSf and PSf-LS membranes. Comparing to the spectrum of PSf blank membrane, PSf-LS spectra show absorption peaks at 3451–3100 cm^{-1} and at 1700–1600 cm^{-1} which are assigned to O–H stretching vibration and C=O stretching, respectively. They refer to the phenolic hydroxyl groups and carbonyl groups of LS [11]. These IR absorption bands revealed that LS was incorporated into the PSf network.

3.2. Scanning electron microscopy

The cross-sections of membranes were scanned by SEM. Fig. 3 shows cross section images of PSf blank, PSf-LS1, PSf-LS2 and PSf-LS3 membranes obtained at 20 °C of water bath. A clear influence of LS on macrovoid formation can be observed. The membrane with high LS concentration showed morphology with reduced macrovoid. At the same time, higher LS concentration caused the presence of larger pores. Macrovoid formation is a liquid–liquid de-mixing process. Instantaneous de-mixing favors macrovoid formation [12]. Therefore, a possible explanation of the reduction in macrovoid formation is that LS, as an ionic polymer, has a good dispersing property. The interaction between LS and DMF would delay the DMF/water exchange process. The consequence of that delay would be the observed decrease in macrovoid formation and the formation of more open and regular morphologies.

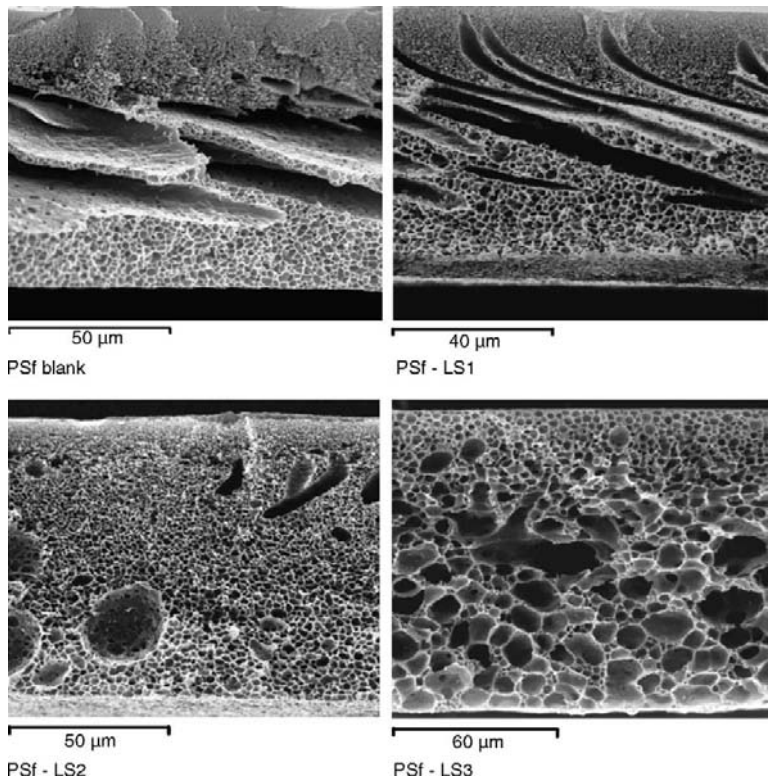

Fig. 3. SEM cross-section images of PSf blank and PSf-LS membranes (precipitated at 20 °C).

Table 1
Asymmetry analysis for PSf-LS membranes at two different loads of LS obtained at several precipitation temperatures

	PSf-LS2				PSf-LS3			
	11 °C	15 °C	20 °C	35 °C	11 °C	15 °C	20 °C	35 °C
Asymmetry %	9	11	13	15	7	10	10	16

Precipitation temperature also has an influence on the morphology of the membrane. The asymmetry analysis results are presented in Table 1. A membrane with a homogeneous pore distribution and less macrovoids has a low asymmetry value. We observed that the membrane tended to be more asymmetric when precipitated at high temperature and more macrovoids were formed at higher precipitation temperature. This morphology change could also be a result of the de-mixing process. High precipitation temperature accelerates the solvent–non-solvent diffusion, which speeds up the de-mixing process and results in the presence of more macrovoids.

These morphologies have a direct influence on mass transport resistance. As expected, larger pores and macrovoids drive to lower mass transport resistance.

3.3. Proton transport

In the present article, we choose the proton transport ability as the main parameter to be considered, although for specific possible future applications, other considerations might gain importance, like methanol cross-over or hydrogen gas permeability.

Different membranes were investigated such as: PSf blank membranes, PSf-LS membranes and Nafion 117. The permeability for proton through Nafion was determined to be 5.17×10^{-4} cm^3 cm^{-2} s^{-1}, and so the resulting flux was calculated as 5.17×10^{-7} mol cm^{-2} s^{-1}. This value is used as the reference to compare with those of PSf-LS membranes.

Proton fluxes of PSf-LS membranes calculated from Eqs. (1) and (4) are presented in Fig. 4. These values range from 0.9 to 5.4×10^{-7} mol cm^{-2} s^{-1}.

We observe that proton fluxes obtained with 1 and 2 wt.% of LS concentration membranes show the same behavior versus precipitation temperature. At these LS compositions 15 °C yields the higher values in proton transport.

We also observe that when LS concentration is 3 wt.%, the proton flux exhibited a different behavior when changing the precipitation temperature. In this case the proton flux continuously increased when increasing the precipitation temperature. This behavior was coincident with the conclusion from SEM images that more macrovoids were observed at higher precipitation temperature. The different behaviors of 1 and 2% membranes to the 3% ones were also evident when analyzing the SEM images.

Finally, at the same precipitate temperature, the proton flux increases when more LS is added to the polymer casting solution. This tendency is clearly due to the facilitated proton transport by acid groups of LS. Under the same conditions, the proton transport through blank PSf membrane was several orders lower (1.53×10^{-12} mol cm^{-2} s^{-1}) than PSf-LS membranes. While we observe in Fig. 3 that PSf blank membrane and PSf-LS1 have similar morphologies so that the main mechanism of proton transport through PSf-LS membranes cannot be diffusion. We think the facilitated transport mechanism will be responsible for the different transport values although diffusion might have a secondary influence due to the morphology change when larger amounts of LS was added.

3.4. Membrane conductivity

Proton conductivity is considered to be the intrinsic property of the membrane and it is conventionally measured by impedance spectroscopy. In order to compare with these reported results, several PSf-LS membranes were tested. For example, PSf-LS3 membranes precipitated at 11 °C were measured by impedance spectrometry and presented an average ion conductivity of 0.9 mS cm^{-1}, which is in the acceptable conductivity range for a proton transport membrane [14,15]. The conductivity of Nafion 117 was reported to be 8.05 mS cm^{-1} under the same experimental conditions [13].

3.5. Methanol transport and membrane selectivity

After the measurements of proton flux, we chose the following five membranes for further measurements: PSf-LS2

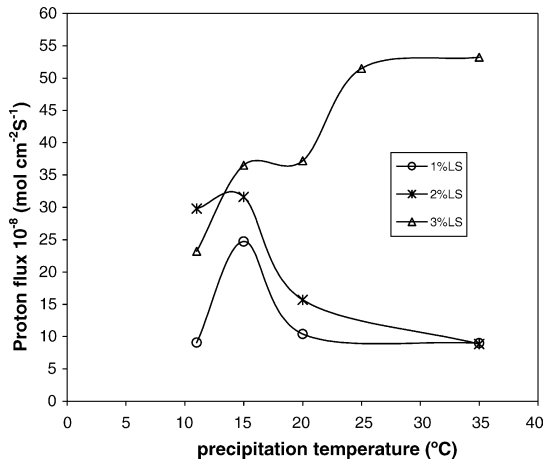

Fig. 4. Proton flux of PSf-LS membranes versus precipitation temperature.

Table 2
Methanol flux through selected PSf-LS membranes obtained at different precipitation temperatures and methanol flux through Nafion 117 as a reference

	PSf-LS2 (11 °C)	PSf-LS2 (15 °C)	PSf-LS3 (20 °C)	PSf-LS3 (25 °C)	PSf-LS3 (35 °C)	Nafion 117
Methanol flux 10^{-7} (mol cm^{-2} s^{-1})	0.347	0.56	0.614	0.719	1.06	1.18

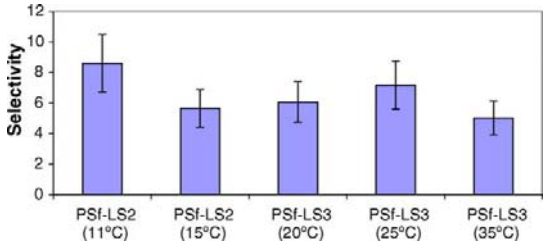

Fig. 5. Selectivity values as proton over methanol for selected PSf-LS membranes obtained at different precipitation temperatures.

precipitated at 11 °C, PSf-LS2 precipitated at 15 °C, PSf-LS3 precipitated at 20 °C, PSf-LS3 precipitated at 25 °C, PSf-LS3 precipitated at 35 °C.

Considering a possible application in DMFC, methanol transport through the membranes is another important factor. Therefore, we measured the methanol flux for the selected membranes precipitated at different temperatures and Nafion 117 under the same measuring condition (25 °C) in order to have a reference value.

Methanol permeability of Nafion 117 calculated by Eqs. (1) and (3) was determined to be 2.54×10^{-6} cm^{-2} s^{-1}, which is very close to the value reported by Pivovar et al. and Won et al. [16,17]. Corresponding methanol flux calculated from Eq. (4) was 1.18×10^{-7} mol cm^{-2} s^{-1}.

Table 2 contains the methanol fluxes obtained with selected PSf-LS membranes.

Methanol flux values observed show the same tendency as that of proton flux. High LS concentration causes an increase in methanol flux. When the LS concentration is the same, high precipitation temperature resulted in high methanol flux due to the open morphology. Comparing to Nafion 117, methanol flux of all the tested membranes is relatively lower. This is due to Nafion's flexible backbone, which causes less resistance for methanol when it swells. On the contrary PSf is an aromatic polymer and LS has an aromatic backbone, so the PSf-LS rigid chains show less methanol transport ability.

Fig. 5 shows the selectivity of all PSf-LS membranes calculated by Eq. (5). PSf-LS2 precipitated at 11 °C shows the highest selectivity value.

4. Conclusions

Reflectance IR revealed that the LS was readily contained in the membrane. Due to its dispersing property, LS presence influenced the membrane morphology. Higher LS concentration reduced macrovoid and made pores more open so that the mass resistance decreased. Precipitation temperature also has influence on the morphology of the membranes. When LS concentration was 3 wt.%, higher temperature resulted in more macrovoids. When LS concentration was less than 3 wt.%, higher temperature reduced the pore size and made the morphology more asymmetric.

PSf-LS membranes showed proton transport ability due to polyionic structure of LS. Higher LS concentration improved the proton transport, so that the proton is mainly transported by a facilitated mechanism that depends on acid group concentration. Selected PSf-LS membranes showed relatively low methanol transport compared to Nafion 117. Results from impedance conductivity demonstrated that PSf-LS membranes exhibited the intrinsic property of proton transport.

Moreover, since LS is a waste or by-product of pulping industry, PSf-LS membrane would present economical and environmental advantages with respect to membranes made by other polymers.

More investigation on thermal and mechanical properties of PSf-LS membranes are undergoing, and long-term stability will be tested in the future.

Acknowledgements

The financial support of the work was provided by Spanish Ministry of Science (projects PPQ2001-1215-C03-01 and PPQ2002-04201-C02) and Rovira i Virgili University.

References

[1] J. Kim, B. Kim, B. Jung, J. Mem. Sci. 207 (2002) 129–137.
[2] N. Carretta, V. Tricoli, E. Picchioni, J. Mem. Sci. 166 (2000) 189–197.
[3] Heinzel, V.M. Barragan, J. Power Sources 84 (1999) 70–74.
[4] R. Gonzalez, E. Reguera, J.M. Figueroa, J.D. Martinez, J. Appl. Polym. Sci. 90 (2003) 3965–3972.
[5] H.H. Tseng, M.Y. Wey, J.C. Chen, Fuel 81 (2002) 2407–2416.
[6] G. Cazacu, M.C. Pascu, L. Profibre, A.I. Kowarski, M. Mihaes, C. Vasile, Ind. Crops Prod. 20 (2004) 261–273.
[7] S. Baumberger, C. Lapierre, B. Monties, D. Lourdin, P. Colonna, Ind. Crops Prod. 6 (1997) 253–258.
[8] C. Torras, IFME® Registered Software, 02/2003/3395, Spain.
[9] R. Garcia-Valls, M. Muñoz, M. Valiente, Anal. Chim. Acta 387 (1999) 77.
[10] M. Mulder, Basic Principles of Membrane Technology, 2nd ed., Kluwer Academic Publishers, The Netherlands, 1997, pp. 350–352.
[11] D. Fengel, G. Wegener, Wood Chemistry, Ultrastructure, Reactions, Walter de Gruyter, Berlin, 1984, pp. 157–163.

[12] M. Mulder, Basic principles of Membrane Technology, 2nd ed., Kluwer Academic publishers, 2003, pp. 138–140.
[13] G. Pourcelly, P. Sistat, A. Chapotot, C. Gavach, V. Nikonenko, J. Mem. Sci. 110 (1996) 69–78.
[14] D.S. Kim, H.B. Park, J.W. Rhim, Y.M. Lee, J. Mem. Sci. 240 (2004) 37–48.
[15] Y. Woo, S.Y. Oh, Y.S. Kang, B. Jung, J. Mem. Sci. 220 (2003) 31–45.
[16] B.S. Pivovar, Y. Wang, E.L. Cussler, J. Mem. Sci. 154 (1999) 155–162.
[17] J. Won, S.W. Choi, Y.S. Kang, H.Y. Ha, I.H. Oh, H.S. Kim, K.T. Kim, W.H. Jo, J. Mem. Sci. 214 (2003) 245–257.

Appendix D

"Porous Lignosulfonate membrane for direct methanol fuel cells", accepted by Journal of Membrane Science, 2005

Corresponds to Chapter 5.

Porous lignosulfonate membranes for Direct Methanol Fuel Cells

Xiao Zhang,[a] Andreas Glüsen,[b] Ricard Garcia-Valls[a,*]

[a] Department of Chemical Engineering, Universitat Rovira i Virgili, Spain
Tel.: +34 977 55 96 11; Fax:+34 977 55 85 44; E-mail: ricard.garcia@urv.net
[b] Institute for Energy Process Engineering (IWV-3), Forschungszentrum Jülich GmbH, Germany

Abstract
Porous lignosulfonate membranes were prepared and considered for their potential application in direct methanol fuel cells (DMFC). Membranes were characterized by impedance spectrometry and water uptake measurement. Both their ion exchange capacity (IEC) and water uptake capacity affected porous membrane conductivity. Membrane conductivities were in the range 5-12 mS/cm at 80ºC. Membrane electrode assemblies (MEAs) based on lignosulfonate membranes were also prepared and characterized in a single cell in order to determine whether they can be used in a direct methanol fuel cell. The current density at 300 mV was of 42 mA/cm^2 at 80ºC.

Keywords: porous membrane, lignosulfonate, proton conductivity, membrane electrode assembly, single cell performance

1. Introduction

For polymer electrolyte membrane fuel cells (PEFC) operating on hydrogen or methanol, Nafion® is the standard proton conducting membrane. Its sulfonic acid groups form micro ion channels where the proton is transported together with its solvating water [1-4]. Based on the same concept, one of the main material developments for DMFC is sulfonated polymer and such blends as sulfonated polysulfone, sulfonated polystyrene and sulfonated poly(ether ether ketone). Both inorganic and organic materials are used as blending composite. With SiO_2, TiO_2 and ZrO_2 in the polymeric network, the membrane can be applied in DMFC operated at temperatures above 100°C [5-10]. Other research groups fill the phosphate and other acids into the polymeric matrix to generate membranes with better proton conductivity [10-14,]. Rigid and hydrophobic polymers are chosen to yield hybrid membranes with less methanol permeation [10, 15-21].
In this study, we prepared a type of porous membrane using polysulfone (PSU) and lignosulfonate (LS) blends. PSU is a hydrophobic, chemically resistant polymer which functions as a methanol barrier and membrane structure support. LS is also called sulfonated lignin. It is a highly crosslinked polyphenolic polymer that contains sulfonic acid groups and is a waste product of the pulping and paper making industry. Every year a huge amount of sulfonated lignin is produced all over the world, but only 1% of it is used. It is still a burden to the environment and needs to be explored further. If membranes were to consist of the LS that is not used today and a standard technical polymer such as PSU, they would be much cheaper than the present standard material Nafion. It is generally accepted that polymers containing a

perfluorinated main chain and polymers containing a fully aromatic main chain are more stable under fuel cell conditions than polymers containing CH_2-groups in the main chain. However, other polymers containing aliphatic components in the main chain have previously been tested successfully under fuel cell conditions [22].
In previous research, we prepared LS membranes under different conditions. Morphology analysis showed that LS was incorporated into the PSU matrix and no obvious phase separation was detected. The pores in the membranes were closed [23]. In the present paper, we characterize the electrical resistance of the LS membrane by impedance spectroscopy. The factors that influence membrane conductivity were investigated. At the same time, we prepared membrane electrode assemblies (MEAs) from the LS membrane. The MEAs were characterized in a Direct Methanol Fuel Cell at 80ºC.

2. Experimental

2.1 Lignosulfonate membrane preparation

PSU (Mw. 35,000) was purchased from Aldrich and LS (Mw. 7000) was provided by Lignotech Borregaard. The casting solution was prepared by dissolving LS and 15 wt.% PSU in N,N-Dimethylformamide (DMF) at 35ºC. Then the casting solution was spread by a coating machine onto a glass surface in a controlled thickness film. After it had been immersed in various precipitation bath solutions, the wet film formed a solid membrane.

2.2 Water uptake measurement

Membrane samples were cut to the size of 42mm × 42mm and weighed after 2h in a 130ºC oven. Then membrane samples were put into a water bath at 60ºC and 80ºC for 2 h and the bath was allowed to cool to room temperature. The membrane was immediately weighed and its dimension was measured after the membrane surface had been wiped dry with filter paper. Finally, the water uptake was calculated by

$$uptake(\%) = \frac{W_{wet} - W_{dry}}{W_{dry}} \times 100 \quad (1)$$

2.3 Membrane protonation

Membrane samples were put into 3.0 M H_2SO_4 solution at 60ºC for 1h. Then they were rinsed with deionized water, and put into deionized water at 80ºC for 1h. Finally, the protonated membranes were rinsed with deionized water and stored in deionized water.

2.4 Proton conductivity measurement

Two cells were used to measure the membrane conductivity. Cell 1, a four-point probe conductivity measuring cell [24] made of Teflon, was used to measure the conductivity under different humidities and temperatures. It consisted of two platinum current-carrying electrodes (distance 3 cm) and two platinum potential-sensing

electrodes (distance 1 cm). The cell was placed in a home built environmental chamber which allowed the cell temperature and relative humidity to be controlled independently [25].
Cell 2 is shown in Figure 1 and has the same structure as cell 1. The distance between the potential-sensing electrodes is 2 cm and the distance between the current-carrying electrodes is 4 cm. The cell was placed in a water bath and the conductivity was measured at different temperatures.
The testing sample was a piece of membrane about 10 cm long and 1 cm wide and was fixed in the cell. The membrane resistance was measured by Impedance Spectroscopy (Potentiostat / Galvanostat model 273A, EG&G Princeton Applied Research). The frequency swept from 65535 Hz to 100 Hz. The data were analyzed by Z plot software.
The conductivity was calculated using

$$\sigma = \frac{d}{RS_c} \tag{2}$$

where σ, d, R, S_c refer, respectively, to proton conductivity (S/cm), the potential-sensing electrode distance (cm), the membrane resistance (Ω) and the membrane cross-section area (cm^2).

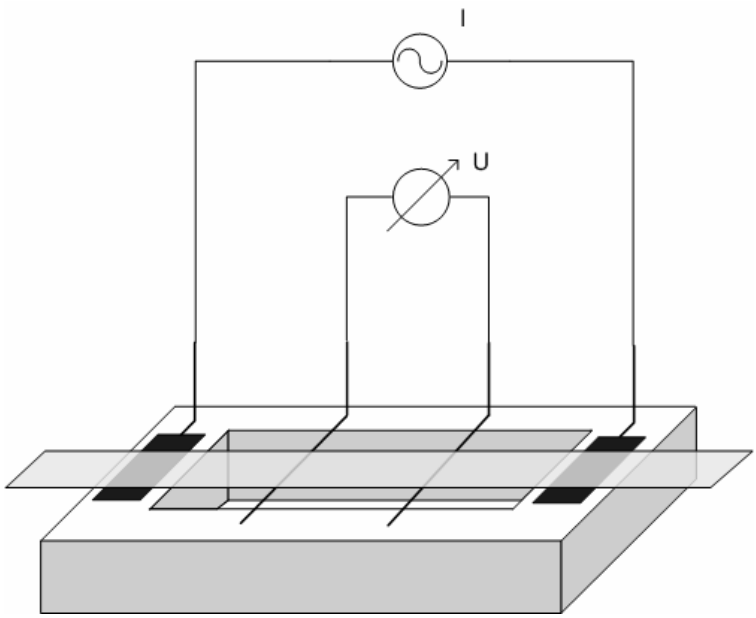

Figure 1. 4-Electrode AC-Impedance measurement cell

2.5 Fabrication of the membrane electrode assembly (MEA)

2.5.1 Catalyst ink preparation

The catalyst ink for the cathode was prepared by proportionally mixing 57.2% Pt/C (Johnson Matthey Hispec 9100) with deionized water, 5% Nafion solution (Fluka

Chemika) and isopropanol (IPA). The catalyst ink for the anode was prepared by proportionally mixing 40% PtRu/C (Heraeus) with deionized water, 5% Nafion solution and IPA. The suspension was mixed by ultrasound for 10 min at room temperature. The suspension was then further mixed by ultraturrax (High shear rotor-stator system).

2.5.2 Gas diffusion electrode preparation

Gas diffusion electrodes (GDE) were prepared by spraying catalyst ink on top of the diffusion layer (Vulcan XC 72, Cabot Corp. and PTFE, Dyneon) [26]. Then, the wet electrode was dried at 60ºC for 2 h. Before use, GDE was sprayed with 5% Nafion solution, and then dried at 60ºC. Nafion loading on GDE was about 1 mg/cm². This Nafion layer on top of the electrode was necessary to obtain a good contact between the electrodes and the membrane without hot-pressing.

2.5.3 MEA preparation

The membrane was pretreated by spraying 5% Nafion solution on both sides, and then it was dried at 130ºC. Very thin Nafion dense layers formed on the surfaces of the LS membrane. Nafion loading was around 2 mg/cm^2. The Nafion layers on the membrane also helped to improve contact between the membrane and the electrodes. Furthermore, the Nafion dense layers sealed the surface of the LS membrane and significantly reduced the risk of pin-holes.

MEA was formed by directly placing GDEs, the pre-treated membrane and the sealing material in a single measure cell. During operation, the GDEs stuck to the treated membrane surface and thus the MEA was formed in situ. Standard MEA-preparation procedures including a hot-pressing step could not be used because they destroyed the membrane.

2.6 Single cell performance and methanol permeation

All MEAs were characterized in a test rig with a single titanium cell. The flow-field had a grid-structure. The channels were 1.0mm deep, 1.0mm wide and spaced 1.0mm from each other. The electrode area was 20cm^2. The anode compartment was fed with 1.0M methanol under 1.0 bar pressure, and the cathode compartment was fed with air under 1.5 bar pressure. The flow rates were 664 ml_N/min of air at the cathode and 249 ml/h of methanol solution at the anode. The operation temperature was 80ºC. Methanol permeating to the cathode was mostly oxidized directly on the cathode. In order to ensure complete conversion of permeated methanol to CO_2 a catalytic converter was placed in the cathode exhaust. Then the total CO_2 in the cathode exhaust was measured by an IR-detector. The amount of CO_2 enabled the amount of permeated methanol to be calculated and from this the current density that could have been generated was calculated (loss current) [27]. The corresponding methanol permeability (P , cm^2/s) was calculated as

$$J_{methanol} = \frac{i}{6F} \tag{3}$$

$$P = \frac{J \times l}{C_{methanol}} \tag{4}$$

where, F is Faraday constant, i (A/cm^2) is the current density, $J_{methanol}$ (mol/cm^{2}s) is the crossed methanol flux , l (cm) is the membrane thickness, $C_{methanol}$ (mol/cm^3) is the methanol concentration of the anode, which was consider as 1.0 x 10^{-3} mol/cm^3 in our case.

3. Results and discussion

3.1 Membrane and properties

Several membranes were formed and their density, thickness and IEC are listed in Table 1.

Table 1. Membrane properties

Membrane	LS content in the dry membrane wt. %	Casting conditions		Dry membrane density g/cm^3	Average membrane thickness μm	Theoretical gravimetric IEC meq/g	Theoretical volumetric IEC meq/cm^3
		LS content in the casting solution wt. %	Precipitation bath solution				
LS6	6.25	1	Water	0.2731	86	0.054	0.0148
LS12	11.70	2	Water	0.2593	89	0.102	0.0264
LS17	16.70	3	Water	0.2143	110	0.144	0.0309
LS17/IPA	16.70	3	IPA	0.3063	77	0.144	0.0438
LS17/IPAW	16.70	3	50%IPA/Water	0.1833	155	0.144	0.0265
Nafion 117	-	-	-	1.98	178	0.909	1.8

From table 1, we see that LS content and precipitation bath solution influence the membrane density. When the precipitation bath solution was water, a high LS content reduced the membrane density. When the precipitation bath solution was isopropanol (IPA), the membrane had higher density. When it was precipitated in a 50% IPA/water bath solution (IPAW), the membrane was more porous. The gravimetric, and particularly the volumetric, IEC were much lower than the standard material Nafion 117.

3.2 Water uptake measurement

To determine the water uptake, we used Nafion 1135 as a reference because it was as thick as the LS membranes. The results are listed in table 2. Since no dimensional change was observed for all the tested LS-membranes after the swelling experiments, we can conclude that LS membranes took water into its pores other than dimensional swelling, which was due to its porous property and rigid and hydrophobic PSU chains. Nafion 1135 swelled by 8-10% in each direction, because of the more flexible backbone of the Nafion polymer. Higher temperatures increased the water uptake for LS membranes and Nafion 1135. This and the fact that even the swollen LS membranes have densities of less than 1 g/cm³ indicates that some pores are not accessible at 60°C but become accessible at 80°C while other pores are not accessible even at 80°C.

The membrane density is related to the water uptake capacity. Low density membranes contain more pores, which results in high water uptake.

Table 2. Membrane water uptake at different temperatures

uptake%	60ºC	80ºC
LS6	131.76	156.62
LS12	162.71	185.44
LS17	245.03	282.95
LS17/IPA	89.18	93.03
LS17/IPAW	313.55	321.98
Nafion 1135	23.67	31.45

3.3 Proton conductivity

We tested the conductivities of LS17 membranes using cell 1 under different humidities and temperatures. The results are presented in Figure 2. Membrane conductivity increases as the humidity and temperature increase.

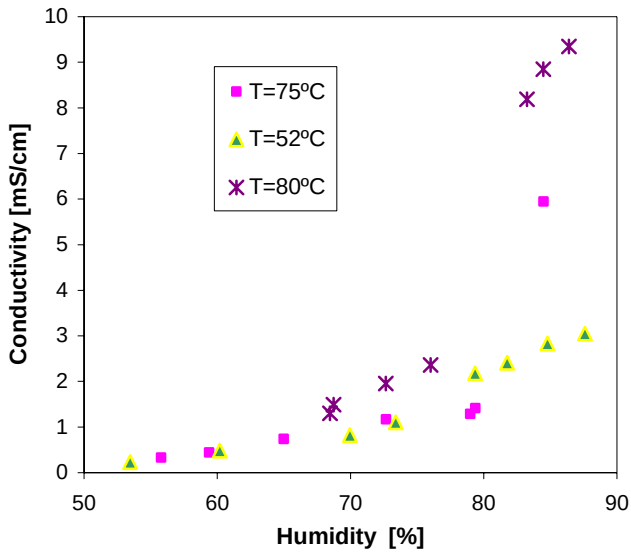

Figure 2. The effect of humidity on the proton conductivity of a protonated LS17 membrane at different temperatures

After immersing the membrane in the water bath, we measured membrane conductivity over time by using cell 2. Figure 3 shows that membrane conductivity improved slightly with the equilibration time in water. After two hours, membrane conductivity reached a plateau. This suggested that the conductivity of LS membranes depends on the water uptake, which agrees with the conductivities measured under different humidities.

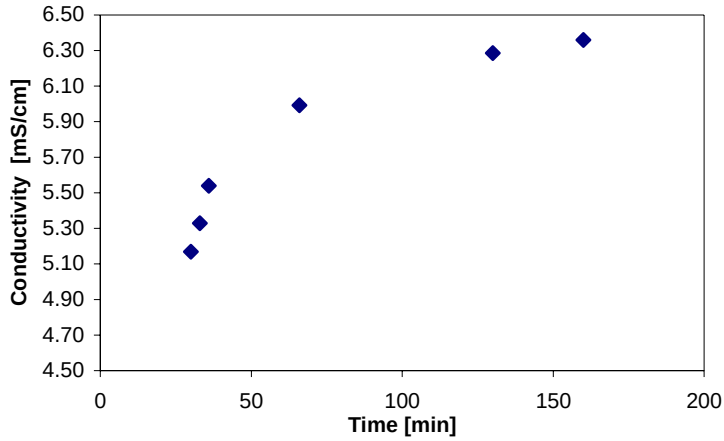

Figure 3. The influence of water uptake time on membrane conductivity at 40ºC

Figure 4 shows the conductivities of LS membranes and Nafion 117 measured by cell 2 at different temperatures. Higher temperatures led to higher conductivities for all the membranes. It is also clear that Nafion 117 showed higher conductivity than LS membranes because its IEC was higher. Likewise, LS membranes with higher IEC showed increased conductivity. Therefore, increasing the LS content in the membrane will improve membrane conductivity.

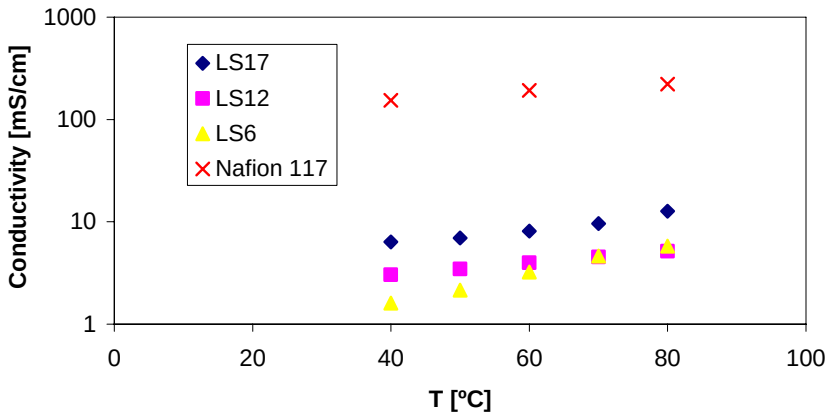

Figure 4. Logarithmic Plot of Proton conductivity of LS membranes and Nafion 117 at different temperatures

LS membrane conductivity also depends on the precipitation bath solution (Figure 5). At the same LS content, the conductivity of the membranes precipitated in a water bath was higher than the conductivity of those precipitated in other solutions. As we observed when measuring the water uptake with IPA as the precipitation bath solution, the membrane was denser and took up much less water, which resulted in lower conductivity. However, LS17/IPAW showed lower conductivity than LS17 although LS17/IPAW took more water than LS17. Obviously the IEC, water uptake and precipitation solvent all play a role in membrane conductivity. It should be pointed

out that the conductivity of the LS17 membrane is fifteen times lower than that of Nafion, while the volumetric acid group density is sixty times lower. The general expectation is that conductivity should be reduced more than the acid group density, because even if only a few acid groups are removed, some conduction pathways will be broken. This leads us to conclude that by choosing the right precipitation solvent, the acid groups can be directed into a very favorable steric arrangement.

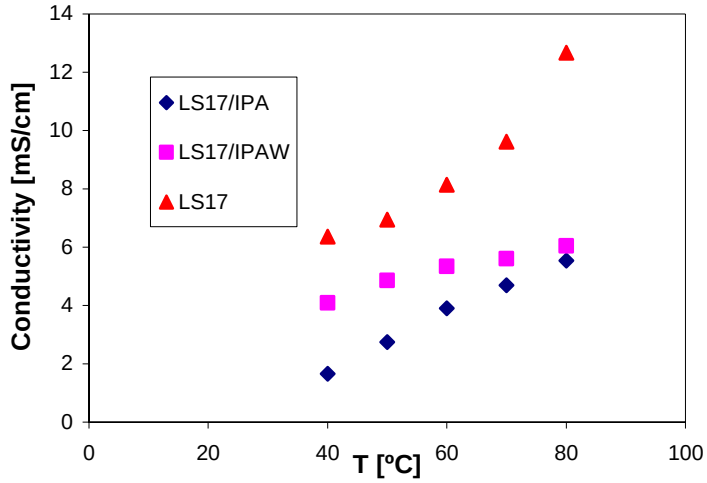

Figure 5. Effect of the precipitation bath solution on membrane conductivity

3.3 Methanol crossover and single cell performance

Three MEAs (Table 4) were formed and measured in a single cell test rig. Cell performance and methanol permeation are presented in Figures 6 and 7. MEA 1 and MEA 2 show very similar performances in spite of the difference in membrane conductivity. This may be an indication of non-perfect proton transfer between Nafion-based catalyst layers and the LS-based membrane. At 300 mV, the current density reached in both cases was around 42mA/cm^2, while Nafion 117 based MEA usually obtains a current density of 214mA/cm^2. This is because the conductivity of Nafion 117 is better than that of LS membranes and also Nafion has better contact with GDEs.

Table 4. List of MEAs prepared

MEA	Membrane	Anode catalyst loading mg/cm^2	Cathode catalyst loading mg/cm^2
1	LS17	1.77	2.38
2	LS12	1.77	2.30
3	Nafion 117	2.70	2.01

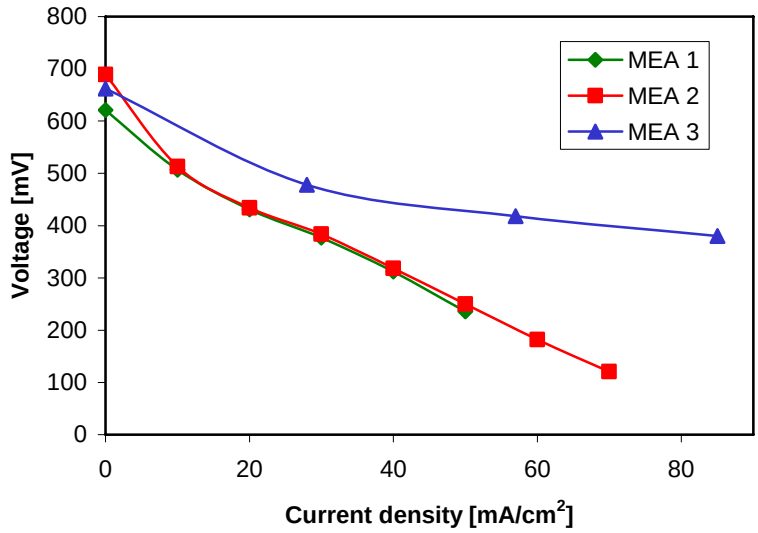

Figure 6. Cell performance curve of MEA1 and MEA2

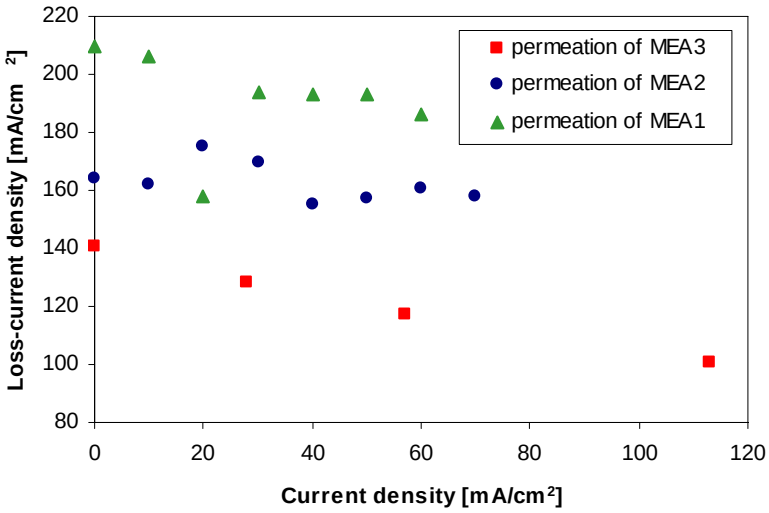

Figure 7. Loss-current density of MEA1, MEA2 and MEA3

Figure 7 shows the loss-current density due to methanol crossover for MEAs based on LS membranes and Nafion 117. The loss-current densities for MEA1, MEA2 and MEA3 were about 210 mA/cm^2, 160 mA/cm^2 and 140 mA/cm^2, respectively. A high loss-current density means high methanol permeation. Using equation (3) and equation (4), we calculated the methanol permeabilities of three MEAs based on the loss-current density obtained at open cell condition. The methanol permeability of MEA3 based on the Nafion 117 membrane was 4.40 x 10^{-6} cm^2/s, and that of MEA1 based on the LS17 membrane was 3.98 x 10^{-6}cm^2/s and that of MEA2 based on the LS12 membrane was 2.45 x 10^{-6} cm^2/s. It was clear that MEAs based on the LS membranes showed lower methanol permeabilities comparing to the MEA based on

Nafion 117. From this result we can also conclude that our lignosulfonate membranes can separate the anode and cathode reactants effectively. The porous structure is a closed pore structure as shown elsewhere [23]. Therefore the method taken during MEA-preparation to avoid pinholes as described above make these membranes very good separators in spite of their low density.

Although we did not test the life time of the LS-membrane-based MEA, MEAs have operated for over 60h and have shown stable cell performance. This demonstrated that LS membranes are stable during the real cell test. Since membranes made of other aliphatic polymers have also been successfully tested under fuel cell conditions [22], it is reasonable to assume that Lignosulfonate membranes are sufficiently stable under DMFC conditions

4. Conclusions

This research has focused on the electrical and electrochemical characterization of lignosulfonate membranes for Direct Methanol Fuel Cells and MEAs based on them. Our swelling experiments showed that porous LS membranes took up water into their pores but did not swell in water. Their dimensional stability in water is an advantage to be used in the DMFC. Impedance analysis showed that LS membranes were more resistant than Nafion 117, which is mainly because of their low IEC. In fact, considering the low IEC, the proton conductivity is remarkably high, so the lignosulfonate in the blend must have a steric distribution which is favorable for proton transport.

MEAs were successfully formed in the single cell build-up. The current density at 300 mV was about 42 mA/cm^2, which was 5 times lower than that of MEA based on Nafion 117. Membrane resistance plays a crucial role in cell performance. The methanol permeability of LS-based MEA was lower than that of Nafion 117-based MEA. LS-based MEA was stable for 60 hours in the test condition.

As a new type of membrane for DMFC, LS membranes still require further investigation if they are to perform as well as the more expensive Nafion membranes. Especially the membrane preparation process has to be improved in order to obtain membranes with higher IEC and higher conductivity. In spite of the low density and high water uptake these membranes show very low methanol permeability, making them highly promising candidates for further development. MEA preparation should also be investigated in the future if cell performance is to be improved.

Acknowledgement

We would like to thank Birgit Kohnen and Hans-Friedrich Oetjen (Forschungszentrum Jülich) for the fuel cell testing. The author X. Zhang would like to acknowledge Deutscher Akademischer Austauschdienst (DAAD) for providing the grant for her research stay in Forshungszentrum Jülich. The work was funded by the Spanish Ministry of Science (projects PPQ2001-1215-C03-01 and PPQ2002-04201-C02) and the Rovira i Virgili University.

References

[1] T. Schultz, S. Zhou, and K. Sundmacher, Current Status of and Recent developments in the Direct Methanol Fuel Cell, Chem. Eng. Technol. 24 (2001) 12

[2] A.-L. Rollet, G. Gebel, J.-P. Simonin, P. Turq and A. Sans, Determination of the Influence of External Conditions on the Nanostructure of Nafion Membrane, Journal of Polymer Science: Part B: Polymer Physics 39 (2001) 548

[3] M. Eikerling, A. A. Kornyshev, A. M. Kuznetsov, J. Ulstrup and S. Walbran Mechanisms of Proton Conductance in Polymer Electrolyte Membranes, J. Phys. Chem. B 105 (2001) 3646

[4] M. Eikerling, Y. I. Kharkats, A. A. Kornyshev and Y. M. Volfkovich, Phenomenological Theory of Electro-osmotic Effect and Water Management in Polymer Electrolyte Proton-Conducting Membranes J. electrochem. Soc. 145 (1998) 2684

[5] V. Baglio, A.S. Arico, A. Di Blasi, V. Antonucci, P.L. Antonucci, S. Licoccia, E. Traversa and F. S. Fiory, Nafion–TiO2 composite DMFC membranes: physico-chemical properties of the filler versus electrochemical performance, Electrochimica Acta 50 (2005) 1241

[6] S.-P. Nunes, B. Ruffmann, E. Rikowski, S. Vetter and K. Richau, Inorganic modification of proton conductive polymer membranes for direct methanol fuel cells, Journal of Membrane Science 203 (2002) 215

[7] D.-S. Kim, H.-B. Park, J.-W. Rhim and Y.-M. Lee, Preparation and characterization of crosslinked PVA/SiO2 hybrid membranes containing sulfonic acid groups for direct methanol fuel cell applications, Journal of Membrane Science 240 (2004) 37

[8] P. Dimitrova, K. A. Friedrich, U. Stimming and B. Vogt, Modified Nafion-based membranes for use in direct methanol fuel cells, Solid State Ionics 150 (2002) 115

[9] N. Miyake, J.-S. Wainright and R.-F. Savinell Evaluation of a Sol-Gel Derived Nafion/Silica Hybrid Membrane for Proton Electrolyte Membrane Fuel Cell Applications, J. Electrochem. Soc. 148 (2001) A898

[10] A. Glüsen, D. Stolten, Membranen für Polymerelektrolyt Brennstoffzellen, Chemie Ingenieur Technik 75 (2003) 1591

[11] Y.-S. ParkT and Y. Yamazaki, Low methanol permeable and high proton-conducting Nafion/calcium phosphate composite membrane for DMFC, Solid State Ionics 176 (2005) 11

[12] F. Bauer and M. Willert-Porada, Microstructural characterization of Zr-phosphate–Nafion® membranes for direct methanol fuel cell (DMFC) applications, Journal of Membrane Science 233 (2004) 141

[13] L. Tchicaya-Bouckary, D. J. Jones and J. Rozière, Hybrid Polyaryletherketone Membranes for Fuel Cell Applications, Fuel Cells 2 (2002) 40

[14] G. Alberti, U. Costantino, M. Casciola, S. Ferroni, L. Massinelli and P. Staiti, Preparation, characterization and proton conductivity of titanium phosphate sulfophenylphosphonate, Solid State Ionics 145 (2001)249

[15] C.W. Lin, R. Thangamuthu and C.J. Yang, Proton-conducting membranes with high selectivity from phosphotungstic acid-doped poly(vinyl alcohol) for DMFC applications, Journal of Membrane Science 253 (2005) 23

[16] J. Kim, B. Kim and B. Jung, Proton conductivities and methanol permeabilities of membranes made from partially sulfonated polystyrene-block-poly(ethylene-

ran-butylene)-block-polystyrene copolymers, Journal of Membrane Science 207 (2002) 129
[17]F.G. Wilhelm, I.G.M. Pünt, N.F.A. van der Vegt, H. Strathmann and M. Wessling, Cation permeable membranes from blends of sulfonated poly(ether ether ketone) and poly(ether sulfone), Journal of Membrane Science 199 (2002) 167
[18]C. Manea and M. Mulder, Characterization of polymer blends of polyethersulfone/sulfonated polysulfone and polyethersulfone/sulfonated polyetheretherketone for direct methanol fuel cell applications, Journal of membrane Science 206 (2002) 443
[19]J. Kerres, A. Ullrich, F. Meier and T. Häring, Synthesis and characterization of novel acid-base polymer blends for application in membrane fuel cells, Solid State Ionics 125 (1999) 243
[20]J.-M. Bae, I. Honma, M. Murata, T. Yamamoto, M. Rikukawa and N. Ogata, Properties of selected sulfonated polymers as proton-conducting electrolytes for polymer electrolyte fuel cells, Solid State Ionics 147 (2002) 189
[21]D. J. Jones and J. Rozière, Recent advances in the functionalisation of polybenzimidazole and polyetherketone for fuel cell applications, Journal of Membrane Science 185 (2001) 41
[22]P. D. Beattie, F. P. Orfino, V. I. Basura, K. Zychowska, J. Ding, C. Chuy, J. Schmeisser, S. Holdcroft, Ionic conductivity of proton exchange membranes, Journal of Electroanalytical chemistry 503 (2001) 45
[23]X. Zhang, J. Benavente and R. Garcia Valls, lignin-based membranes for electrolyte transference, Journal of power sources 145 (2005) 292
[24]Y. Sone, P. Ekdunge and D. Simonsson Proton Conductivity of Nafion -117 as Measured by a Four-Electrode AC Impedance Method, Journal of the Electrochemical Society 143 (1996) 1254
[25]M. Schonert and M. Veldhuisen, personal communication 2004
[26]M. Schonert, K. Jakoby, C. Schlumbohm, A. Glüsen, J. Mergel and D. Stolten, Manufacture of Robust Catalyst Layers for the DMFC, Fuel Cells 4 (2004) 175
[27]H. Dohle, J. Divisek, J. Mergel, H.F. Oetjen, C. Zingler and D. Stolten, Recent development of the measurement of the methanol permeation in a direct methanol fuel cell, Journal of power sources 105 (2002) 274